Università degli Studi di Napoli "FEDERICO II"

Dottorato di ricerca
in
Valorizzazione e gestione delle risorse agro-forestali
XXIV ciclo

Tesi di dottorato
in
Pedologia Applicata

Insight into the mechanisms of soil structure formation: an experimental approach using soil micromorphology and image analysis

Tutor
Prof. Fabio Terribile

Cotutor
Ing. Giacomo Mele

Coordinatore:
Prof. Guido D'Urso

Dottoranda
Laura Gargiulo

Acknowledgements

I would like to thank all the persons that make it possible the realization of this PhD thesis. Firstly my gratitude goes to professor Fabio Terribile who give me the opportunity for my scientific growth. Then a particular appreciation is reserved to Giacomo Mele, who introduced myself in the field of soil pore image analysis.
Furthermore I say thank you to all persons that actively participate my effort spent during this years: Antonietta Agrillo, Angela Balsamo, Angelo Basile, Antonello Bonfante, Gilda Buscemi, Roberto de Mascellis, Bruno Di Matteo, Giuliano Langella, Piero Manna, Antonio Mileti, Luciana Minieri, Pierpaolo Moretti, Nadia Orefice and Simona Vingiani.
Finally I reserve a special thank to my family and my boyfriend for their support.
THANK YOU!

Contents

1. Introduction

1.1 The soil structure

"The soil is a world of darkness, of caverns, tunnels and crevices, inhabited by a bizarre assortment of living creatures . . ." (Wallwork, 1975).

Soil is the most diverse and important ecosystem on the planet. Myriad of biophysical and biochemical processes persist in parallel that are required to sustain all of the other trophic levels in the biosphere. A key to this is the physical complexity of the soil physical structure that provides the habitat for soil organisms and the conduit for essential resources (Young and Crawford, 2004).

Soil structure is characterized by physical and temporal heterogeneities across all measured scales, from nm to km (Young and Ritz, 2000). The geometrical complexity of the pore pathways determines the biochemical processes that govern life on Earth, such as plant productivity (Hillel, 1980), water retention (Dexter and Richard, 2009; Vogel, 2000), and greenhouse gas emissions (Kuka et al., 2007), and offer an unrivaled buffering capacity against potential pollutants entering the waterways (Zhang et al., 2002).

Dexter (1988) broadened the definition to "the spatial heterogeneity of the different components or properties of soil". This definition includes within it the earlier concepts of particles and aggregates, but has been expanded to include all possible soil features. In particular, it introduces the concept: structure = heterogeneity. According to this definition, the formation of structure implies that the soil is becoming more heterogeneous.

Soil structure is dynamic, complex, and is not very well understood. One of the reasons for the complexity of soil structure is the dynamic nature of soil structure. Structural attributes vary in time and space, and the attributes observed at any given time reflect the net effect of numerous interacting factors which may change at any moment (Lal, 2004). The importance of soil structure and its complex nature are well summarized in this phrase of Jacks (1963): "the union of mineral and organic matter to form the organo-mineral complexes is a synthesis as vital to the continuance of life as, and less understood than, photosynthesis."

The formation of soil structure is the result of the actions and interactions of chemical, physical and biological factors with intricate feedback mechanisms.

Over time, several theories have been proposed on its formation. Edwards and Bremner (1967) formulated a theory in which the solid-phase reaction between clay minerals, polyvalent cations and SOM is the main process leading to microaggregate formation. Based on this concept, Tisdall and Oades (1982) coined the aggregate hierarchy concept and subdivided organic aggregating agents into transient (polysaccharides), temporary (roots and fungal hyphae) and persistent (humic substances). Oades (1984) suggested a modification to the aggregate hierarchy concept by theorizing the formation of microaggregates within macroaggregates. Subsequent research on aggregate formation and SOM stabilization extensively corroborated this modification (Six et al., 2004).

Among the aggregating agents the soil organic matter has been widely studied for its effect on the formation of soil structure. The SOC creates regions of heterogeneity in the soil, leading to ‘‘hot spots’’ of aggregation (Bronick and Lal, 2005) . Increased SOC is related to increased aggregation (Chenu, 2000). The aggregate binding effect of labile SOC is rapid but transient (Kay, 1998) while slower decomposing SOC has subtler effects on aggregation, but the effects may be longer lived (Piccolo et al., 1997; Martens, 2000).

The role of iron oxides on the aggregation and stabilization of soil structure has been extensively analyzed (Arduino et al., 1989; Rhoton et al., 2003; Six et al., 2002). Their aggregating effect is especially noticeable at the scale of microaggregates, but also the formation of macroaggregates was related to the content of oxides in the soil (Six et al., 2000, Imhoff et al., 2002). They may increase the aggregation adsorbing organic substances on their surfaces (Oades et al., 1989), establishing electrostatic bonds with negatively charged clay minerals (El-Swaify and Emerson, 1975) or forming coatings on the surface of minerals and binding together primary and secondary particles (Müggler et al., 1999). Calcium carbonate in soil acts as aggregating agent, through the formation of segregations and coatings including other components of the soil with the formation of aggregates. A large amount of scientific literature is focused on the effect of Fe oxides and $CaCO_3$ on the stability

of soil aggregates (Boix-Fayos, 2001; Rhoton et al., 1998; Cammeraat and Imeson, 1998; Igwe al., 1995; Colombo and Torrent, 1991; Oades and Waters, 1991).

A natural process that can affect soil structure is wetting and drying (W/D) cycles (Pagliai et al., 1987; Hussein and Adey, 1998; Bresson and Moran, 2003). Telfair et al. (1957) and Newman and Thomasson (1979) observed that alternations of W/D cycles can result in aggregate formation in non-aggregated soils, which can confer specific structures to damaged soils. Investigations carried out in clayey soils (Pagliai et al., 1987) revealed that W/D cycles can cause changes in the pore system and induce soil aggregation. Sequences of W/D cycles can lead to the rearrangement of soil particles, because during these processes soil particles may change their individual orientation, modifying the pore system as a whole (Pires et al, 2008).

Soil freezing has been reported both as beneficial and detrimental to soil structure (Dagesse, 2011). Lehrsch et al. (1993) emphasized the non-uniformity of structural changes induced by frost. One general consistent trend is that the disruptive effects of frost are enhanced with increasing water content (Bullock et al., 1988).

Soil fauna and plant roots play an important role in the formation and stabilization of soil structure. Earthworms and enchytraeids are the soil organisms most studied in relation to soil structure formation (Jones et al., 1994; Edwards and Boholen, 1996; Francis and Fraser, 1998; Brown et al., 2000). Also termites are important for their role in building soil structure (Jungerius et al., 1999; Holt and Lepage, 2000; Bignell and Holt, 2002). Mycorrhizal and saprophytic fungi are are involved in the formation and stabilization of soil aggregates, but also extracellular polysaccharides (EPS) produced by soil micro-organisms influence soil aggregation (Meadows et al., 1994; Chantigny et al., 1997; Czarnes et al., 2000; Schutter and Dick, 2002). Plant roots affect soil structure penetrating in the soil, changing soil water regime, releasing organic material within the rhizosphere and entangling soil particles (Angers and Caron, 1998; Gale et al., 2000; Puget and Drinkwater; 2001; Gulser, 2006; Zhou and Shangguan, 2007).

In 2004, Six et al. reviewed the results obtained in the study of the main factors influencing aggregate formation and stabilization. They stated that although the important contribution of the study of aggregation process in the understanding of

the soil structure formation, the quantification of the single influences and involved feedback mechanisms remain lacking. Most experiments focusing on mechanisms are designed to yield simple correlations between the factors and aggregation. Promising solutions could be integrating aggregation measurements with morphological characterization and with 2 and 3D spatial information.

In fact, in relation to functional properties soil structure is better thought as a framework or architecture, and the investigation of discrete aggregates or distributions of aggregates does not offer any spatial information. Functional traits of soil structure, at all scales, rely on the connectivity, tortuosity and the heterogeneity of pore space (Young et al., 2001).

Soil micromorphology provides insights into soil structure and aid interpretation of the mechanisms of soil structure formation and image analysis, although not a standardized technique such as the measure of aggregate stability, allows to obtain quantitative information on soil structure better related to soil functions. The image analysis is a technique used successfully for over thirty years in the quantitative study of soil structure.

The technique is traditionally based on the acquisition of images of plane sections of impregnated soil samples and the subsequent "objects analysis" (Jongerius et al. 1972; Pagliai et al., 1984), which means that each pore is considered as an individual object having certain specific properties (area, perimeter, elongation, etc.). Although the usefulness of this approach, thereafter alternative soil image analysis approaches became available in order to produce soil pores information which can be easily compared with functional soil properties (Velde, 1999; Mele et al., 1999). They base the quantitative analysis of soil porosity on mathematical morphology algorithms, allowing to determine a pore size distribution conceptually related to the soil water retention.

1.2 Aims and outline of the thesis

The aim of this work was to study some mechanisms of soil structure formation by means of soil micromorphological approach and the soil two-dimensional image analysis approach cited above. Given the complexity of interactions among factors influencing soil structure formation, we used an approach based on experimental tests in pots in order to better isolate and distinguish the effects of certain soil structuring factors. In fact recently Bockheim and Gennadiyev (2009) highlighted that the experimental approach to pedology has many advantages, including the support of observational evidence, the establishment of causal rather than simply correlative relations and the linking of basic and applied pedology.

The thesis was produced as a compilation of three research papers and a technical note, all written by myself as the principal author.

In the second chapter is firstly presented a brief overview of the two-dimensional image analysis technique applied to the study of soil structure. Since this technique is not yet standardized and many problems are related to each stage of the image analysis, in this work we have highlighted the main limitations about the image acquisition stage and we attempt to find possible solutions in order to give a contribution to the standardization of the two-dimensional image analysis.

In the third chapter is reported the work on the study of the effect of calcium carbonate ($CaCO_3$) and iron (Fe) oxides on soil structure formation. These two inorganic compounds are well-known as aggregating factors, then we investigate the physical mechanisms of soil pore development as consequence of the distribution of calcium carbonate ($CaCO_3$) and iron (Fe) oxides. In order to isolate their effects we performed an experimental test on simplified soil-like systems, that were successively analyzed by soil micromorphological and soil image analysis approach.

In the fourth chapter is presented a study on the effect of the interaction between rock fragments and some soil physical properties, such as the characteristics of shrinkage and plasticity, on the mechanisms of soil pore formation. For this purpose was investigated, by means the preparation of an experimental test and the use two-dimensional image analysis, the effect of several concentrations of rock fragments

with different sizes and shapes on the surface cracking and the pore size distribution of five soils different in shrinkage-swelling dynamics and plasticity.

In the fifth chapter is presented a preliminary methodological work on the use of a micromorphological image analysis approach that allows to quantify the contribution of different biological activities on soil pore size distribution and on aggregate size distribution.

2. Soil pore analysis from resin impregnated soil blocks: methodological aspects of 2D image acquisition

2.1 Introduction

The application of image analysis techniques to study the soil structure has become an indispensable tool for research in soil science. Essentially this technique provides a powerful tool for a direct evaluation of the soil pore system.

The characterization of the porosity using image analysis was first carried out by Jongerius et al. (1972) and Murphy et al. (1977a,b), in the early 1970s when image analysers, like the Quantimet 720 (Fisher, 1971; Nawrath and Serra, 1979), became available contributing significantly to promote the quantitative use of photographs in the study of soil structure. The measurement of macroporosity by image analysis were compared with data from water retention measurement already in the 1979 by Bullock and Thomasson (1979). Ringrose-Voase and Bullock (1984) developed a system (ANOPOR) to recognize and measure the three different classes of pores (channels, planar voids and vughs) in impregnated soil blocks and successively Ringrose-Voase (1987) proposed two scheme to describe several soil structural spectra using these classes. In 1987 Protz et al. (1987) stated that it was possible to measure the size, shape and distribution patterns of voids and pedological features at different moisture contents and they hypothesized that improvements in image analysis equipment in the future would allow the use of spectral data in order to distinguish features in soil samples. Significant contributions to the quantification and characterization of soil pores by 2D image analysis procedures are those by McBratney and Moran (1990) and Ringrose-Voase (1990, 1991) who proposed various way of parameterizing micromorphological observations and of using these structural parameters to compare different soil structures. To bridge the gap between description of soil in the field, i.e. macromorphology (which is usually qualitative), and micromorphology (which may be quantitative), Koppi and McBratney (1991) proposed a technique for mesomorphological description at a scale that permitted details of horizons to be quantified and the relationship between features of interest

in different horizons to be discerned. In order to quantify micromorphological features Terribile and Fitzpatrick (1992) presented a multilayer approach to the image analysis of soil thin sections that allowed the creation of multilayer images on which supervised and unsupervised classification procedures were applied to distinguish and quantify features such as quartz, clay coatings, matrix and pores. The principles and the progresses of 2-D image analysis system used for the characterization of soil structure were presented and discussed by Ringrose-Voase (1996). The application of mathematical morphology for analyzing soil structure from images was showed by Horgan (1998). In order to analyze the three-dimensional characteristics of soil pore space, Vogel (1997) proposed a method for the morphological determination of pore connectivity as a function of pore size using serial sections. Mele et al. (1999) used a system based on mechanical tomography applied to optical serial sectioning to perform several kinds of analysis such as pore size distribution, exchange surfaces, pore-connectivity, etc. Also Moreau et al. (1999) used sequential images of an impregnated soil block to compare two dimensional and three dimensional aspects of pores in a Vertisol.

The characterization of the soil pore system from the 2D soil image analysis has been used for a variety of purposes: to evaluate the effect of management practices on soil structure (Pagliai et al., 2004: Hubert et al., 2007), to quantify dye transport in preferential flow pathways (Ohrstrom et al., 2004; Duwig et al., 2008), to assess repair of soil structure due to wetting and drying cycles (Pires et al., 2007), to observe pores and aggregates during aggregation (Li et al., 2004), etc.

In recent years, synchrotron based X-ray computed tomography (CT) and desktop X-ray micro- CT scanners have allowed researchers to visualize in three dimensions the structure and composition of soils at micrometric resolutions, and have enabled significant advances to be made in our understanding of the functioning of soils at previously unexplored spatial scales (e.g., Baveye et al., 2002; Elliot and Heck, 2007; Sleutel et al., 2008).

Although it is currently possible to use 3D image analysis to observe and quantify soil porosity, 2D image analysis on impregnated soil blocks remains attractive and is still commonly used (e.g. see Li et al., 2004; Bartoli et al., 2005; Mooney et al.,

2006: Hubert et al., 2007; Carof et al., 2007; Glab and Kulig, 2008; Miralles-Mellado et al., 2011) because of its low cost and easy accessibility. This is additionally so because porosity and pore size distributions of a 3D soil block can be adequately predicted using 2D images (Moreau et al., 1999).

The 2D soil image analysis is a technique based on the impregnation of a dried undisturbed soil sample with resin and fluorescent dye (FitzPatrick, E.A., 1984). After the soil sample is hardened it is cut into slices and analyzed in an optical microscope. The dye impregnated blocks permit the sections of the voids to fluoresce under ultraviolet light (Murphy et al., 1977a). At the stage when pictures of the soil are taken (in the field or in the laboratory), different lighting arrangements, cameras, lenses, resolutions, aperture and settings for exposition have to be selected among many possible choices. Finally, the resulting 2-D images of the soil have to be thresholded or segmented to produce a binary image, to which are then applied a wide range of statistical or mathematical methods.

In the 1992 Thompson et al. (1992) advised caution in the interpretation of data generated by analysis of images of soils, arguing that, in effect, image analysis begins in the field when the soil is sampled, and researchers should be aware that artifacts may be introduced at several steps in the process. Each laboratory must address a number of relevant problems before meaningful analyses and comparisons can begin. Some problems include: establishing adequate contrast between pores and soil matrix on the image; choosing images representative of pore space at the resolution of interest; identifying relevant statistical tests to compare pore-space patterns. By controlling as many variables as possible during image preparation researchers can use image analysis as an important tool to study soil pore space.

Moreover, all these steps involve operational decisions that can vary from one observer to another.

Despite the progresses made in this field, Marcelino et al. (2007) renewed call for standardization. They compared soil porosity measurements preformed by manual, semiautomatic and automatic 2D-image analyses on three sets of images of the polished surfaces of soil blocks impregnated with a fluorescent resin and on the thin

sections made from them, respectively. A scanning electron microscope in backscattered mode was used to acquire the third set of images on the thin sections.

They observed that porosity measurements carried out on images acquired using different methods cannot be compared. On the other hand, because different interventions and methods used to increase image quality and segment images also affect porosity results significantly, these results can only be compared if the images are subjected to the same treatment.

Recently Baveye et al. (2010) determined how much variation exists among the outcomes of various image thresholding strategies (including any image pretreatment deemed appropriate), routinely adopted by soil scientists and observed that there is considerable observer influence associated with this thresholding. They proposed different strategies to cope with this situation, including the use of physical "standards", adoption of procedures to assess the accuracy of thresholding, benchmarking with physical measurements, or the development of computational methods that do not require binary images.

Even within the same soil sample preparation method the quality of the images obtained from different scientists also can show a variability which significantly affects the successive image processing procedures and analysis results This is mainly due to the procedure used in the image acquisition stage. Therefore such preliminary stage would require firstly to be standardized .

The objective of this work is then to provide a contribution to the discussion of some of the many problems related to the stage of image acquisition, which is one of the most delicate and critical to achieve a standardization of the entire soil image analysis process.

Among the major limitations about the acquisition stage the following will be investigated here: (i) pore and solid phases detection limits, (ii) the determination of the "representative elementary area" (REA), (iii) the choice of the resolution to be employed and (iv) real pore shape against pixel grid geometry of digital images.

This work is an attempt to both highlight these limitations and to find possible solutions by means of specific tests performed using two soils with very different soil structure.

2.2 Materials and methods

Dried undisturbed samples have been collected from A and B horizons of both a Typic Haploxerert (Suelli, Avellino; Italy) and Fluventic Haplustepts (Vitulazio, Caserta, Italy) (USDA, 1998). The samples were treated with acetone (FitzPatrick, 1984) and then impregnated with the polyester resin (Crystic 17449, Scott-bader Ltd.) containing a fluorescent dye (Uvitex OB) having a spectral emission in the blue band under UV illumination (365 nm). After the hardening the samples were cut and grind in order to have a flat surface (vertical with respect to the orientation of the profile). Digital images of the four vertical sections (7.2x5.4 cm) were acquired under UV illumination. A Nikon D200 camera was used, controlled by a PC using Nikon Capture 4.1 software. Images were pre-processed and segmented using a technique of supervised "thresholding" using Corel Photo-Paint X3, in order to obtain binary images where the two separate solid and pore phases are in black and white, respectively.

Below are presented brief overviews of the different issues addressed and methods used to investigate them.

2.2.1 Detection limits

Overview

In soil structure study it is of paramount importance to have a very good differentiation between the pore and the solid phase of the soil; this is typically done illuminating with UV light a soil block impregnated with a fluorescent dye. Under the UV light the pore containing the dye fluoresces becoming bright against the solid dark phase. Such treatment produce the contrast between the two phases: solid and pore.

This step of image production is critical, yet some modifications to the image are difficult to avoid. For example, pores can be "lost" because they are too small to contain sufficient dye to fluoresce adequately. Alternatively, pores may be "gained" because dye can fluoresce through clear sand grains at the surface of the block. Unfortunately, there is no simple way to verify the accuracy of the image that is produced, except by careful visual checking of the print to be analyzed against the

sample itself. The question to be answered is whether the pores to be measured, and only they, are fully delineated (Thompson, 1992)

A good visual differentiation is reflected, in the best of the cases, by a clear bimodal distribution of the histograms of grey levels. Such bimodal distribution is a good prerequisite for obtaining a good "pore-solid" segmentation of the image and therefore good material for a reliable image analysis of the pores. Unfortunately, such nice scenario in most of the cases is not approachable and grey levels histograms having not very clearly expressed bimodality generally result.

This may be due to problems of impregnation or interaction between the dyes and the elements present in the soil or additives added to the resin. The critical connection between soil impregnation problems and image analysis is this: measurements of soil pore space by image analysis are compromised to the extent that samples are poorly impregnated. Both polyester and epoxy resins have been used for impregnation of dried soil samples. Neither provides perfect impregnation in all situations. In fact, there are so many variables associated with the soil sample itself, mineralogy, clay content, porosity, organic matter, etc., that it is probably unrealistic to expect any impregnating resin to be "universal" (Thompson, 1992).

Regarding the interaction between dyes and elements in the soils, certain metal ions are known to cause color changes and loss of brightness with fluorescent colorants. Several studies have shown that plastic processing additives containing "free" zinc, magnesium, calcium and iron will cause deleterious color effects when used in a plastic resin system containing NX-Pigment. If an additive containing metal must be used, it should be thoroughly tested to ensure the color stability of the NX-Pigment.

As a consequence it can be difficult (if not impossible) to locate a proper grey level threshold for obtaining a good pore-solid differentiation. The overall result is a large increase of the inaccuracy produced in the analysis.

In order to address such limitation it must be reminded that digital images are actually acquired by means of Charge Coupled Devices (CCDs of digital camera, video camera or scanner) or more recently by means Complementary metal–oxide–semiconductor (CMOS) sensors. The quantum efficiency of these image sensors is a

property of the photovoltaic response defined as the number of electron-hole pairs created and successfully read out by the device for each incoming photon.

Typical spectral sensitivity curves for IS under different illuminations are illustrated in Figure 1 (http://www.vision-systems.com). For comparison, Figure 1 also illustrates spectral sensitivity curves for the human eye, corresponding to photopic and scotopic vision, arising from the cones and rods structures of the retina, respectively.

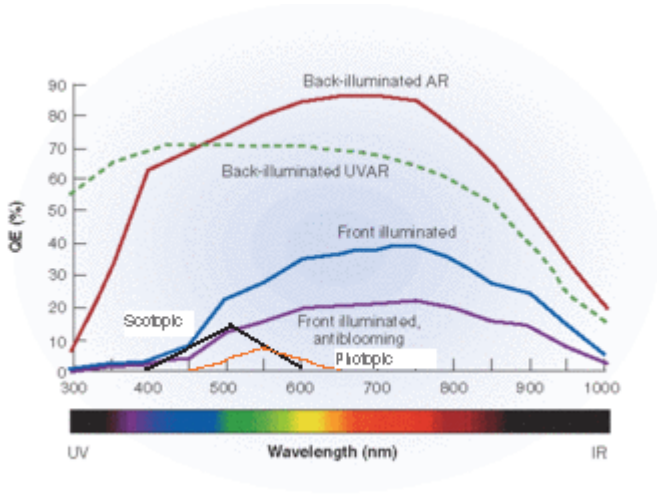

Figure 1. Typical spectral sensitivity curves for image sensors under different illuminations and for the human eye.

Peak sensitivity is in the green (photopic at 555 nanometers and scotopic at 507 nanometers) with a maximum quantum efficiency of 3 percent for photopic vision and 10 percent for scotopic. From this data it is obvious that compared to our eyes, a scientific-grade camera has a broader spectral sensitivity with a much higher quantum efficiency.

The image sensors have their peak sensitivity in the near-infrared- red portion of the spectrum and a much lower sensitivity in the visible blue part of the spectrum; this is unfortunate because most widely used dyes which are used for pores studies (i.e. Uvitex) emit in the blue part of the spectrum. This situation means that the optimal signal/noise ratio is not achieved.

Methods

In this work a test was performed to evaluate the possibility of using pigments that emit in the range of wavelengths, other than blue, in which the image sensors show a greater sensitivity. In addition to the pigment that emits in the blue, two different fluorescent pigments have been used: one that emits in the red (SC-25 Angstrom Technologies, Inc.) and one that emits in the green. These pigment were selected for their solubility in acetone, which is normally used as a diluent in the mixture of polyester resin. Were prepared three blocks of epoxy resin (Araldite PY 303-1, Ciba) with gravel (see fig.2), each containing one of the three pigments added to the same concentration (1% by weight). RGB images of resin blocks were acquired under UV light. We compared histograms of intensities of R, G and B respectively to quantify the intensity of the signal obtained.

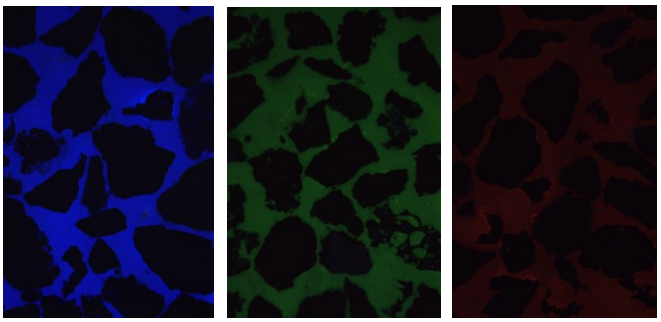

Figure 2. Images of resin blocks containing different pigments.

2.2.2 Determination of representative elementary area

Overview

One of the most delicate and difficult task to be addressed in soil porosity studies is the choice concerning the size of the analyzed area or volume. The choice of the analyzed area or volume, in the ideal case, should follow a preliminary investigation concerning the analysis of the minimum elementary volume/area necessary to represent the porosity of a selected horizon to be studied.

The perceived macroscopic properties of natural porous systems may be strongly affected by the geometrical characteristics of the measuring instruments used to evaluate them. In soil science the term “representative elementary volume” or REV is known especially in terms of modeling the transport of fluids and solutes (Bear, 1972). The representative elementary volume can be defined as the minimum volume

of a soil sample required from which a given soil parameter measurement becomes independent of the size of the sample. In other words if the sample volume is large enough it should account for the spatial heterogeneity of the parameter of interest within the scale of interest. To assess the true nature of the instrumental dependence of macroscopic variables, one has to be able to perform nondestructive measurements of specific soil properties over a series of volumes of increasing sizes, which are all 'centred' on the same point, like Matrioshka dolls. Baveye et al. (2002) demonstrated the potential of calculations based on x-ray CTdata to simulate the dependence on sampling volume of a range of macroscopic soil parameters.

In two dimensions, an equivalence of the representative elementary volume can be the representative elementary area. Bear and Bachmat (1984) concluded that in an isotropic medium an REV was well represented by a representative elementary area (REA).

Sweeney (1994) was the first to utilize the concept of the REA on voids from soil thin sections. Subsequently VandenBygaart and Protz (1999) stated that a fundamental question to be answered for quantitative micromorphology studies at varying scales is: What is the minimum area on a soil thin section or block that is required to represent the pedofeature of interest based on its distribution in soil space? They suggested that the REA determination should be performed in every quantitative soil micromorphological study in order that the parameter of interest is an adequate representation of that feature in soil space. VandenBygaart and Protz (1999) proposed a methodology to estimate the REA: the REA was attained at the area where the measurements made on a parameter in three successive areas of measurements do not change ± 10% relative to the next greater area of measurement. The 10% level was selected arbitrarily and could vary depending on the pedofeatures of interest. That is, the relative change between successive sampling areas could vary depending on: (i) the parameter of interest (i.e., soil porosity; aggregates, Fe concretions, etc.) for which the spatial variability is not known; (ii) the number and differences in area of successive frame subset areas; (iii) the absolute size of the soil parameter being measured.

This methodology is still employed currently, for example it has been used in a study on the effect of tillage and no-tillage practices on pore morphology to determine which images of section of soil blocks reached the REA for the total macroporosity measurement and for the pore morphological classes measurement (Hubert, 2007). Li and Zhang (2010) analyzed digital images of a cracked soil surface to determine the REV of a crack network in soil. They used a method similar to that of VandenBygaart and Protz, they calculated the crack porosity and crack polygon density values for 10 square windows of increasing size and found the REV size when the variation of these values in relation to domain size was negligible (when gradient errors became less than 20%).

This work has further explored the problem of identification of the REA with respect to the total porosity by comparing each four binary images of soil structure very different from each other.

Methods

It has been performed an evaluation of the representative elementary area for measuring the total porosity. For the determination of the REA with respect to the total porosity, the porosity percentage was determined on areas of increasing size of four digital images of the same size (400 pixels). These images were obtained from photos of sections of impregnated soil blocks characterized by different types of soil structure. In particular, the images of the samples described previously have been used (see fig.3), i.e. images of an Ap horizon of a Fluventic Haplustepts (Vitulazio) and of a B horizon of a typic Haploxerert (Suelli), and also two images of a sandy soil and of a Vertisol. The image analysis for the determination of total porosity was performed using Solicon - PC Version 1.0 software (Cattle *et al.*, 2000).

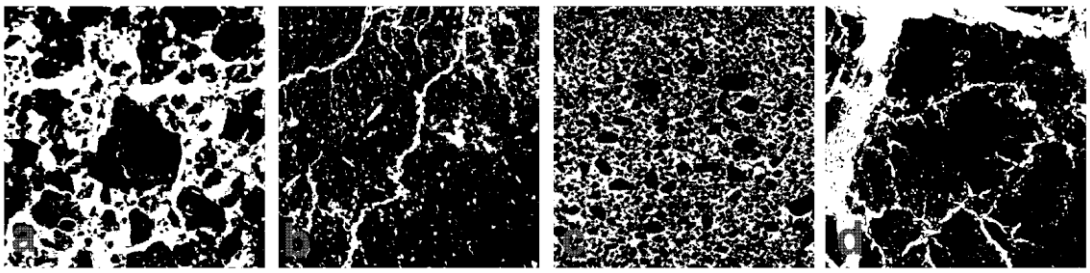

Figure 3. Images acquired from samples of: a) Ap horizon of Vitulazio (Vertic Inceptisol) soil, b) B horizon of Suelli soil (Vertisol), c) a sandy soil, d) A horizon of a Vertisol.

2.2.3 Choice of spatial resolution

Overview

Baveye et al. (2010) stated that the choice of image resolution is one of the Achille's heels of image analysis and it is necessary to identify a way to deal with it. The soil image analysis is influenced by the image resolution because it is limited by a lower pore size class related to the image resolution. Therefore the choice of the spatial resolution to be used must be considered of paramount importance for any image analysis work on soil pores. It is relevant to address such important issue because little research efforts have been produced on it, such as the evaluation of the influence of image resolution on the surface fractal dimension of soil pores (Dathe and Baveye, 2003) and on estimates of the lacunarity of porous media (Pendleton, 2005). Therefore what is missing is an evaluation of the choice of the resolution that takes into account its effect on properties of the soil pore system as the total porosity and pore size distribution. The resolution of a given image depict the reality at that specific scale of information, therefore a pore system not detectable at a coarser resolution (i.e. pore much smaller than the pixel area) may show up at higher resolution producing another and novel aspect of the reality of that sample. Of course the finest achievable resolution (given a set of camera and optics) give the closest picture to reality and therefore it may be the most desirable. Despite such obvious statement it must be emphasised that this is not always the case; in fact finest resolution means high amount of data to be processed especially when dozens or hundreds of images have to be processed together as it is the case when a large mosaic image has to be produced from very small field of view. This implies at least very long time if not the impossibility of image processing. In such scenario since the finest resolution is the best but the more hardware demanding while the coarsest resolution is the worst but the least hardware demanding it is crucial to set up a methodology enabling to select the most appropriate resolution for the problem to be addressed considering the choice of image resolution depends also on the purpose of the analysis. For example the level of resolution required to study fine pore space produced by enchytraeid worms is different from the one required to study large Vertisols cracks. Therefore it is necessary to set up a methodology in order to help

the choice of resolution. This is generally the case when a specific case study has to be addressed such as for instance the change of porosity before and after a given soil treatment (e.g. tillage practice). In this case, the user has to select the best resolution which enables both (i) to analyse the change in porosity before and after the treatment with (ii) as less data as possible in order to enable the many image processing analysis required.

In this work we analyzed the effect of the variation of resolution at the acquisition stage on the results (i.e. total porosity, mean width of the soil pores, pore size distribution) of some pore image analysis performed on samples with very different soil structure and we tried to set up a methodology to help scientists to select the most appropriate spatial resolution for the soil pore system analysis.

Method

We have carried out soil image analysis on four samples of the A and B horizons of the Vitulazio and Suelli soils with different soil pore system organization (see fig.3a and b). A set of 2D images were acquired under UV light at the eight following resolution: 25, 50, 75, 100, 125, 150, 250, 500 μm for each of the four samples. After the acquiring stage and the thresholding of the images, image analysis was performed using Solicon - PC Version 1.0 software (Cattle *et al.*, 2000) to determine total porosity. Pore size distribution and mean width of the pores were determined by image analysis using Micromorph 1.4 (TRANSVALOR 2000), through the application of the "opening" algorithm (Horgan, 1998; Serra, 1982), which classifies the pore phase according to the spacing from the walls.

2.2.4 Effect of pore orientation on total porosity measurement

Overview

The accurate analysis of the complexity of the system of pores, characterized by many pores with different shapes and orientations, not always is such trivial as it may seems.

In fact a highly oriented porosity parallel or otherwise oblique to the arrays of the image sensors may induce for each of these cases some more or less evident defects in pores representation. In this work we have checked the amount of artefacts

introduced in the soil pore analysis based on the orientation of the pores with respect to the elements of the image sensors at the time of image acquisition stage.

Method

We acquired a series of images at different angles and then we calculated the variation in frequency and connectivity of the porosity. The rotation test was performed on the images of the Ap horizon of Vitulazio soil having a not oriented porosity and of the B horizon of Suelli soil showing a strong pore orientation. These images has been acquired 7 times after a rotation of 15° of the sample. Then for each rotation the image analysis was performed using Solicon - PC Version 1.0 software (Cattle *et al.*, 2000) to determine total porosity. In order to better understand the variation in pore frequency of the highly oriented pore system, the rotation test was performed also on an artificial image with an oriented pore (Fig. 4).

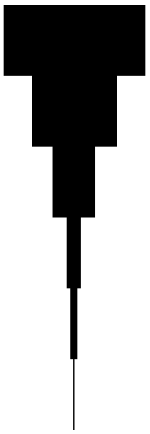

Figure 4. Artificial image of oriented pore.

This image has a true calculated porosity (calculated on the base of the pore shape) of 11.44 %.

2.3 Results and discussion

2.3.1 Detection limits

Form the histograms of the images of three blocks of resin containing different pigments (fig.2) was obtained a graph of the relative intensity expressed as a percentage of the pigment that emits in the blue.

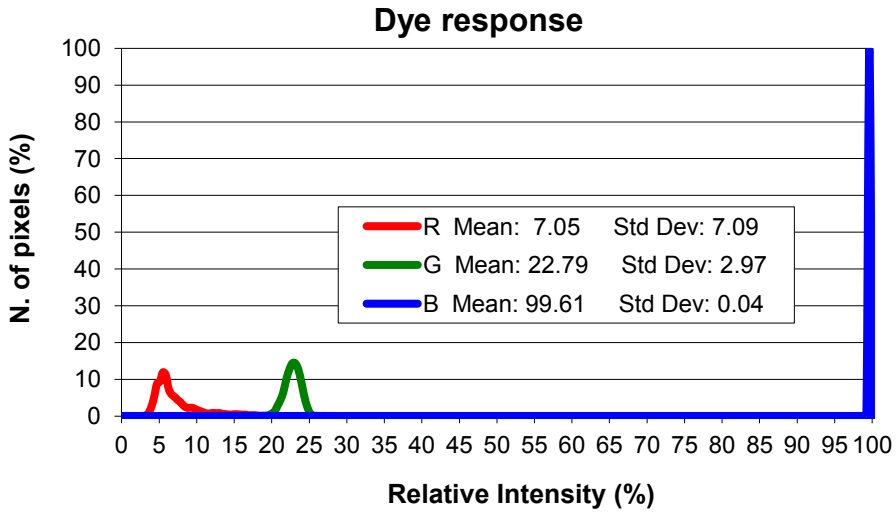

Figure 5. Relative intensity of the three pigments used.

From the graph in figure 5 it was observed that the pigment that emits in the green range of the spectrum produces an average intensity which is equal to 22.79% compared to that of the blue and the pigment that emits in the red produces an intensity even lower (7.05% compared to blue pigment).

Furthermore, while the relative peak intensity produced by the blue pigment is very narrow, with a standard deviation of 0.04, the peaks produced by pigments that emit in green and red are much larger, with values of standard deviation of 2.97 is 7.09 respectively.

This comparison therefore shows that to have the same intensity of the signal produced by the pigment that emits in the blue it should be necessary to use a higher amount of pigment that emits in the green or an even greater amount of pigment that emits in the red. Since at lower values of standard deviation corresponds the greater homogeneity of the signal, can also be observed that the pigment that emits in the blue produces a most homogeneous signal than that produced by the other two pigments. It is also noteworthy that the used red pigment was the only commercially available soluble in acetone and its cost is an order of magnitude higher than that of the blue.

Therefore even if the image sensors have their peak sensitivity in the near-infrared-red portion of the spectrum, however, for both technical and economic reasons, is more convenient to use the pigment that emits in the blue.

2.3.2 Determination of representative elementary area

In figure 6 are shown the images with their REA.

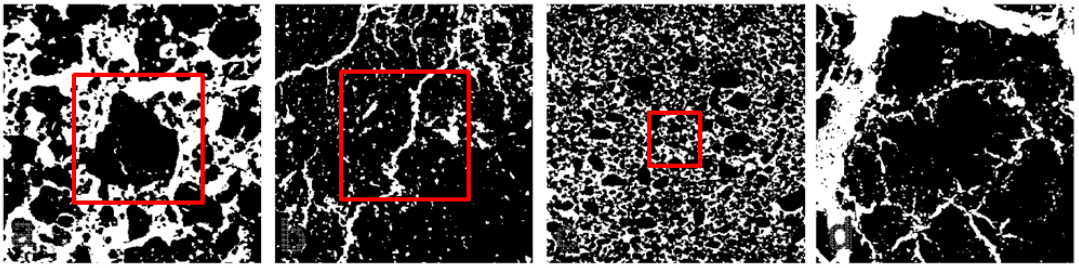

Figure 6. Images acquired from samples of: a) Ap horizon of Vitulazio (Vertic Inceptisol) soil, b) B horizon of Suelli soil (Vertisol), c) a sandy soil, d) A horizon of a Vertisol.

The graph (fig.7) resulting from the determination of the REA with respect to the total porosity showed that, with respect to the Vertisol (fig.6d), the size of the total image was too small to reach the REA; in fact, the value of total porosity has not stabilized with the increase of the area analyzed.

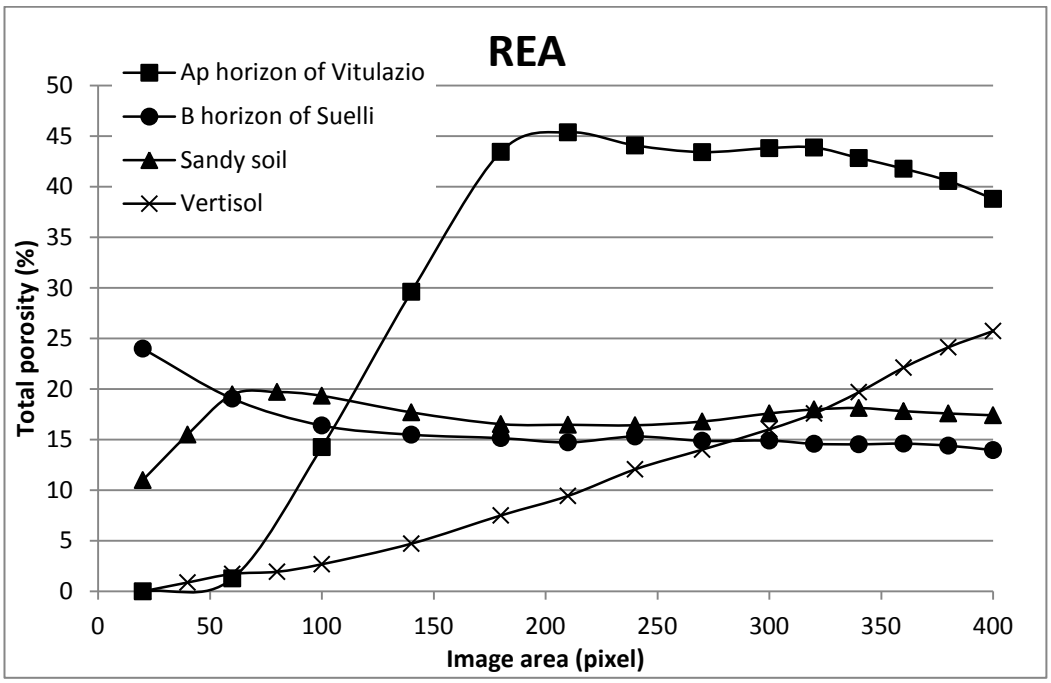

Figure 7. Determination of REA for the total porosity measurement.

So to get a measure representative of the total porosity of this type of structure (Fig.6d) is necessary to analyze larger area. As for the sandy soil was observed that the measure of total porosity has already stabilized from an area of 140 pixel^2. So for a homogeneous soil structure like that of a sandy soil (fig. 6c) a small area resulted sufficient for the determination of total porosity. The most interesting results were

related to the images of both Ap and B horizons from two different soils (Fig.6a and b). The area from which the values of total porosity have stabilized was the same (180 pixel^2) for both soils, although they had very different total porosity: 15% for the B horizon and 43% for Ap horizon. In addition, as it can be seen by the pictures and results presented below, the pore size distributions of two soils were very different. Therefore, the REA needed to measure the total porosity was the same for two soils with very different pore geometry, in terms of both total porosity and pore size distribution. Consequently, it is possible to deduce that the REA is actually influenced by the periodicity of a particular organization of the pores of the soil.

2.3.3 Choice of spatial resolution

Prior to the results obtained from measurements of total porosity, pore size distribution and mean pore width as a function of resolution is necessary to make some preliminary considerations. The image sensors have a square array of photodiodes (or a row with a scanning device) which gather and arrange the sampled points in a square grid of pixels and the side of a pixel corresponds to the image resolution. Because the pores have a size continuous variability which can only be approximated by the discrete spatial distribution of the pixels in the image, you can make measurement errors (overestimate, underestimate or failure detection) of the porous phase depending on the ratio between the resolution and pore size.

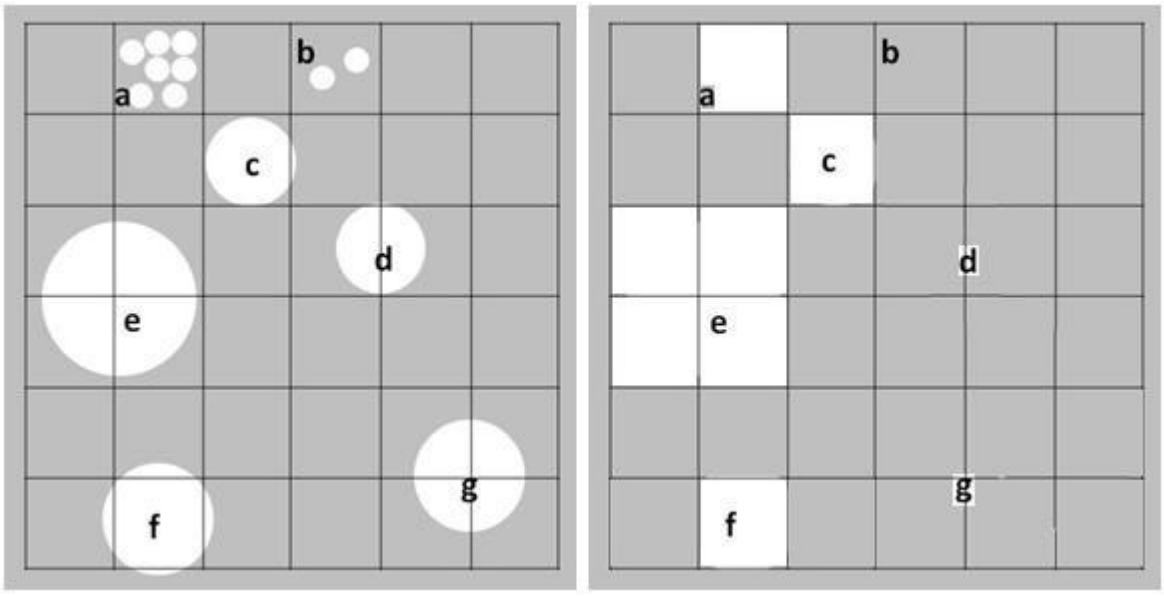

Figure 8. Square grid of pixels and the corresponding circular porous phase.

In Figure 8 are shown the most common circumstances useful in explaining the reasons for these errors. In it we refer, for simplicity, to portions of the porous phase of circular shape and it is assumed a configuration of hardware and acquisition (illumination, optics, image sensor sensitivity, etc.) such that a pixel change state from a solid (black) to a pore (white) when the area of corresponding real porous portion is greater than 50% of the pixel. Note, however, that similar schemes could be made for any shape of porous phase and for state change thresholds of pixels different from 50%. The portions of the porous phase smaller than the resolution may be overestimated (Fig. 8a) or undetected (Fig.8b), those with the same size as the resolution may also be overestimated (fig.8c) or undetected (fig.8d) and those of the largest dimension of resolution can be either overestimated (Fig. 8e) or underestimated (Fig. 8f). The portions of porous phase larger than the resolution may also be undetected, but only if their size is less than $\sqrt{8}/\pi$ in the case of circular pores (fig. 8g). Note, however, that similar results would be obtained for any shape of porous phase and for state change thresholds of pixels different from 50%.

These measurement errors lead to different results of the analysis of pores as a function of resolution. The influence of image resolution was then observed in reference to the results of pore image analysis performed on samples of both the horizons of Vitulazio and Suelli soils.

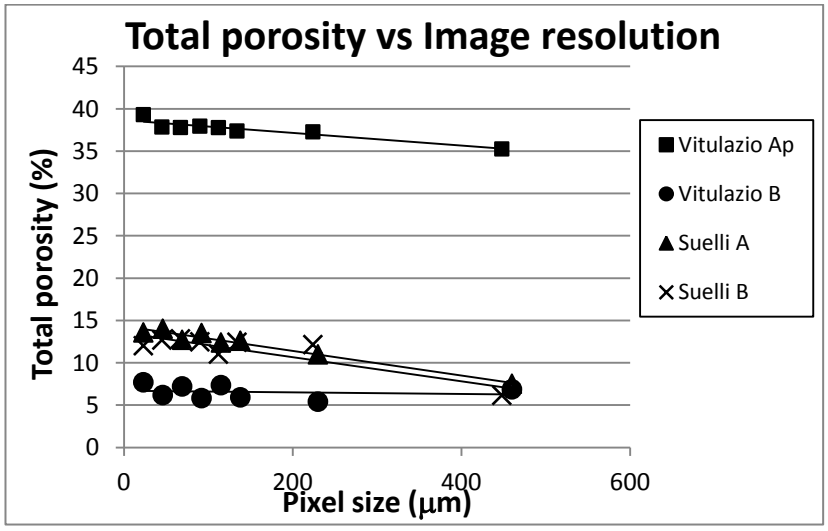

Figure 9. Total porosity values obtained for images (of the four samples analyzed) acquired at 8 different resolution.

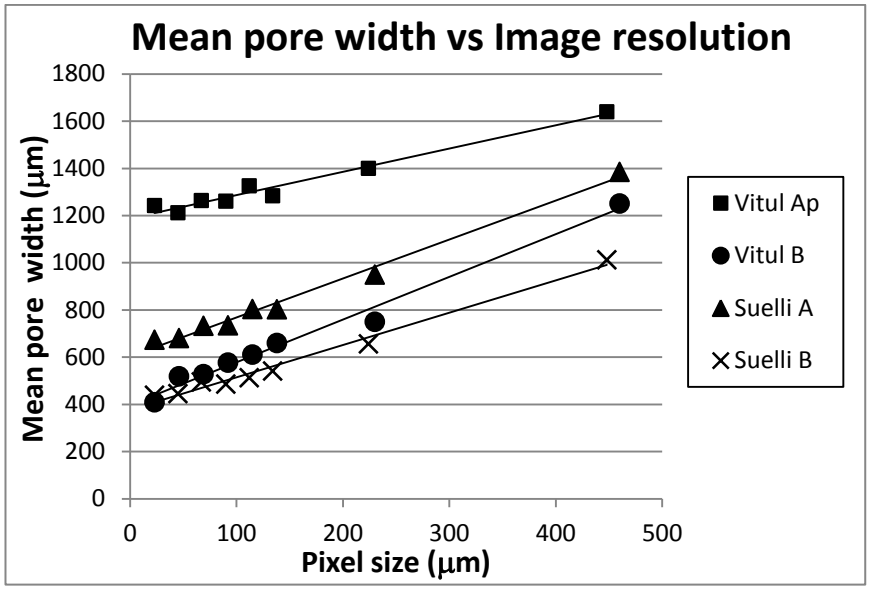

Figure 10 Mean pore width values obtained for images (of the four samples analyzed) acquired at 8 different resolution.

In Fig. 9 and 10 are given respectively the graphs concerning the total porosity and the mean pore width for each resolution; from the data of the different samples it can be seen that as resolution get coarser total porosity decreases while mean width increases, although these trends have some changes in elevation or oscillations depending on the structure of the samples analyzed. Such behaviour can be related both to the fact that as pixel area get coarser (coarser resolution) small pores (which at finer resolution are included in the pore phase) cannot be detected or can be underestimated and also to the fact that large pores can be overestimated, with a consequent increase in mean pore width.

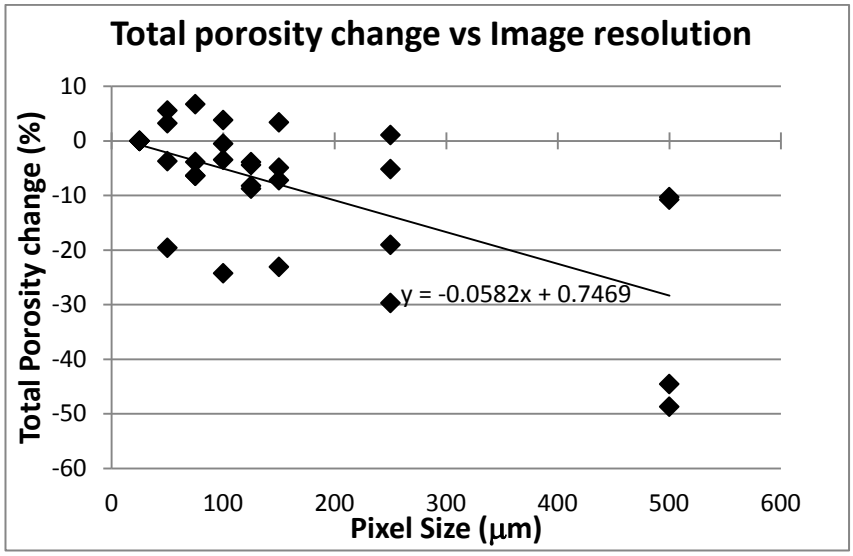

Figure 11. The percentage change in total porosity respect to the value obtained at finer resolution for all four soils samples.

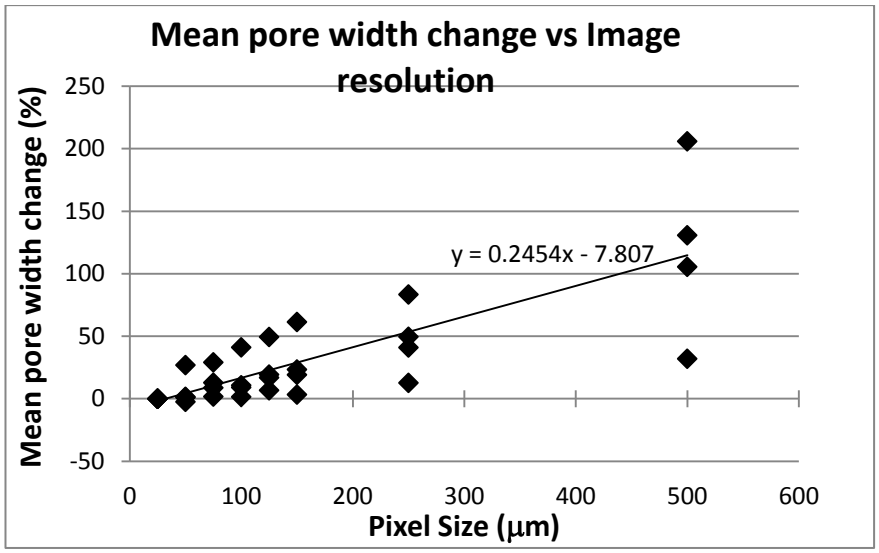

Figure 12. The percentage change in mean pore width respect to the value obtained at finer resolution for all four soils samples.

From the results of all 4 different soils analyzed are realized two graphs (figures 11 and 12) that, for each resolution, showing: a) the percentage change in total porosity respect to the value obtained at finer resolution and b) the percentage change of mean pore width respect to the value obtained at finer resolution. The regression line shown, referring to four soils with very different structures, could be used as a first approximation to estimate the reduction in total porosity and mean pore width

increase, which would be expected for any soil with decreasing of the resolution chosen.

In Fig. A1 of the appendix are given the cumulative pore size distribution for all the samples and all the resolutions.

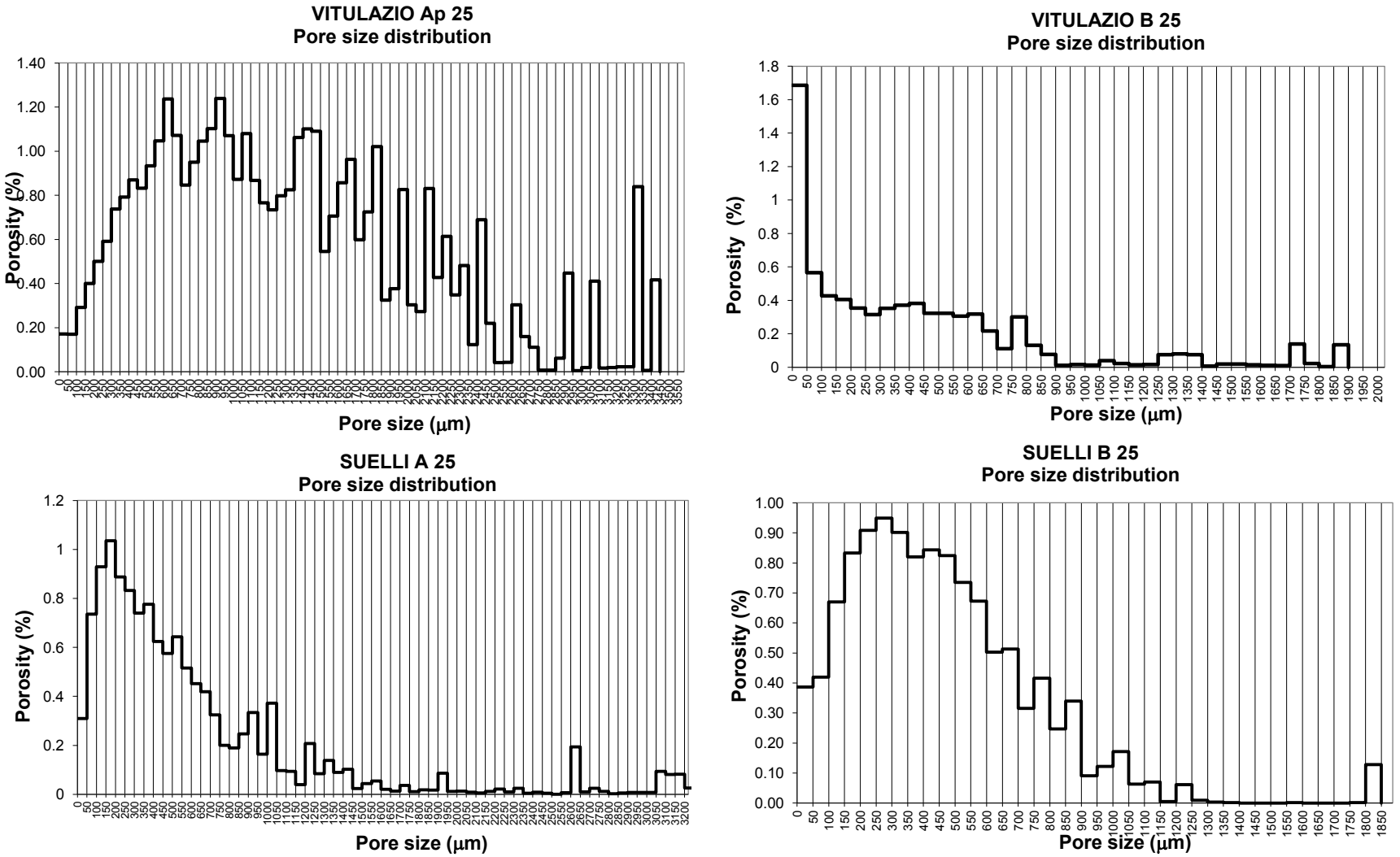

Figure13 Pore size distribution histograms at the maximum chosen resolution (23μm).

The assemblage of the pore size distribution histograms at the maximum chosen resolution (23μm) for each of the samples is given in Fig 13. These PoSDs show that the surface A and Ap horizons have a more complex PoSD of the lower B horizon; this may be related to the influence of the biological activity in the surface horizon. It is also relevant to note that there are very different pattern of multimodal PoSD with a much simpler pattern in the A horizon of Suelli compared with the much more complex PoSD distribution of the Ap of Vitulazio; it is likely that this last behaviour depends from the tillage practices. In the case of Vitulazio soil it can be seen that PoSD is multimodal and it has a very complex pattern for Ap and simpler for the B horizon. Moreover the general shape of the two distribution are very different with an asymmetric bell shape for Ap and an arc of hyperbola for the other horizons ; Ap has pores up to 3,2 mm while B has pores smaller than 1,8 mm.

The pore size distributions for each resolution of the sample of Ap horizon of Vitulazio are reported in fig. 14. The overall data concerning the pore size distribution (PoSD) for each resolution and for each of the other 3 samples are reported in the appendix. In both the samples, moving from 23 μm to coarser resolution, there is a clear averaging effect due to the larger pixel area; this averaging effect, step by step, simplify the distribution in unimodal. To be noticed that due to the pore image analysis procedures the width of the pore size classes increases with the resolution being twice this latter.

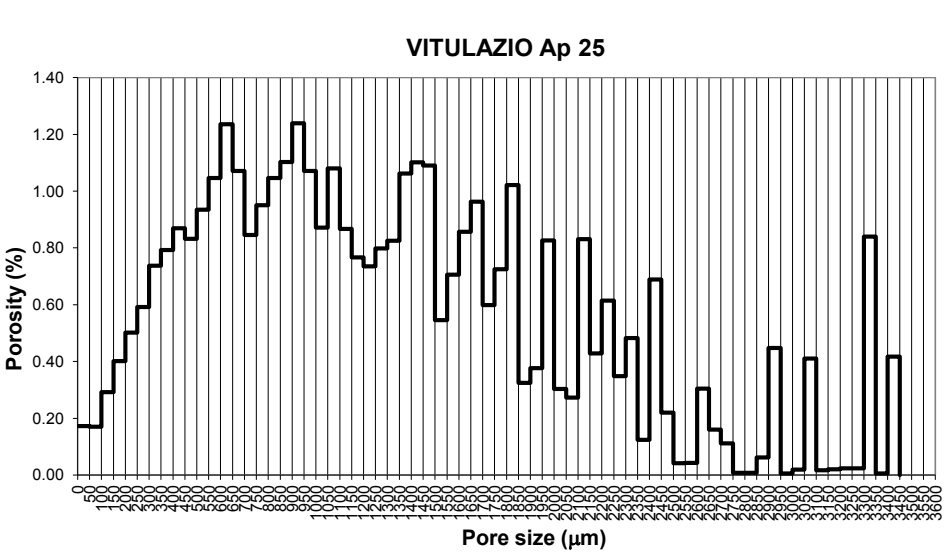
VITULAZIO Ap 25
Porosity (%)
Pore size (μm)

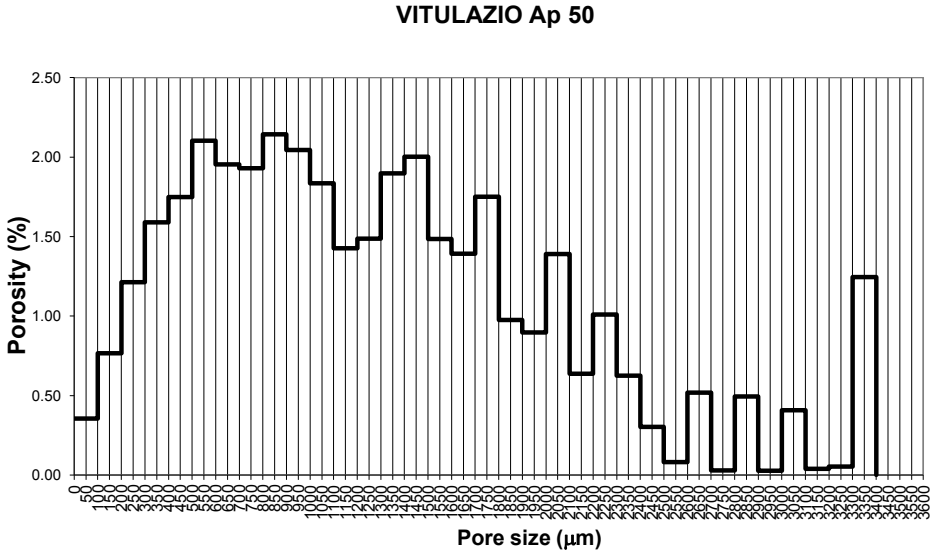
VITULAZIO Ap 50
Porosity (%)
Pore size (μm)

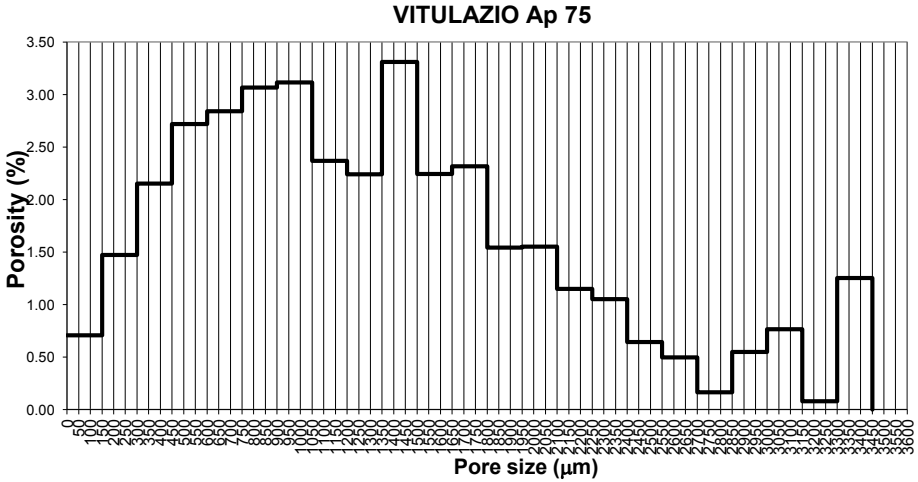
VITULAZIO Ap 75
Porosity (%)
Pore size (μm)

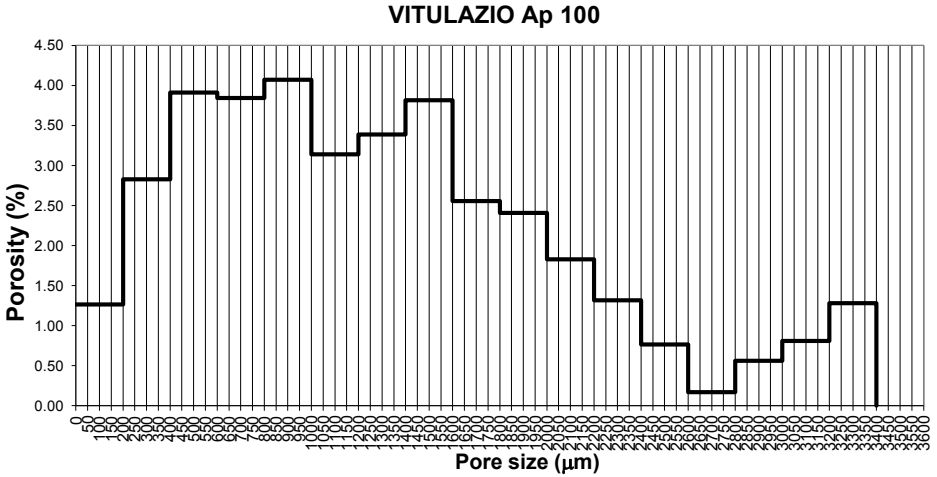
VITULAZIO Ap 100
Porosity (%)
Pore size (μm)

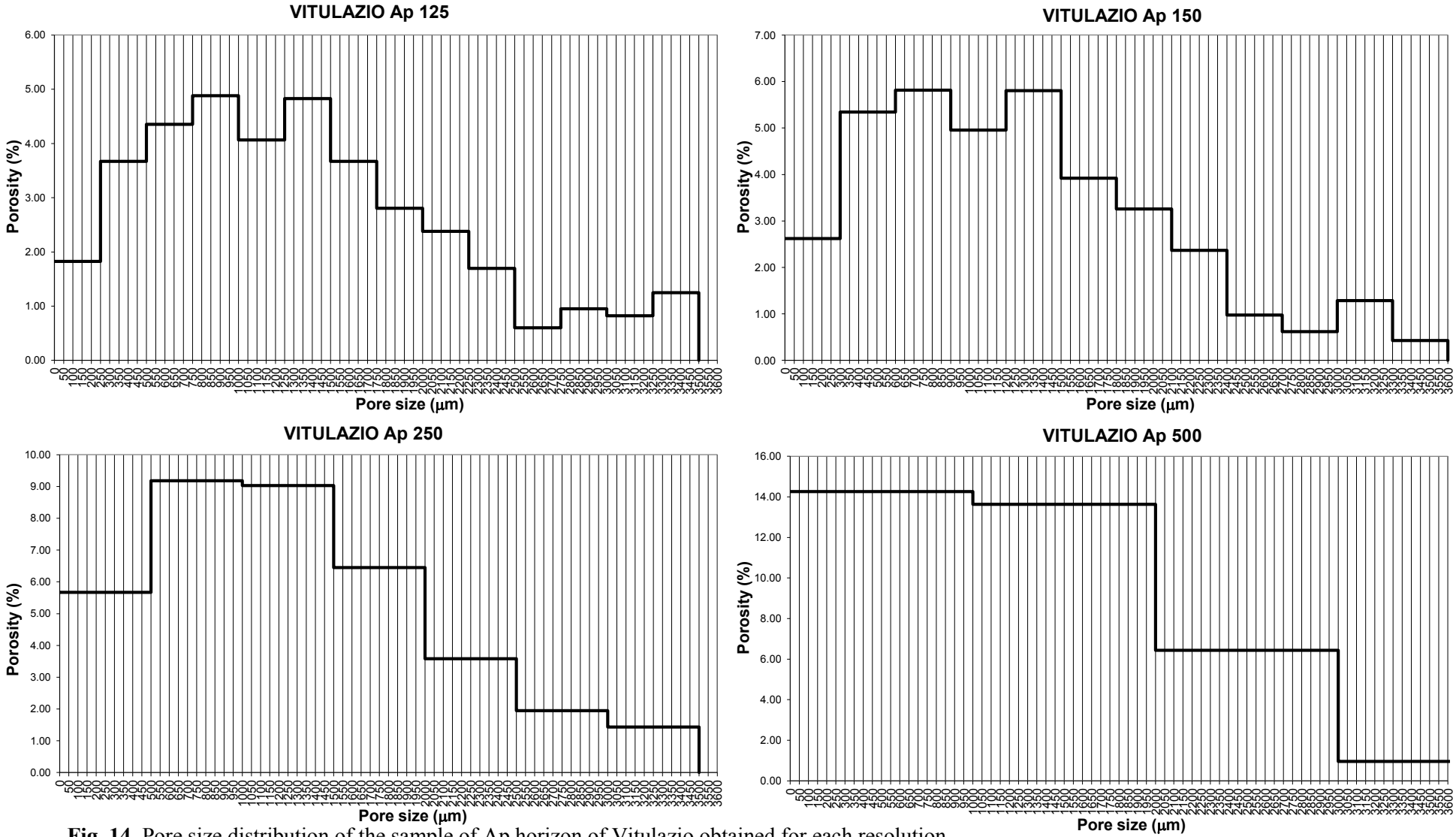

Fig. 14. Pore size distribution of the sample of Ap horizon of Vitulazio obtained for each resolution.

Since the goal is to find the coarser resolution which allows to make a fixed level of error in measuring the porosity, below a method to select the most appropriate resolution is proposed. Assuming that the measurement error of the porosity mainly concerns the porous phase portions closer to the size of the resolution, was calculated the percentage difference between the porosity of the first class of pore size obtained at a given resolution and the cumulative porosity up to the class obtained at finer resolution. The percent porosity changes for each resolution and for each of the 4 samples are given in figures 15.

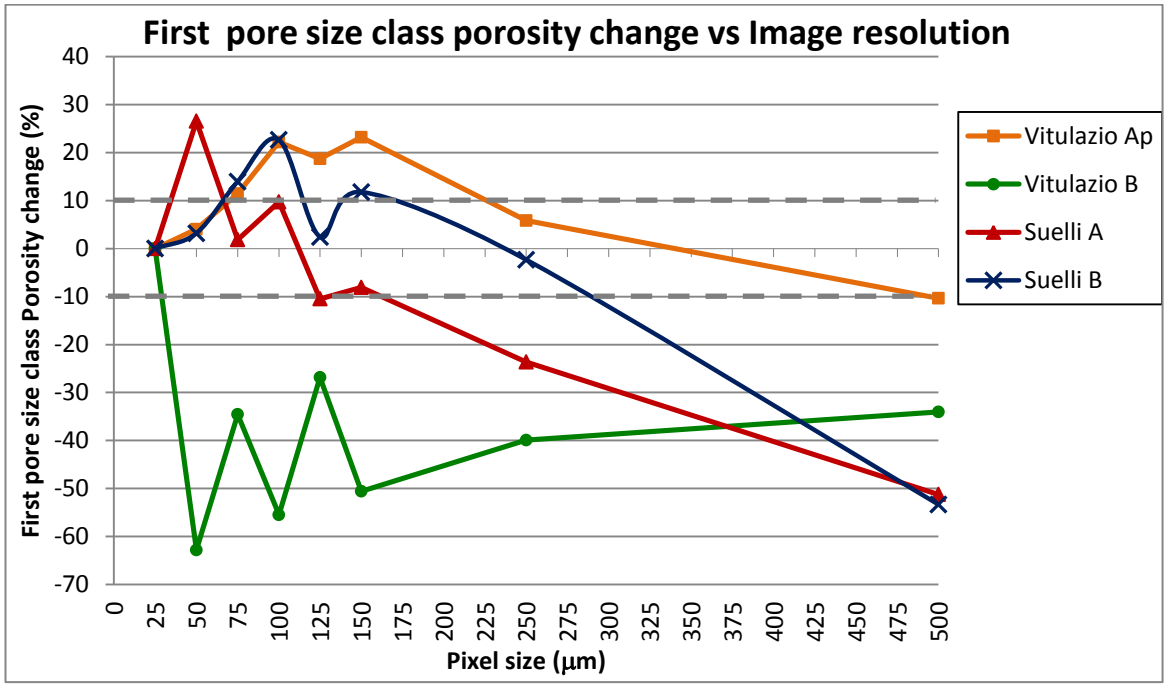

Figure 15. First pore size class porosity change obtained for each sample with the variation of image resolution**.**

The appropriate resolution may be the least able to produce a measurement error for the first class of pore size not greater than a predetermined value. Suppose you want to accept an error of estimate of the pores smaller than 10% compared to the case of finer resolution technically achievable (25 µm in the case of images considered in this work) from figure 13 we observe that the resulting resolutions are 50 µm, 25 µm, 25 µm and 50 µm respectively for the images of samples of Ap horizon of Vitulazio, B horizon of Vitulazio, A horizon of Suelli and B horizon of Suelli.

2.3.4 Effect of pore orientation on total porosity measurement

The results given in Table 1 show that in the Ap horizon the rotation does not affect much the overall analysis giving a standard deviation of 0,11%; such situation is different for the highly oriented B horizon giving a standard deviation of 0.77 %. Regarding to the artificial image the results of the rotation test show that the true porosity value is approachable only when the planar pores are aligned with the elements of the image sensors (90° rotation) giving the highest estimated porosity. Such behaviour is related to the fact that the oriented planar pore, representing a minority phase in the image, is able to produce the largest influence on the final pixel values only when it occupies the larger part of the pixel area which means when it is parallel to the image sensors.

Samples	**Rotation steps**								
	0°	**15°**	**30°**	**45°**	**60°**	**75°**	**90°**	Mean	St. dev.
Ap horizon; Inceptisol	10.44	10.24	10.47	10.52	10.52	10.68	10.51	10.48	0.13
Bss horizon; Vertisol Total porosity (%)	7.63	7.69	7.56	6.05	6.07	6.22	6.42	6.81	0.78
Artificial sample (theorical porosity 11,44) Total porosity (%)	11.42	11.31	11.21	10.94	11.34	11.35	11.44	11.29	0.17

Table 1. Variation in total porosity against rotation steps.

Finally it can be concluded that this preliminary rotation test is an important prerequisite when reliable results have to be produced since it estimates the amount of artefact introduced in the system. It must be emphasised that in many cases, where not highly oriented pores are present, the results show very little change in percent porosity against rotation; this result can be different when dealing with highly oriented pores where it is necessary to estimate whether the artefact introduced is compatible with the analysis.

2.4 Conclusion

In this work an attempt was made to investigate in particular the problems related to the acquisition phase of image analysis in order to provide a contribution to the standardization of this procedure. The results obtained, although still far from providing a standardized procedure may be usefully considered as guidelines or recommendations that should be followed during the acquisition stage of image analysis.

2.5 Appendix

In this appendix are reported the cumulative pore size distribution obtained for the 4 soil samples analyzed and the pore size distributions of the samples of A and B horizons of Suelli soil and of B horizon of Vitulazio soil obtained for each resolution.

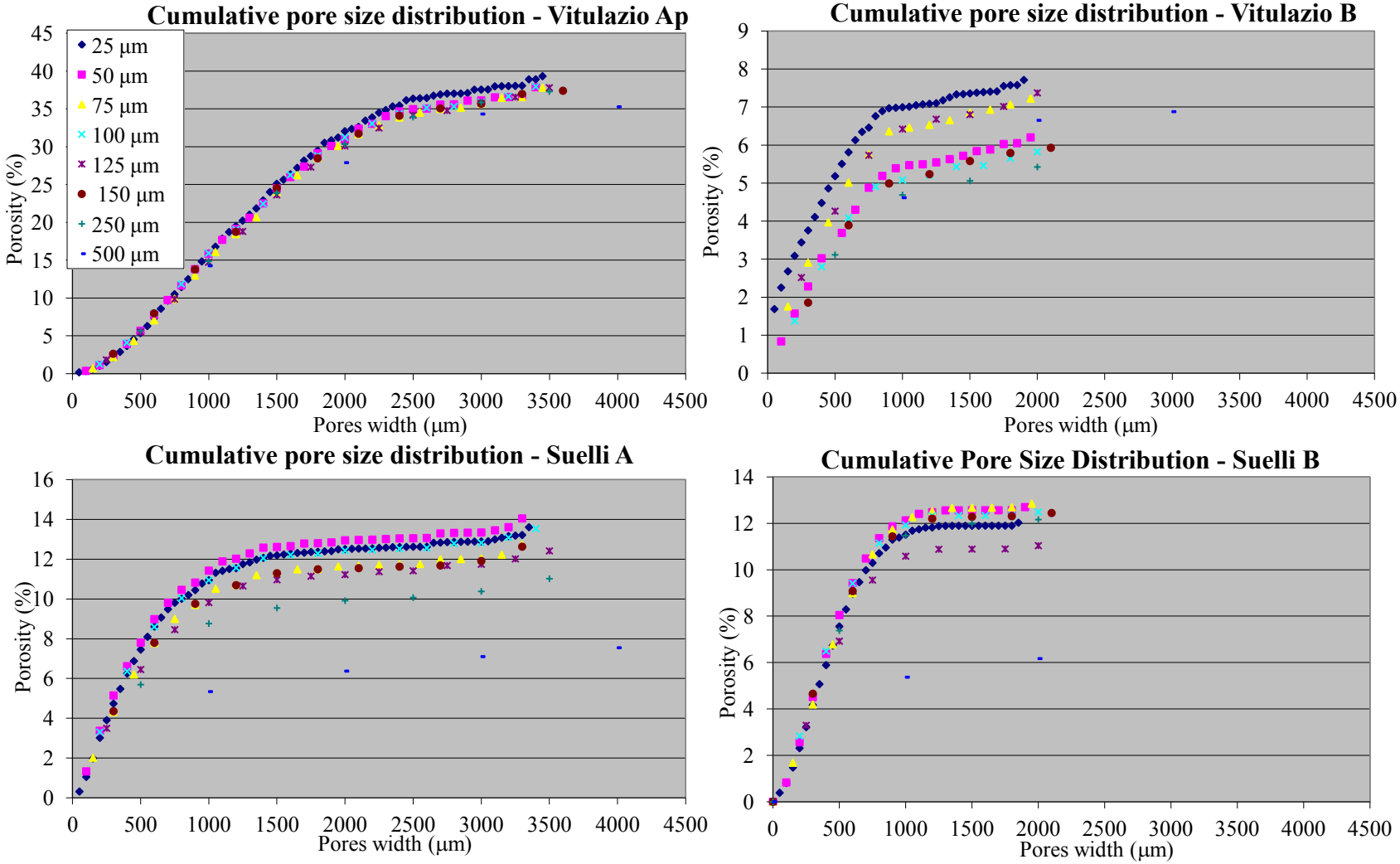

Fig. A1. Cumulative pore size distribution obtained for the 4 soil samples analyzed.

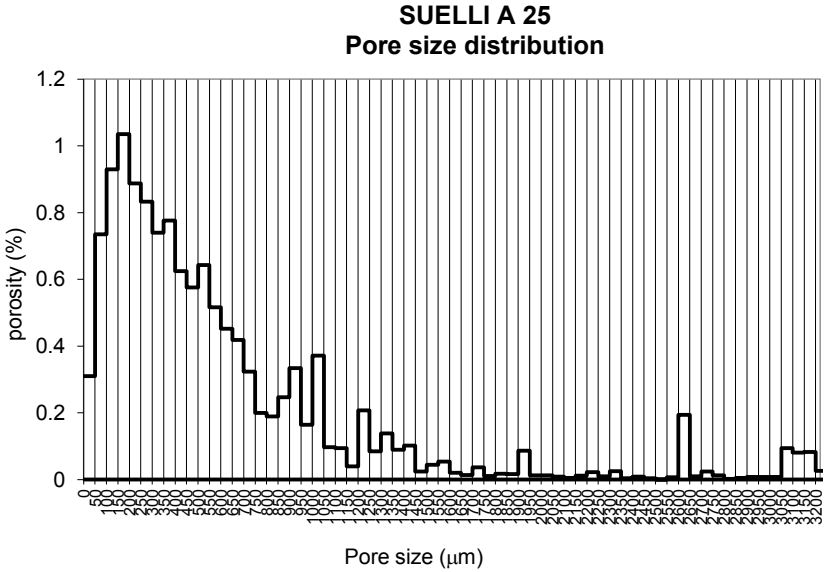
SUELLI A 25
Pore size distribution
porosity (%)
Pore size (μm)

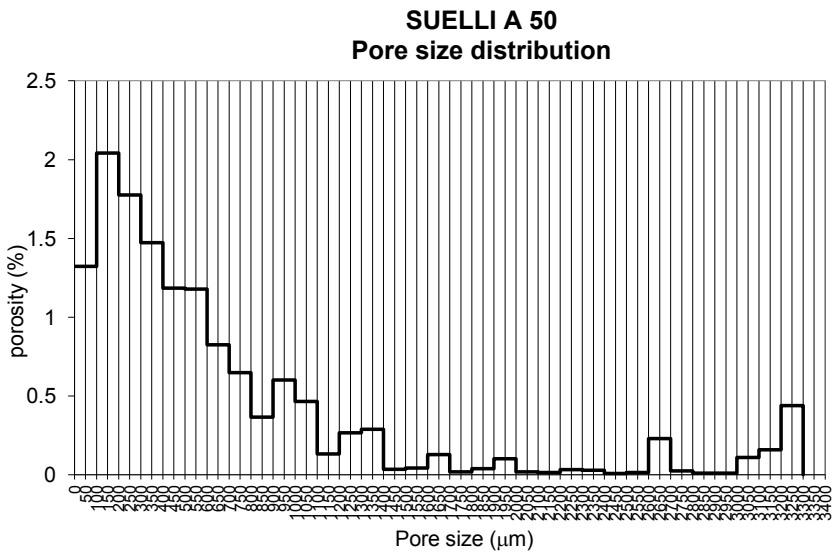
SUELLI A 50
Pore size distribution
porosity (%)
Pore size (μm)

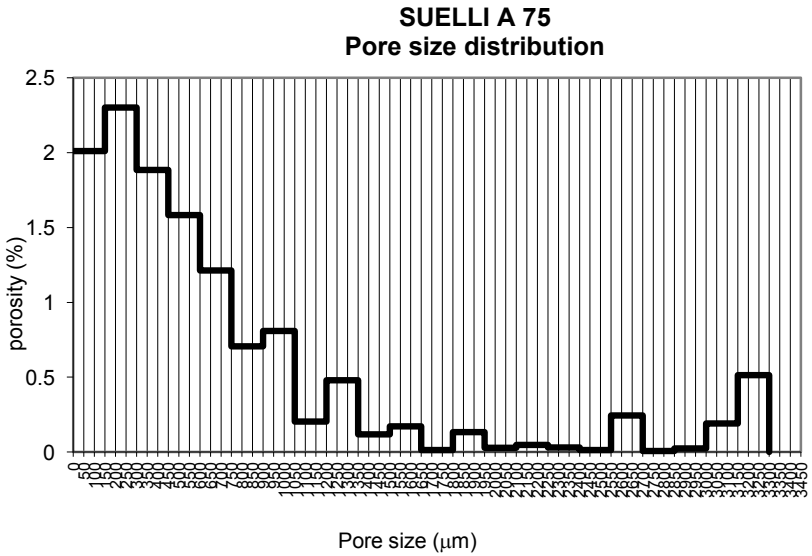
SUELLI A 75
Pore size distribution
porosity (%)
Pore size (μm)

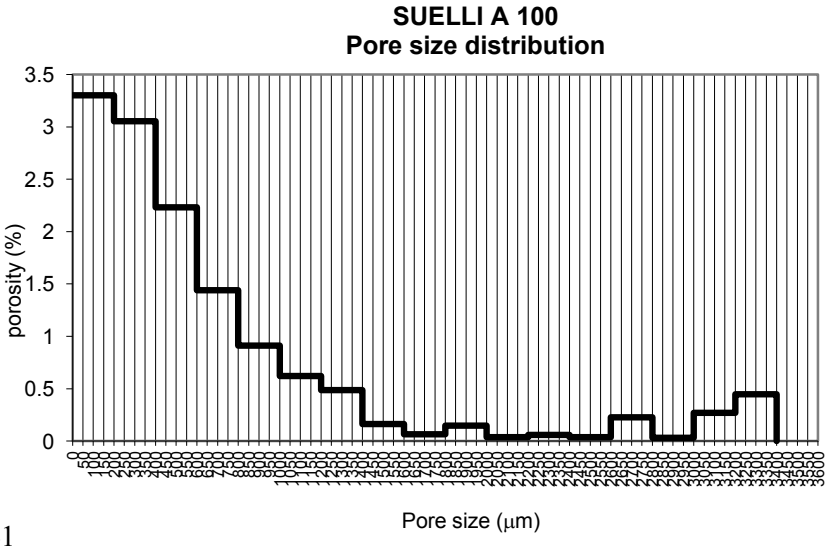
SUELLI A 100
Pore size distribution
porosity (%)
Pore size (μm)

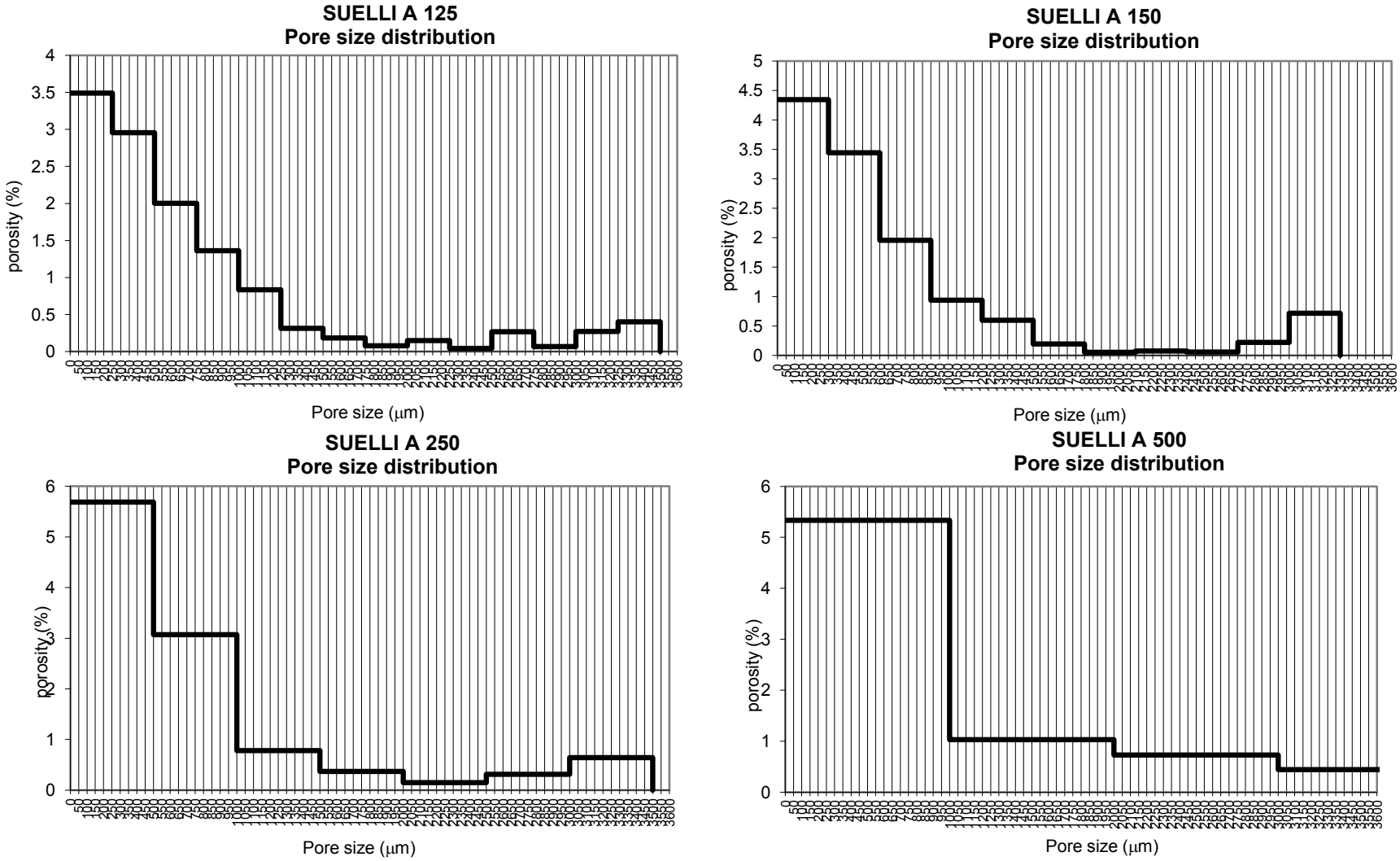

Fig. A2. Pore size distribution of the sample of A horizon of Suelli obtained for each resolution.

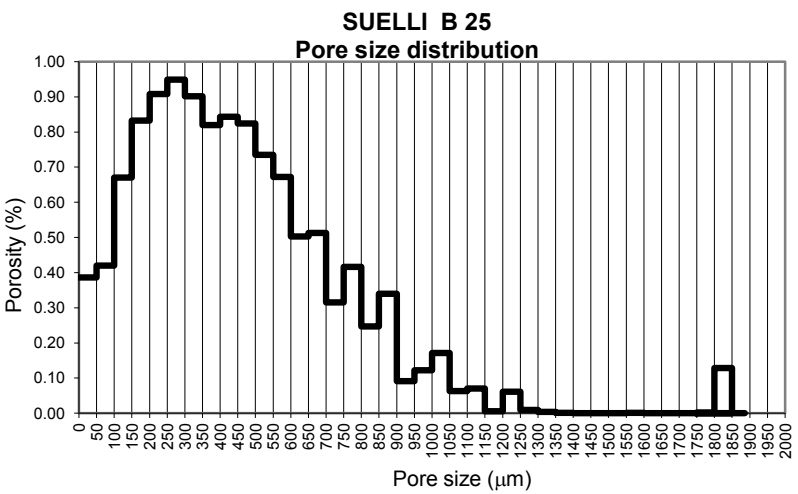
SUELLI B 25
Pore size distribution
Porosity (%)
Pore size (μm)

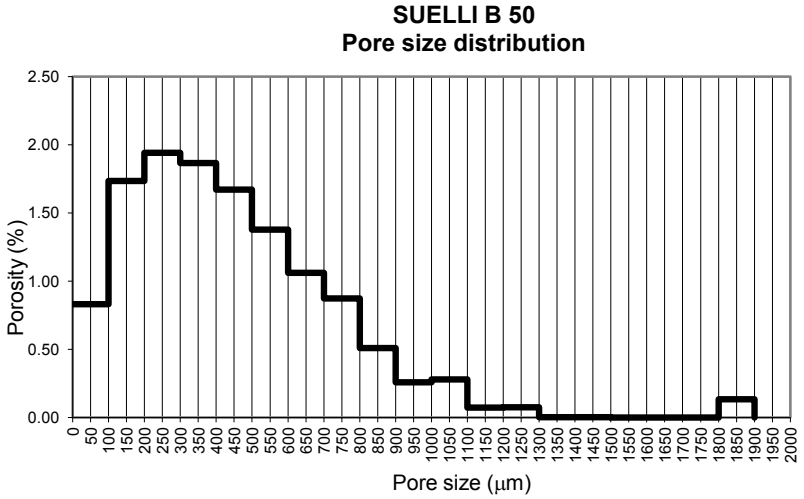
SUELLI B 50
Pore size distribution
Porosity (%)
Pore size (μm)

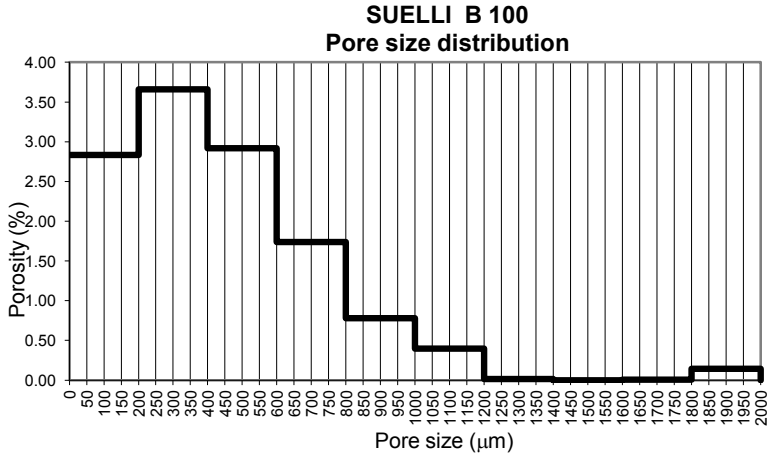
SUELLI B 100
Pore size distribution
Porosity (%)
Pore size (μm)

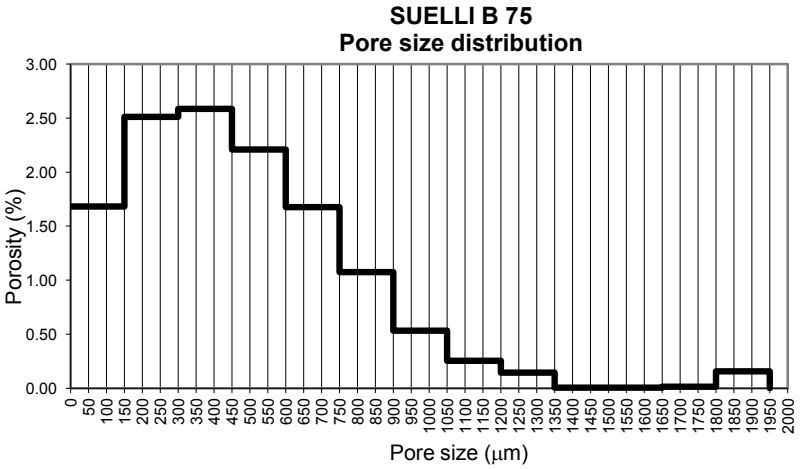
SUELLI B 75
Pore size distribution
Porosity (%)
Pore size (μm)

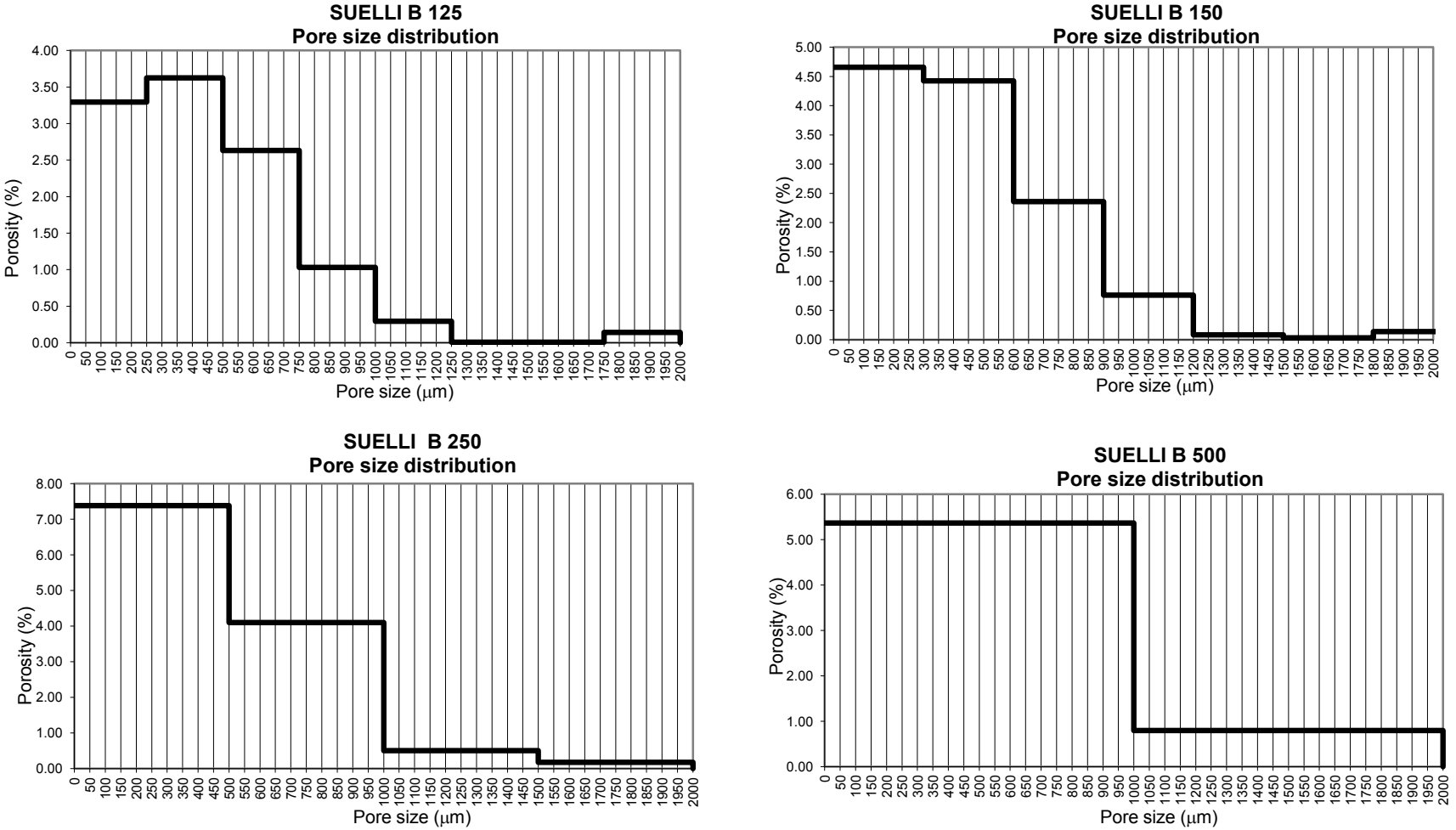

Fig. A3. Pore size distribution of the sample of B horizon of Suelli obtained for each resolution.

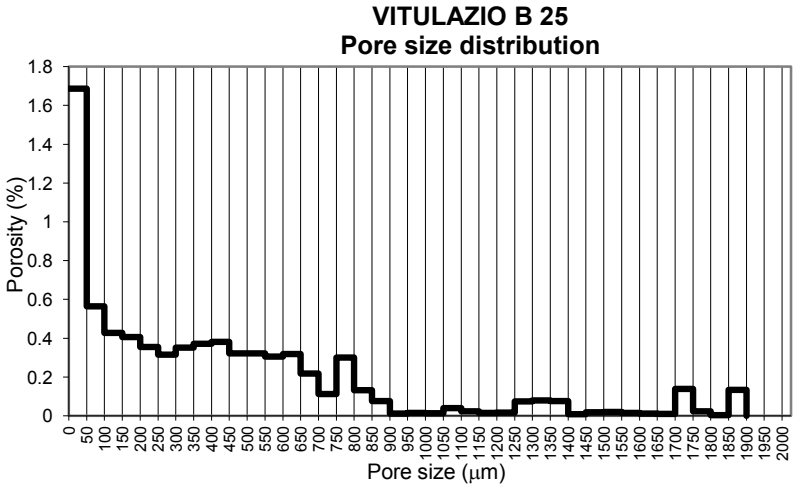
VITULAZIO B 25
Pore size distribution
Porosity (%)
Pore size (μm)

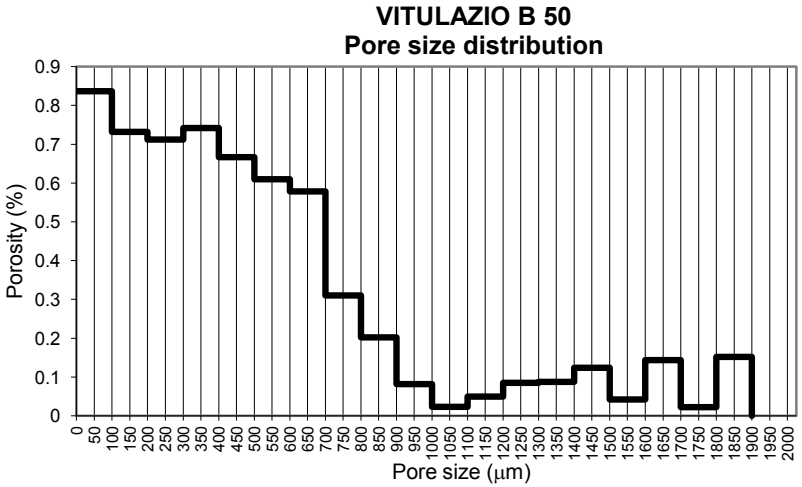
VITULAZIO B 50
Pore size distribution
Porosity (%)
Pore size (μm)

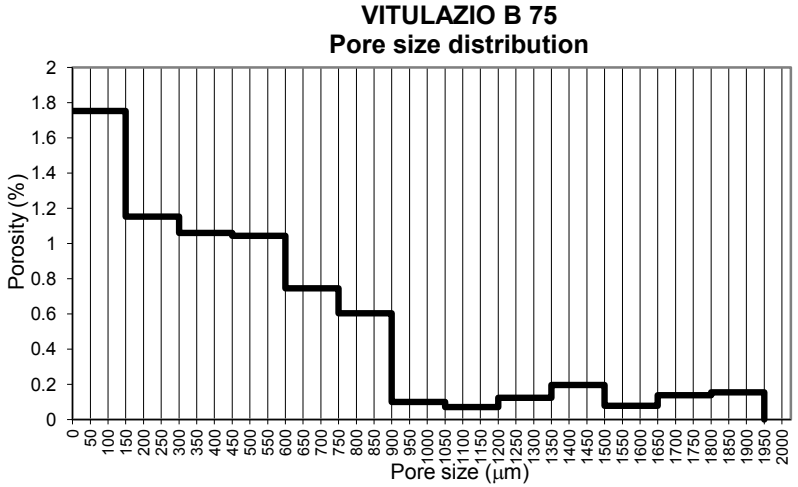
VITULAZIO B 75
Pore size distribution
Porosity (%)
Pore size (μm)

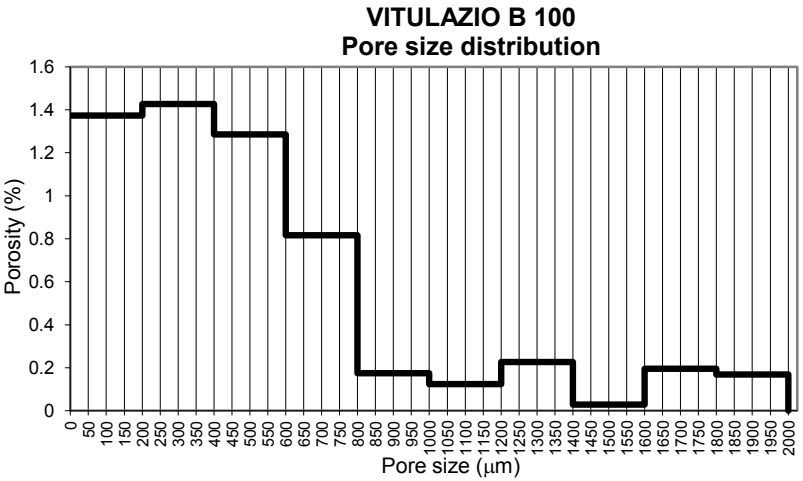
VITULAZIO B 100
Pore size distribution
Porosity (%)
Pore size (μm)

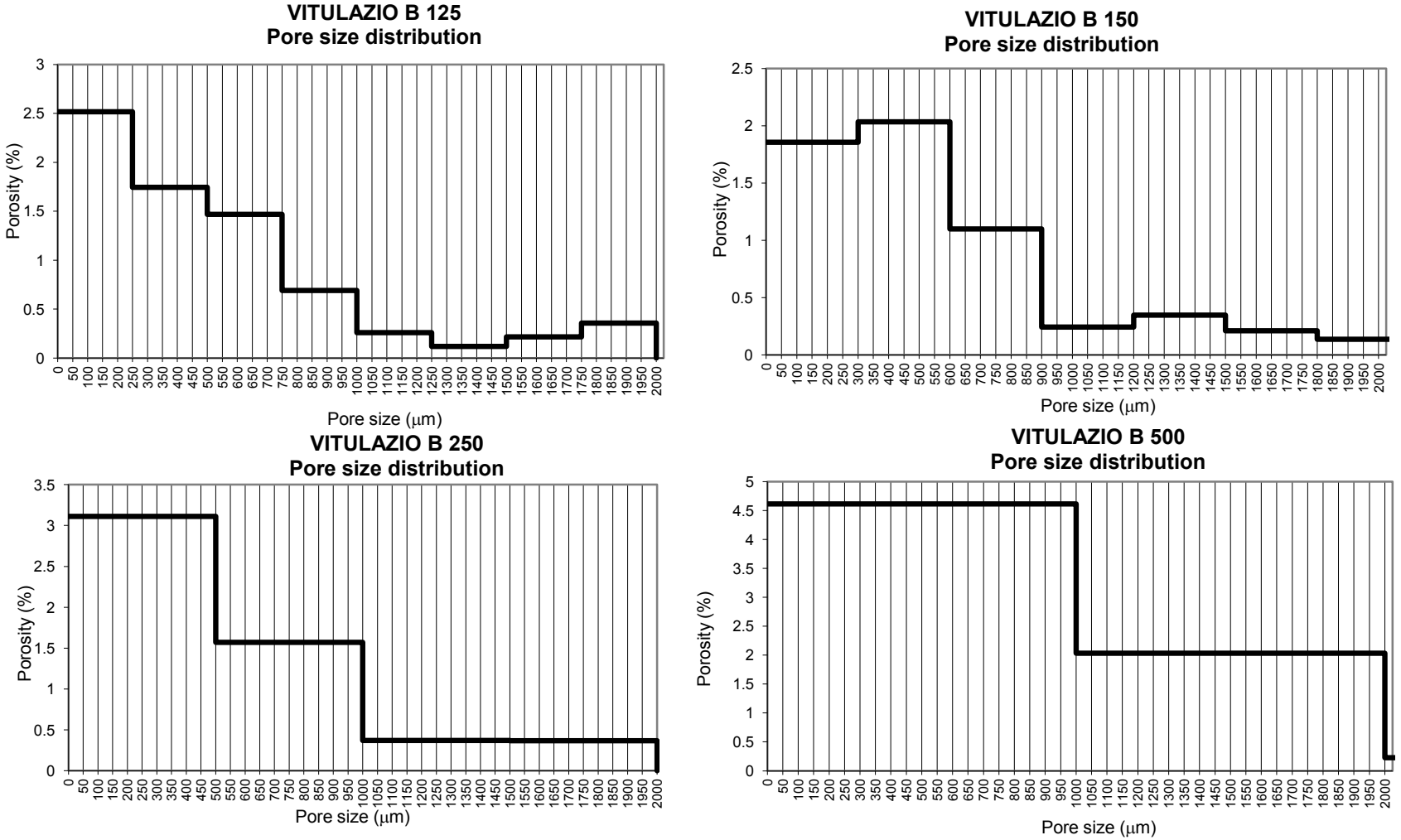

Fig. A4. Pore size distribution the sample of B horizon of Vitulazio obtained for each resolution.

3. Micromorphological study on physical mechanisms of soil pore development: an experiment using iron oxides and calcium carbonate

3.1 Introduction

The fundamental importance of soil structure in the maintenance of healthy terrestrial ecosystems is well known. Indeed soil as environmental compartment has become one of the last frontiers in the study of biodiversity (Sugden *et al.*, 2004). Soil structure is a critical physical property that affects soil ability to sustain plant and animal life and, therefore, is instrumental in maintaining agricultural productivity (Hillel, 1980) as well as local and global environmental quality (Bronick and Lal, 2005).

Soil functions are very much affected by a key feature of the soil structure, namely the pore system and its size distribution (Bouma, 1990; Dexter and Richard, 2009). Pore size distribution (PoSD) strongly affects the content and distribution of both gases and water in soils (Dexter and Richard, 2009; Horn *et al.*, 1994), which, in turn, determine the species and distribution of chemical compounds (e.g., Kuka *et al.*, 2007) as well as soil organisms.

The bulk of scientific research over the last half century has been focused on biological, physical and chemical factors that influence soil structure and their complex interactions (Six *et al.*, 2004). Aggregate stability measurement has been one of the most used approach to evaluate the effect of these factors on the soil structure. While rapid and inexpensive, it is an indirect method of soil structure characterization (Díaz-Zorita *et al.*, 2002) and the use of aggregates as a surrogate of whole soil structure does not allow inference of spatial and functional information (Young *et al.*, 2001). Actually direct investigations of the soil pore system, such as soil image analysis, are available and provide valid tools to analyze both shape and size distribution of pores (Mele *et al.*, 1999; Pagliai and Vignozzi, 2002; Velde, 1999). Unfortunately they are still little used to investigate the role of the numerous factors influencing pore architecture. Among all inorganic agents influencing soil structure, Fe oxides and $CaCO_3$ are especially important in soils due to their

widespread natural occurrence and importance in determining soil structure properties of many types of soil horizons. For example, $CaCO_3$ coatings cement together sand and silt particles during the formation of both calcic and petrocalcic horizons (Gile *et al.*, 1966; Lal, 2006) and cementing coatings of Fe oxides may explain the highly stable granular structure of Oxisol topsoils, which are typically characterised by high porosity and low bulk density (Yerima and Van Ranst , 2005), and the compacted nature of Gleysol subsoils and of petroferric, placic and fragipan horizons (Ajmone Marsan *et al*., 1994).

Several studies have focused on the effect of Fe oxides and $CaCO_3$ on the stability of soil aggregates (e.g.: Boix-Fayos *et al.*, 2001; Colombo and Torrent, 1991; Igwe *et al*., 1999; Wuddivira and Camps-Roach, 2007). Although the importance of these contributions in understanding the role of Fe oxides and $CaCO_3$ in the soil, little is known about the relationship between their spatial distribution at pore scale and the soil pore system development.

With respect to $CaCO_3$, Baghernejad and Dalrymple (1993) showed that this chemical agent can be mobilized in the pore networks as suspension and argued that such physical mechanism plays an important role in the process of structure formation of calcic horizons.

More recently, Falsone et al. (2010) investigated the effect of calcification directly on the soil pore system, analyzing it at a nanometer scale by means of nitrogen adsorption and mercury porosimetry. With regard to the Fe oxides, Taina et al. (2010), by means of micromorphological analysis, have linked the spatial distribution of typical redoximorphic features in a Gleysol with the architecture of the soil pore system.

Much of these work emphasised physical mechanisms of soil structure formation including the role of particle migration/deposition (e.g. micrite coatings, Fe coatings; Mn coatings, etc.).In such framework, our work aims to investigate, through micromorphological analysis, the physical effects of $CaCO_3$ and Fe oxides on the soil pore development. An aggregate stability test was also performed.

Given the complexity of the interactions among the factors that influence soil pore system formation, we chose to perform our work on simplified soil-like systems, prepared adding separately Fe oxides and $CaCO_3$ to three mineral substrates.
We have purposely chosen three mineral substrates (sandy, silty and clayey) having poor ability to develop soil structure and soil pores; thus we avoided swelling clays, soil material rich in organic matter, soil material rich in biota, etc.

3.2 Materials and experimental design

The experiment was performed on three very different mineral materials that in the following sections we have named as sandy, silty and clayey materials. Sandy substrate was obtained from a *Psamment* that had developed over a recent sand dune at Palinuro (Salerno, South Italy, 40°02'18"N - 15°17'33"E). Silty substrate was obtained from an *Orthent* developed over recent alluvial sediments sampled near the dam of the Alento River (Salerno, South Italy, 40 ° 19'34"N - 15 ° 06'08"E). Clayey material was purchased as pure kaolinite from a company that supplies ceramic products (SOKA, France).
The Fe oxides and $CaCO_3$ powders used in the experiment are given in Table 1.

Aggregating agents	Concentration /g kg^{-1}		
Fine Fe oxides (grain size <5 μm)	0.5	5.0	50.0
Coarse Fe oxides (grain size <170-350 μm)	0.2	2.0	20.0
Calcium carbonate (grain size 10 μm)	0.5	5.0	50.0

Table 1 Properties of aggregating agents and employed concentrations.

Iron oxides were of two different grain size classes, coarse (170-350 μm) and fine (mainly < 5 μm but also including a mode in particle size distribution in the range 0,3-0,5 μm), consisting of mixtures of hematite (Sigma-Aldrich Inc.) and goethite (Sigma-Aldrich Inc.). We combined hematite and goethite because of the frequent contemporary presence of these Fe-containing minerals in soils (Schwertmann and Taylor, 1989). Two different (fine and coarse) Fe oxide grain sizes were used in this study in order to simulate separately Fe coatings formation (Imhoff *et al.*, 2002;

Yerima and Van Ranst, 2005) and the presence of already formed Fe concretions (Pawluk and Dumanski, 1973; Schwertmann and Fanning, 1976).

Fine-grain $CaCO_3$ (about 10 μm; Sigma-Aldrich Inc.) powder was used in order to obtain a near-colloidal suspension of micrite crystals resembling natural carbonate in many illuvial calcic horizons (Lal, 2006).

Each factor was dry-mixed at three different concentrations (Table 1) with all substrates. The concentrations (ranging over three orders of magnitude) were selected based on a review of related literature (Muneer and Oades, 1989; Rhoton *et al.*, 2003; Schwertmann and Taylor, 1989). Six replicate polypropylene pots (6.0 cm high x 6.5 cm in diameter) for each study case and six untreated control pots for each mineral material were prepared. In order to induce soil structure development the 180 samples were put in a tank and subjected to nine wetting/drying (W/D) cycles, consisting of a wetting phase of 24 hours at 25 °C and drying phase of 40 °C for 4 days. Sample dry weight returned to the initial value after the 4 days drying period. Minimum and maximum moisture ratio values for the silty and clayey substrates are shown in Fig. 2.

In order to avoid possible soil structure artefacts induced by drop impact or runoff, wetting (with deionized water) was performed via capillary action from the bottom of the container. Nine cycles were used based on previous research that indicated stabilization of the pore size distribution after four cycles in clay loam and sandy loam soils (Gargiulo, 2008).

3.3 Methods

3.3.1 Substrate characterization

Prior to the analysis and experiment, all three materials were dried at 40 °C for 72 hours and sieved to 2 mm. Substrates were analyzed for grain size distribution (GSD) by sieving a humid sample, for the fractions between 0.2 and 2 mm, and by sedimentation (pipette method) (Day, 1965), using Stockes law, for <0.2 mm fractions.

Soil chemical analyses were completed by following standard methods. Soil pH was determined potentiometrically with a pHmeter (10pH/ISE, Beckman) in soil: water

suspensions (ratio of 1:2.5) (Peech, 1965). Organic carbon content was determined with the Walkley and Black (1934) method, by means of organic matter oxidation with potassium bichromate, in the presence of sulfuric acid. Electrical conductivity was measured in soil:water suspensions (ratio of 1:5) using a conductivity meter (microCM 2201,CRISON) (Rhoades, 1996). Total carbonates were determined using a Dietrich-Fruehling calcimeter (Loeppert and Suarez, 1996); cation exchange capacity (CEC) was determined with $BaCl_2$ (Summer and Miller, 1996).

Mineralogical analysis was performed by X-ray diffraction (XRD) (Wilson, 1987). Samples were dispersed and separated into different grain size classes through sieving to obtain sand (50 μm - 2 mm), and centrifuged to obtain clay (<2 μm). The clay was saturated with $CaCl_2$ and washed with water and acetone to remove chloride. Spectra were determined using a Rigaku Geigerflex D / Max IIIC diffractometer with CuKa radiation and a Ni filter, at 40 kW and 25 mA. Oriented clay samples solvated in ethylene glycol were analyzed to identify expandable secondary minerals. Powder samples from the sand fraction were analyzed randomly in order to define the primary mineral components.

Soil plasticity was also measured on thoroughly puddled samples of the three substrates at a water content where maximum plasticity is expressed, according to the field method described in the Soil survey manual (Soil Survey Division Staff, 1993).

The shrinkage dynamics of the three substrates were investigated using the method of Tariq and Durnford (1993) to obtain the shrinkage characteristic curves (Groenevelt and Grant, 2004).

3.3.2 Two-dimensional image analysis

A mixture of acetone and polyester resin (Crystic 17449, Scott-Bader Ltd.) was added with fluorescent dye (Uvitex OB, Ciba Ltd.), having a spectral emission in the blue band under UV illumination (365 nm). Three of the six replicates from each treatment were saturated with that mixture under a moderate vacuum. This procedure yielded a low viscosity mixture for optimal resin penetration into the pore networks (Fitzpatrick, 1993). After resin polymerization, the substrate blocks were cut into regular parallelepipeds. Digital images (10 μm pixel resolution) of the four vertical

sections (3 x 5 cm) were acquired under UV illumination. A Nikon D200 camera was used, controlled by a PC using Nikon Capture 4.1 software. To merge the variability of the three replicates in each treatment, four images of each sample were placed side by side to obtain a single large 2D image (36 x 5 cm) consisting of all twelve vertical sections of the treatment (Fig. 1).

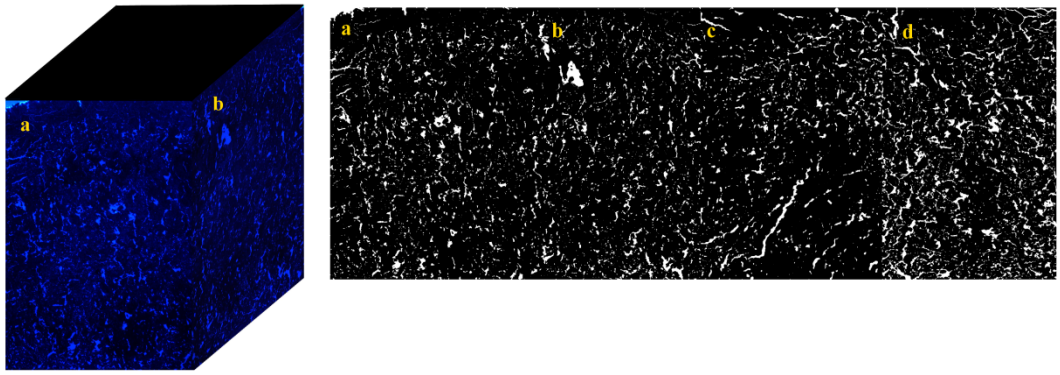

Figure 1 Vertical sections of soil blocks under UV light and the correspondent binary image that was analyzed.

Images were pre-processed and segmented using a technique of supervised "thresholding" using Corel Photo-Paint X3, in order to obtain binary images where the two separate solid and pore phases are in black and white, respectively.
Image analysis was performed using Solicon - PC Version 1.0 software (Cattle *et al.*, 2000) to determine total porosity. Pore size distribution was determined by image analysis using Micromorph 1.4 (TRANSVALOR 2000), through the application of the "opening" algorithm (Horgan, 1998; Serra, 1982), which classifies the pore phase according to the spacing from the walls.

3.3.3 Micromorphological analysis

After acquisition of digital images, each substrate block was used to prepare one thin section (Fitzpatrick, 1993) which was analyzed by optical microscopy using transmitted light (TL), cross polarized light (XPL) and incident light (IL) to identify the different micromorphological features. Micromorphological analysis was performed to detect features relevant for understanding the influence of Fe oxides and $CaCO_3$ on pore development. Such features were described following FitzPatrick

(1993). In particular, the degree of accordance was employed as a useful parameter to describe the association between concretions and pores development. Such parameter classifies opposing surfaces of soil features on the basis of the percentage of their similar outlines (Fitzpatrick, 1993). The provided classes are: <5% (not-accordant), 5-25% (weakly accordant), 25-50% (moderately accordant), 50-75% (strongly accordant) and >75% (very strongly accordant).

The proportion of all micromorphological features of interest was estimated by the point counting technique (McKeague *et al*., 1980). A minimum of 3000 points (1000 per thin section) were counted for each feature, in order to obtain the percentage of the solid phase area represented by that feature. Standard error *e* was calculated according to the following formula (Murphy, 1983):

$$e = \left[\left(\frac{N-F}{N}\right)\left(\frac{F}{N}\right)\left(\frac{1}{N-1}\right)\right]^{1/2} \quad (2)$$

Where N is the total number of points counted (3000) and F is the total number of points counted as a micromorphological feature.

3.3.4 Aggregate stability

The effect of Fe oxides and $CaCO_3$ on aggregate stability was determined by comparing the mean-weight diameter (MWD) of water-stable aggregates in the control and the treated samples (Kemper and Rosenau, 1986). Twenty grams of the <2 mm oven-dried material were placed in the upper sieve of a stack of three (1.00, 0.50 and 0.25 mm mesh size) and pre-soaked in distilled water for 30 min. The nest of sieves was oscillated vertically in water 20 times using an amplitude of 4 cm at a rate of one oscillation per second. After wet-sieving, the resistant materials on each sieve and the unstable (<0.25 mm) aggregates were transferred into beakers, dried at 50 °C for 48 hours and weighed. Mean-weight diameter (MWD) of water-stable aggregates was calculated as

$$MWD = \sum_{i=1}^{n} X_i W_i \quad (1)$$

Where X_i is the mean diameter of the *i*th sieve size and W_i is the proportion of the total aggregates in the *i*th fraction. Higher values indicated the predominance of large and stable aggregates in the analyzed samples.

3.4 Results

Results presented here focus on the highest concentrations tested for each aggregating substance (fine Fe oxides, coarse Fe oxides, $CaCO_3$). However, results obtained at lower concentrations confirmed trends observed at highest ones.

3.4.1 Substrate characterization

The main properties of the three materials are given in Table 2.

Material	GSD[a]			pH (H_2O)	EC[b] ($\mu S\ cm^{-1}$)	OC[c] ($g\ Kg^{-1}$)	Total carbonate ($g\ Kg^{-1}$)	CEC[d] ($cmol(+)\ Kg^{-1}$)
	Sand (%)	Silt (%)	Clay (%)					
Sandy	95	3	2	8.7	71	1.3	79.4	1.3
Silty	21	59	20	7.7	382	7.4	102.3	9.8
Clayey	4	49	47	8.6	273	0.4	1.9	3

[a] Grain size distribution obtained by sieve method.
[b] electrical conductivity.
[c] organic carbon.
[d] cation exchange capacity.
Table 2. Properties of the mineral materials.

The actual grain size classes of sandy, silty and clayey materials were, respectively, sandy, silty loam and silty clay. Sandy and clayey substrates were strongly alkaline while the silty material was slightly alkaline. All three substrates were nonsaline. The organic carbon concentration was low in all three substrates. The clayey material was poorly calcareous, with a low carbonate concentration (1.9 g kg^{-1}), while the carbonate levels in the sandy and silty substrates were much higher (79.4 g kg^{-1} and 102.3 g kg^{-1}, respectively), corresponding to classifications of moderately calcareous and calcareous, respectively. Although this variability in carbonate concentrations was not planned, it was a consequence of selecting two natural soils for study. The CECs of the sandy and clayey material were very low (1.3 and 3 cmol(+) Kg^{-1}, respectively); the CEC of the silty substrate was moderate (9.8 cmol(+) Kg^{-1}). Not surprisingly, the clayey material was identified as pure kaolinite (peaks at 0.71 nm

and 0.38 nm corresponding to d(001) and d(002) reflections). Three clay minerals were identified in the silty substrate: interstratified kaolinite – smectite (peaks at 0.83 nm and 1.78 nm after ethylene glycol treatment), kaolinite (peaks at 0.71 nm and 0.38 nm corresponding to d(001) and d(002) reflections) and illite (peaks at 0.99 nm, 0.51 nm and 0.33 nm corresponding to d(001), d(002) and d(003) reflections). Quartz (peaks at 0.43 nm and 0.33 nm), calcite (peak at 0.30 nm) and albite (peak at 0.32 nm) were identified in the sandy material.

The sandy material was not-plastic, the silty substrate slightly plastic and the clayey material very plastic.

In fig. 2 the shrinkage characteristic curves of clayey and silty materials are shown.

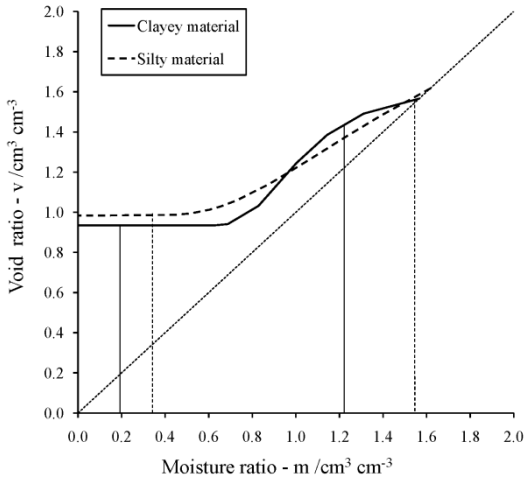

Figure 2 Shrinkage curves of clay and silty materials. Vertical solid (for clayey material) and dotted (for silty material) lines indicate minimum and maximum moisture ratio values achieved during the W/D cycles.

Though tested, the sandy material did not produce a consistent shrinkage curve because of its very limited shrink dynamics. During the drying process the clayey material exhibited a reduction of void ratio as high as that of the moisture ratio (slope = 1). This change implies that, as the sample loses water, the pore volume simultaneously diminishes, which suggests no entry of air into the pore network during drying. The shrinkage curve of the silty material showed a shallower slope across the entire shrinkage range. The resulting slope value <1 implies a lower reduction of the void ratio at a given moisture ratio reduction, thus the shrinkage process is always accompanied by air entry in pores.

Clayey and silty substrate showed similar void ratio range during the shrinkage process, notwithstanding kaolinite is less expandable than smectite and illite present in the silty material. This is clearly a consequence of the purity of the clayey substrate.

3.4.2 Two-dimensional image analysis

In fig. 3 total porosity values and the pore size distributions (PoSD) of treated and control samples of sandy, silty and clayey materials are reported; also differences in percent with respect to total porosity of the controls are drawn. In the graphs the amount of each pore size class is expressed as percentage of the total surface of the analyzed sample. Since images were acquired at pixel resolution of 10 μm, the values for total porosity refer to all pores larger than 10 μm. The identified PoSD classes have an interval of 20 μm because of the iterative application of the "opening" algorithm with circular "structuring elements" having diameter which increases two pixels per step.

Regardless of the treatments, total porosity was highest in the sandy material, while silty and clayey substrates porosities were similar and lower (Fig. 3). PoSDs showed the presence of pores having width till 800 μm, even if most of pores varied in the range 100-300 μm.

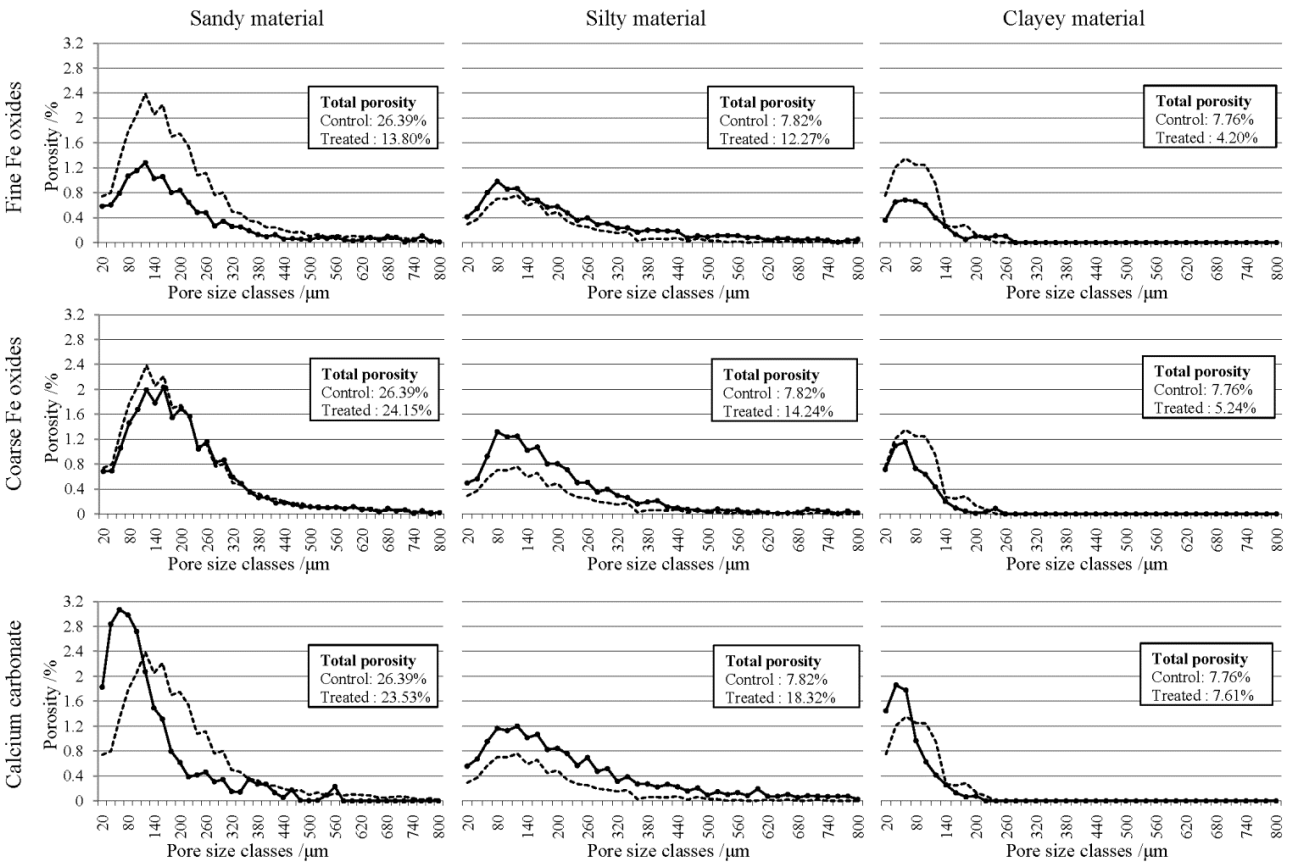

Figure 3 Pore size distribution (PoSD) of control and treated samples (left vertical axis) and percent difference between them (right vertical axis). Total porosity includes only >10 µm pores.

3.4.2.1 Fine Fe oxides (grain size <5 μm)

The application of fine Fe oxides in sandy material resulted in a decrease in total porosity relative to the control from 26.4% to 13.8% (Fig. 3). This reduction in porosity occurred in all pore size classes smaller than 500 μm, but was especially important in the 100-300 μm range where the decrease in porosity was at least 50% for each of the pore classes. Fine Fe oxides applied to silty material caused an increase in total porosity from 7.8% (control) to 12.3%; the increase occurred in all pore size classes. Porosity decreased from 8.7% in the control to 4.2% in the fine Fe oxide-treated clayey samples. There was a substantial decrease of pores <220 μm, and a moderate increase of pore size classes in the 220 – 300 μm range.

3.4.2.2 Coarse Fe oxides (grain size 170-350 μm)

The application of coarse Fe oxides produced a small decrease of total porosity in sandy material (26.4% in the control to 24.1% in the treated sample). This reduction of approximately 10% occurred in the <220 μm pore size classes (Fig. 3). In silty substrate there was a substantial increase in porosity (7.8% to 14.2%) upon coarse Fe oxide treatment, a change that occurred primarily in <420 μm pores. Total porosity was reduced in clayey material from 7.8% in the control to 5.2% in the treated samples, with the decrease occurring mainly in the 60-120 μm pore size classes. Formation of new macropores (220 μm) was observed in the treated samples.

3.4.2.3 Calcium carbonate (grain size 10 μm)

The application of $CaCO_3$ to the sandy material produced a slight decrease in total porosity (26.4% in the control and about 23.5% in the treated samples). PoSD showed that the overall reduction in porosity was a result of the combined effect of a decrease in the larger pore size classes (>120 μm) and an increase in the smaller pore size classes (<120 μm). Calcium carbonate in silty material caused an increase of total porosity from 7.8% to 18.3% across all pore size classes (Fig. 3). The effect of $CaCO_3$ on porosity in clayey substrate was negligible (7.8% to 7.6%). A slight reduction occurred in all pore sizes >70 μm, with an increase in pores <70 μm in size.

3.4.3 Micromorphological analysis

Among the micromorphological features found in the treated samples, the following were selected as they resulted the most important in explaining mechanisms of soil structure formation and soil pore development:

1) Fe coatings. They partially-occluded pore spaces between grains in the sandy material (see Fig. 4a) or aggregates in the other substrates (see Fig. 4b).
2) Fe concretions inducing pore development. They were those observed in pores having walls strongly accordant with the outline of Fe concretions (Fig. 5a). Because mineral substrates and Fe concretions react differently when shrinking and swelling during the W/D cycles, the presence of those strongly accordant surfaces demostrate the connection between that Fe concretions and the formation of the surrounding pore. These Fe concretion were furtherly classified in those originating or not planar pore formation (see Fig. 5b, 5a).
3) Fe concretions not inducing pore development. They were distributed among the sand grains and occurred in pores with not-accordant surfaces in silty and clayey materials. Their main effect was pore filling (an example in Fig. 5c).
4) Micrite coatings. They are microcrystalline calcium carbonate deposits covering pore walls in all three mineral materials (Fig. 6a) and having stabilizing effect.
5) Micrite segregations. They were localized in pores and formed bridges between sand grains (Fig. 6b) and between silty and clayey aggregates (Fig. 6c). Their main effect was pore space fragmentation.

The results of the point counting of the above micromorphological features are reported as the percent of the solid phase area of the analyzed thin sections (Table 3). Standard errors were always <0.009, and are therefore not included in the table.

Aggregating agents	Materials	Fe coatings (%)	Fe concretions inducing pores development (strongly accordant surfaces)		Fe concretions not inducing pores development (not accordant surfaces) (%)	Micrite coatings (%)	Micrite segregations in pores (%)
			with planar pore (%)	without planar pore (%)			
Fine Fe oxides	Sandy	19.9			3.1		
	Silty	10.1	0.3	1.5	0.5		
	Clayey	18.1	0	0.3	0.1		
Coarse Fe oxides	Sandy				2.7		
	Silty		1.8	0.5	0.9		
	Clayey		0.2	1.9	1.1		
Calcium carbonate	Sandy					1.7	16.6
	Silty					3.6	1.5
	Clayey					0.8	6.0

Table 3. Frequencies (%) of micromorphological features expressed in percent area of the solid phase.

3.4.3.1 Fine Fe oxides (grain size <5 µm)

The treatment of sandy material resulted in 19.9% Fe coatings (Fig. 4a).

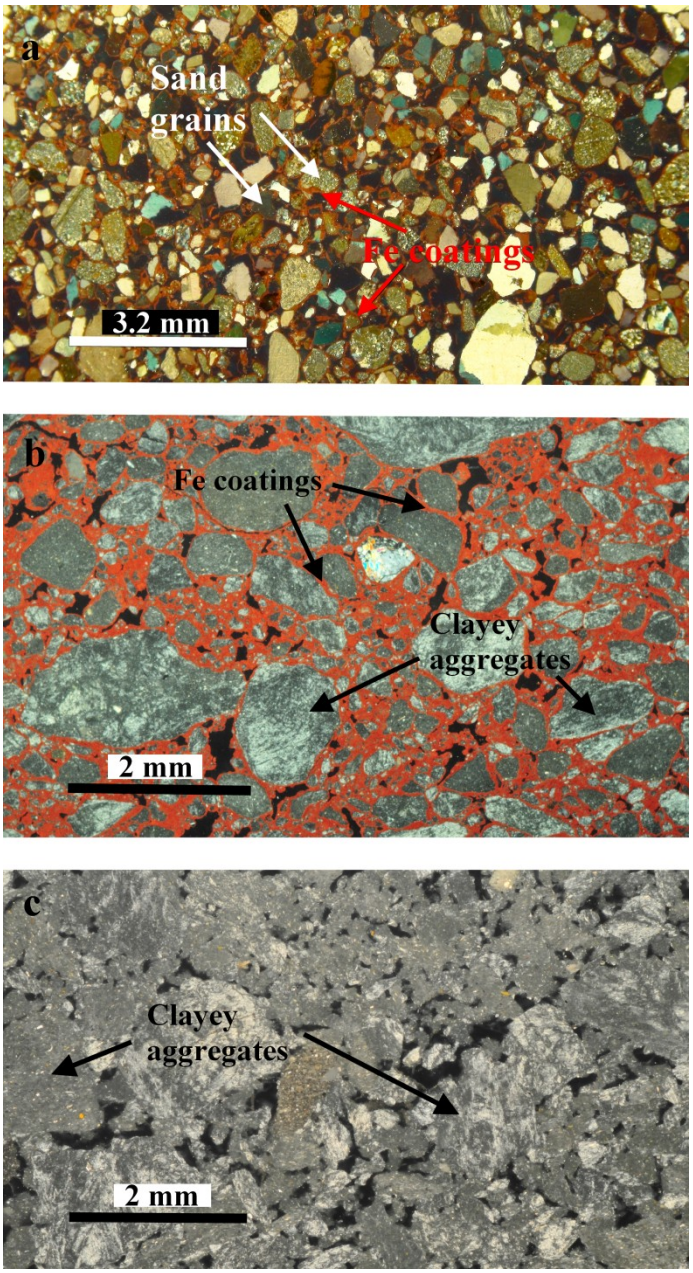

Figure 4 Fe coatings in samples treated with fine Fe oxides (<5µm): a) on sand grains in sandy material, b) on aggregates of clayey material and c) the control of clayey material. Photos were acquired with cross polarized light (XPL) and incident light to detect Fe oxides (appearing red). Pores appear black.

The presence of Fe concretions not inducing pore development was also observed. Fe coatings in silty material treated with fine Fe oxides were lower (10.1%) than the other two materials, but there was a higher percentage (1.5%) of Fe concretions

inducing pore development without planar pores, with respect to sandy and clayey substrates. In addition, only in silty material did Fe concretions induce planar pore formation. When applied to clayey substrate, fine Fe oxides produced 18.1% Fe coatings (Fig. 5b) and very few Fe concretions inducing pore development without planar pore formation.

3.4.3.2 Coarse Fe oxides (grain size 170-350 μm)

In the samples treated with coarse Fe oxides we observed them as isolated grains (as they were) and we classified each of them as a Fe concretion.

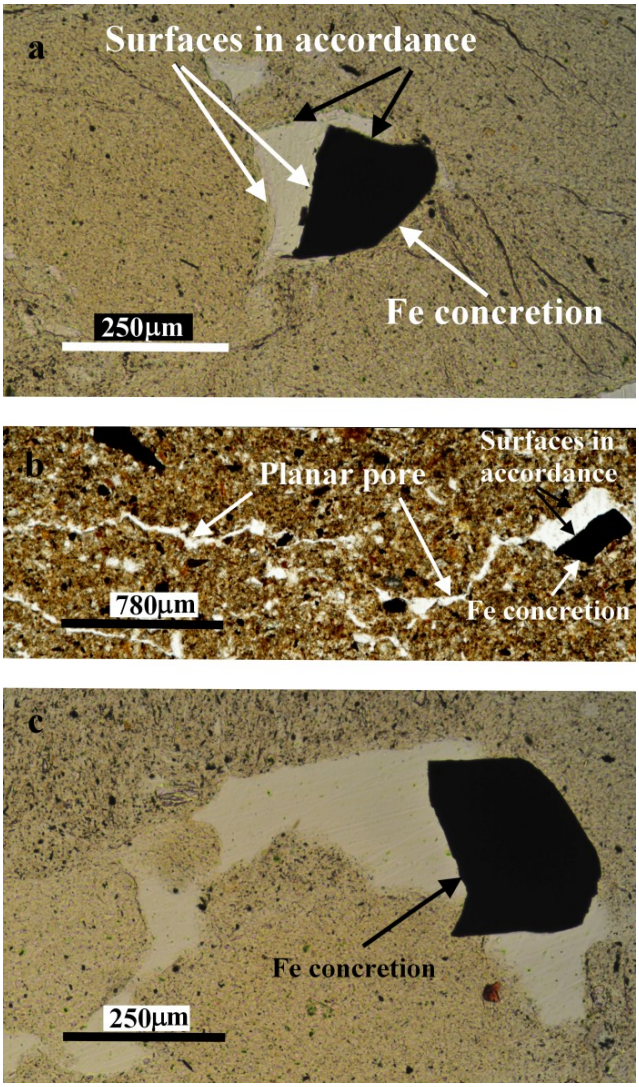

Figure 5 Samples treated with coarse Fe oxides: a) Fe concretion inducing development of pores with strongly accordant surfaces (without planar pore formation), b) Fe concretion inducing pore development with planar pore formation, c) Fe concretion not inducing pore development, in pores with not accordant surfaces. Photos acquired with incident reflected light (pores appear white).

In sandy material, only Fe concretions not inducing pore development were observed, in a percentage of 2.7%. In the silty material treated with coarse Fe oxides there was a higher percent (1.8%) of Fe concretions inducing pore development with planar pore formation (Fig. 5b) than in the clayey material (0.2%). In the clayey material there was the highest value (1.9%) of Fe concretions inducing pore development without planar pore formation.

3.4.3.3 Calcium carbonate (grain size 10 µm)

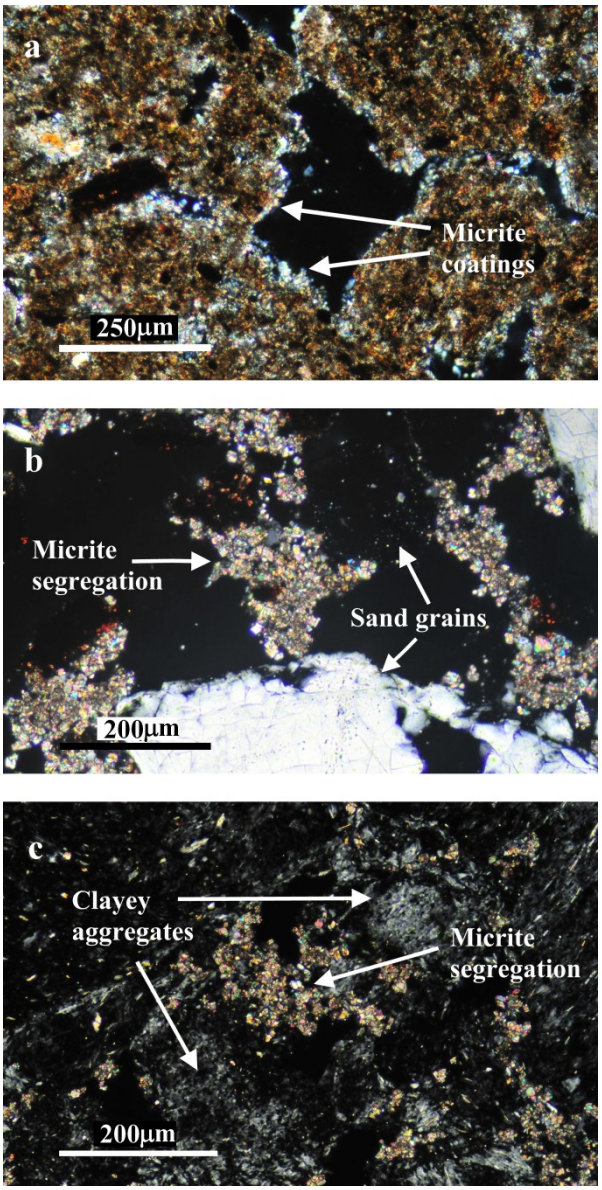

Figure 6 Micrite features: Micrite coatings on the pore walls in silty material sample (a), Micrite segregations in pores in sandy material sample (b) and in clayey material sample (c). Photos acquired with cross polarized light (XPL). Pores appear black.

The application of $CaCO_3$ to sandy material induced the formation of micrite coatings (1.7%) and a high percentage of segregations (16.6%) which formed "bridges" between sand grains in many sites (Fig.6b). In $CaCO_3$-treated silty material the highest percentage (3.6%) of micrite coatings (Fig. 6a) and the lowest percentage (1.5%) of micrite segregations were found. The percentage of micrite coatings in treated clayey substate was the lowest (0.8%) of the three substrates. The percentage of micrite segregations (6.0%) was higher than in silty material, although less than half of what was observed for sandy substrate.

3.4.4 Aggregate stability

Averages on three replicates of Mean-weight diameter values with their standard errors are shown in table 4, while figure 7 shows the percent differences (ΔMWD) between the mean values of MWD of the treated and control samples with their standard errors, also expressed in percent of the control values.

	Material		
	Sandy (mm)	Silty (mm)	Clayey (mm)
Control	0.686 (0.008)	0.325 (0.001)	0.374 (0.015)
Fine Fe oxides	0.705 (0.003)	0.279 (0.004)	0.273 (0.002)
Coarse Fe oxides	0.649 (0.020)	0.334 (0.018)	0.369 (0.001)
Calcium carbonate	0.705 (0.015)	0.300 (0.002)	0.403 (0.048)

SE, Standard error of the mean.

Table 4 Mean (SE) values of Mean weight diameter (MWD) of water-stable aggregates.

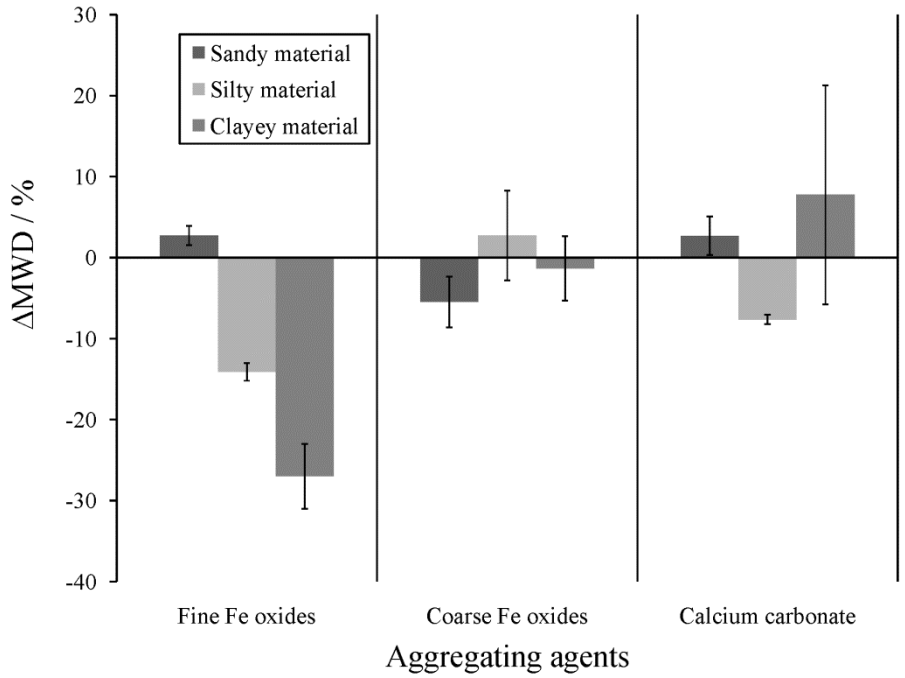

Figure 7 Percent differences of Mean-weight diameter (ΔMWD) of water-stable aggregates between the control and the treated samples.

Upon treatment with fine Fe oxide the mean values of mean-weight diameter (MWD) of the sandy material increased, while MWD decreased in both silty and clayey substrates (Table 4; Fig. 7). The decrease from the control indicates a drop in aggregate stability. The MWD decrease was somewhat less in silty material (0.325 mm to 0.279 mm) than in clayey substrate (0.374 mm to 0.273 mm), but nevertheless significant (Table 4).

When coarse Fe oxide was applied, there was a reduction in MWD in the sandy material (0.686 mm to 0.649 mm) and no significant effect on silty or clayey substrates (Fig. 7).

MWD increased in sandy material that was treated with $CaCO_3$, while no effect was seen in clayey substrate (Fig. 7). However, in silty substrate the $CaCO_3$ produced a significant reduction of MWD from 0.325 mm to 0.300 mm (Table 4).

These results indicate that, despite the effect observed on the PoSDs, the aggregating agents generally did not improve the aggregate stability of the

mineral materials. Only in sandy material the treatments with fine Fe oxide and $CaCO_3$ increased MWD.

3.5 Discussion

Soil image analysis allowed overall to observe evident changes of the pore size distribution (fig.3) induced by the redistribution of Fe oxides and $CaCO_3$, in the three tested materials, due to the shared W/D cycles as basic structuring process (Pires *et al.*, 2008; Scott, 2000).

Intrinsic features of the test materials, such as granulometry, shrink-swell behavior and plasticity were found useful keys to understand the effects of the inorganic agents on the development of pore architecture. For this reason in the following sections results are discussed for each substrate separately, except for aggregate stability. To help discussion all results and comparisons between control and treated samples were summarized in the synoptical Table 5.

Aggregating agents	Analysis	Sandy Material	Silty Material	Clayey Material
Fine Fe Oxides	Total Porosity	-50%	+60%	-45%
	PoSD /µm	--(<500)	+(everywhere)	--(<200), +(>240)
	Micromorph.	++Coatings, ++NA Concretions.	+Coatings, ++A Concr.	++Coatings
	Aggr. Stability	0%	-15%	-25%
Coarse Fe Oxides	Total Porosity	-10%	+80%	-30%
	PoSD / µm	-(<220)	++(<420),	--(40-220), +(>220)
	Micromorph.	++NA Concretions	++APP Concretions	+A Concretions, +NA Concretions
	Aggr. Stability	-5%	0%	0%
$CaCO_3$	Total Porosity	-10%	+ 135%	0%
	PoSD / µm	+ (<120), - (>120)	++ (everywhere)	+(<70), -(>70)
	Micromorph.	+ Coatings, +++ Segregations	++ Coatings, + Microsegregations	+ Microsegregations + Segregations
	Aggr. Stability	0%	-10%	0%

Table 5 Summary of the main results of the quantitative comparison between control and treated samples. Percent variation in total porosity and mean MWD are rounded to the nearest 5%. Changes in Pore Size Distributions (PoSD) are summarized indicating (in brackets) the pore size ranges where porosity has increased or decreased (symbols are: "-" = decrease; "- -" = strong decrease"; "+" = increase; "++" = strong increase"). The most frequently encountered (>1% of solid phase) micromorphological features induced by the treatments are preceded by "+","++" or "+++" for "sufficiently", "much" or "very much" frequent, respectively (see % in Table 3); "NA", "A" or "APP" Concretions indicates Fe concretions having surfaces that are "Not Accordant", "Accordant" or "Accordant with Planar Pore development", respectively, with pore walls.

3.5.1 Sandy material

Since it is well known that shrinkage-swelling dynamics increases soil porosity (Scott, 2000; Pires *et al.*, 2008), the lack of such dynamics in the sandy substrate can be considered the underlying factor to the reduction in total porosity, observed for all treatments (see first column in Table 5).

Treatment with the fine Fe oxides resulted in a 50% reduction of total porosity which may be due to pore filling. Micromorphological analysis allowed to observe that (i) the newly formed Fe concretions are not associated with pore development (pores have not accordant surfaces with the outline of the concretions) and (ii) a high percentages of Fe coatings covered sand grains. The latter finding, though important, is not entirely unexpected since this process is observed in many Oxisols, where sand-size quartz grains are coated with Fe coatings, and in most gley and pseudogley soils. In our experiment during wetting the fine Fe oxides behaved like a colloidal suspension and deposited on solid phase during drying. In this manner the quartz surfaces of the sand grains may have served as nuclei to which the Fe coatings were attracted and accumulated (such as those observed by Padmanabhan and Mermut, 1996). The Fe oxide coatings had a thickness of about 50 μm, thus reducing distance between the pore walls (Fig.5a). Together with the Fe concretions in pores with not accordant surfaces, this phenomenon likely contributed to the observed reduction of frequency of almost all pore size classes, as compared to the control (Fig.3).

In the samples treated with coarse Fe oxides, micromorphological analysis did not show any evidence of their association with newly formed pores (concretions classified as not inducing pore development). The larger Fe concretions (>300 μm) were randomly distributed among the sand grains confusing with them, while the smallest ones (<200 μm) were located in small pores, and thus were the likely cause of the small decrease in porosity in size classes <220 μm, producing a 10% decrease in total value.

The mobilization of $CaCO_3$ in suspension during W/D cycles induced the formation of a high percentage of micrite segregations, most likely forming as the coalescence of multiple micrite coatings (Table 4). These micrite segregations are frequently arranged as bridges between sand grains, thus fragmenting the pore space (Fig. 7b).

Development of the segregations resulted, in fact, in a decrease of pores >120 μm, and a corresponding increase in <120 μm pores (Fig.3). Overall, there was a 10% reduction of total porosity partially due also to the formation of micrite coatings on the sand grain surfaces.

3.5.2 Silty material

Unlike sandy material, in silty substrate all treatments induced an evident increase of porosity in all pore size range. The substantial shrink-swell dynamics of silty material (see Fig. 1) may have been the primary factor driving this increase in porosity.

In both the fine and coarse Fe oxides treatments new pores formed which, based on micromorphological analysis, could be attributed to differential shrink-swell behavior at the interface between the Fe concretions (little or no shrinkage-swelling dynamics) and the substrate (significant shrinkage-swelling dynamics). These new pores were recognizable because their wall surfaces followed the outline of the concretions, providing strong evidence as to their origin.

Treatment of silty material with coarse Fe oxide resulted in a substantial increase in total porosity (~80%), which was attributable also to the development of planar pores from the outer border of the concretions. In fact, in the fragile (slightly plastic) silty material the stress induced during the shrink-swell process by the presence of the not shrinkable coarse Fe concretions caused breakage of the substrate matrix, having as result the development of planar pores (Fig. 7b). Overall, this process increased the frequency of <420 μm pores. Fine Fe oxides also increased total porosity (60%), although the increase was less than in the presence of the coarse Fe oxides. This difference was attributed to both the near absence of planar pore development with fine Fe oxides, and pore filling produced by Fe coatings.

The greatest increase in silty material porosity, across all pore sizes, occurred when samples were treated with $CaCO_3$ (Fig.3). In these samples, the micromorphology revealed a high percentage of micrite coatings on the pore walls (Fig. 7a). Unlike the fine Fe oxide coatings, these produced a very porous microstructure, as is typically observed in the formation of both calcic and petrocalcic horizons (Gile *et al.*, 1966;

Lal, 2006). In this substrate $CaCO_3$ transported in suspension acted as cement and stabilized the pores with each successive W/D cycle. This produced a cumulative effect in the pore development with the succession of the cycles, which explains the high level of porosity observed

3.5.3 Clayey material

Understanding of the results obtained for clayey material requires further clarification about the substrate itself. Thin sections of the clayey material observed by light microscopy (Fig. 5c) revealed that such material was naturally arranged in relatively large compact aggregates (within a typical sand-size range) and due to its high plasticity it shrunk and swelled rather homogeneously during the W/D cycles without further breakage. This may explain the reason of some analogous results to sandy substrate, regardless of the differences in the shrink-swell dynamics. Like sandy material, treatment of clayey substrate with fine Fe oxides resulted in Fe coatings but covering, in this case, aggregates rather than individual grains (Fig. 5a, 5b). As a result, porosity decreased (-45%) across nearly the entire pore size range (<200 μm).

Unlike sandy material, coarse Fe oxides in clayey substrate produced pores with walls that were in accordance with the outline of the Fe concretions (Fig. 6a). This was clearly due to shrink-swell dynamics, while the absence of planar pores formation was most likely associated with high plasticity of the clayey material. Fe concretions were also found in pores having “not accordant surfaces”. This latter features seem to have partially occupied the inter-aggregate pore space (Fig. 6c), reducing <40 μm pores, and possible accounting for the 30% reduction of total porosity.

In contrast to sandy and silty material, the addition of $CaCO_3$ almost did not produce micrite coatings in clayey substrate, a response that is linked to shrinkage-swelling behavior of the clayey material (Fig. 2). In fact the shrinkage curve suggests that the pores remained nearly saturated with water during the shrinkage, thus reducing the probability of sedimentation of the micrite coatings on the pore walls. The nearly absence of micrite coatings could also be related to the breakage of newly formed

micrite coatings at each W/D cycles during the shrink-swell dynamics, as happens in Vertisols.

Also observed were micrite segregations generating bridges between aggregates (Fig. 7c), similar to the situation in sandy material. The resulting effect on PoSD was analogous (see Fig. 3). In fact, pore space fragmentation, induced by these bridges, yielded an increase of small pores and a drop in the frequency of large pores, although total porosity was not affected.

3.5.4 Aggregate stability

With the exception of sandy material, the inorganic agents studied here did not increase the aggregate stability of the mineral materials (relative to the controls) This could be considered an unexpected result, but it can be attributed to the following factors: (i) the added substances were simply intercalated between mineral particles or deposited on them (as coatings), possibly without a more complex interaction with the mineral materials, thus contributing to reduced adhesion among mineral particles and reduced aggregate stability; (ii) the limited duration of our experiment did not provide enough time for development of an intimate and strong chemical interaction with the mineral materials.

While some previous research found that Fe oxides improve aggregate stability (Barral *et al.*, 1998; Igwe *et al.*, 1999), our data indicate that fine Fe oxides actually reduced aggregate stability in the silty and clayey material and that coarse Fe oxides reduced aggregate stability in sandy substrate.

3.6 Conclusion

This experiment on soil-like substrates allowed to observe the consequences of W/D cycles on the mobilization of Fe oxides and $CaCO_3$ in the soil pore system. Influence of Fe and micrite coatings as well as Fe concretions and micrite segregations on soil pore development have been quantified by soil micromorphometry.

Our results showed that micrite coatings induced a cumulative effect on porosity during W/D cycles cementing the walls of newly-formed pores in the silty substrate.

In sandy and clayey materials, micrite segregations produced bridges between sand grains and between clayey aggregates respectively fragmenting the pore space.

In all substrates Fe coatings induced filling of pores.

Fe concretions produced new pores in accordance in clayey and silty materials and also new planar pores in silty material.

The aggregate stability test did not show any improving effects from the addition of the agents.

Shrinkage-swelling behavior and plasticity have resulted physical properties of the substrates strongly influencing pore development due to presence of Fe concretions. We believe that our results can be correlated directly to real-world soils.

The observed effects of micrite coatings and segregations in the soil pore development demonstrate the importance of the not always well recognized role of the suspensions rich in calcium carbonate in the formation of soil structure in the calcic horizons.

About Fe concretions, in Vertisols their occurrence is very common. We can speculate, therefore, that these soil features may play a still unrecognized role both in the well known fertile self mulching structure of surface soils and in the development of wedge structure-associated slickensides of deeper soil horizons.

Many questions remain as to the individual and combined effects of different factors on soil structure development. In order to quantitatively investigate interactions of those agents in natural soils we believe that the role of physical simulation tests should be reassessed matching multiple and integrated analytical approaches.

4. Effect of rock fragments on soil pore system development

4.1 Introduction

Stones play a role in soil by modifying the pore space (Fiès et al., 2002). Rock fragments are often present in soil as a result of soil forming processes and human activity. Since the 1950s, scientists have studied the effect of rock fragments on several soil physical processes, but most studies focused on the effect of rock fragments on water infiltration and runoff (e.g. Abrahams and Parsons, 1991; Agassi and Levy, 1991; Dunkerley, 1995; Cerda`, 2001). Rock fragments resting on a wettable soil surface or partly incorporated into the topsoil affect rainfall interception, overland flow, together with evaporation, percolation and infiltration rates. They can also promote runoff generation (Poesen & Lavee, 1994) and water storage through their effect on soil porosity and water flow paths, which can have land use and site productivity repercussions (Brakensiek & Rawls, 1994; Poesen & Lavee, 1994). According to Sauer & Logsdon (2002), the infiltration rates and hydraulic conductivities of wettable soils with rock fragments strongly depend on the water content and tend to increase with rock fragment content near saturation.

Recently Zhou et al. (2009) studied the effects of different gravimetric rock fragment contents in a soil (Rw) on infiltration, saturated hydraulic conductivity (Ks) and solute transport. Both infiltration rates and the saturated hydraulic conductivity initially decreased with increasing rock fragment content to minimum values for Rw = 40%, and then increased. They observed that the increases in Ks and infiltration above rock fragment contents of about 40% were ascribed to the development of a more continuous macropore system. In fact although macropores are more likely to exist at the soil-to-rock interface, these are not continuous when the rock fragments are not in contact with each other, as would be the case in the mixtures with low rock fragment contents. Thus, increasing the rock fragment content initially increases the impedance of water flow and consequently Ks values become smaller. However, at a critical rock fragment content, which we observed to be about 40%, there are sufficient rock fragments in the soil to create more continuous macropores. Furthermore, fragment-to-fragment contact is more likely to create larger voids than

those existing at the fragment to- soil interfaces and induce the creation of such larger and more continuous macropores.

Urbanek and Shakesby (2009) have showed the potential effect of stones on water flow in a water-repellent soil. They observed that stones in both single and mixed sizes can only promote water movement once their content is sufficiently large for the development of continuous flow paths along their surfaces. Both these works have deduced from the effect of rock fragments on the hydrological properties of the soil their influence on soil pore system development. In fact, few studies have investigated the mechanism of formation of soil pores induced by the presence of rock fragments, and most of them have investigated their effect on bulk density. It was observed that, in natural soils, an increase in the content of rock fragments is correlated with a decrease in the bulk density of the fine earth (Torri et al., 1994). Van Wesemael et al. (1995) observed that the effect of rock fragments on final bulk density of the fine earth was strongest when rock fragments were small (1.7-2.7 cm) and dispersed throughout the soil profile and they concluded that crushing of large rock fragments into smaller ones is to be preferred over removal of rock fragments from the plot layer.

This decrease in bulk density is due to extra porosity resulting from contact between the stones and the fine earth, which in turn arises because the space between the stones is incompletely filled by fine earth or because the larger particles prevent the smaller ones from packing (Stewart et al., 1970). Also, fine earth and rock fragment react in a different way when expanding and contracting (e.g. during the processes of wetting and drying or of freezing and thawing). This might cause voids to form at the contact between rock fragments and fine earth (Poesen and Lavee, 1994).

Relatively to this mechanism, Spomer (1980) suggested that dying mixtures that contain a clay soil leads to the formation of pores as a result of the shrinkage of fine earth between stones. Towner (1988) observed that cracking occurred during drying on mixtures of kaolinite clay and various size of coarse particles when the size of the particles was larger than 2mm.

In order to analyze the contribution of stones and fine earth to porosity and water retention Fiès et al. (2002) prepared mixtures of glass fragments <6mm with silty-

clay soil and a clay soil in the 10-80% glass range. These mixtures were prepared in a moistened state and then were air-dried. The samples obtained were used to determine water contents and bulk densities. Dry samples were impregnated with a polyester resin and the images of the surface of the section were obtained, but they were only used for a qualitative assessment of the soil porosity, in fact in this work the pore volume was calculated based on the values of bulk density. Fiès et al. (2002) observed that in a soil with clay content <30% the two mechanisms behind coarse pore formation were the substitution, when the glass content was <50%, and the filling, when the glass content was >50%, while in a clay soil pores formation was determined by shrinkage. The mechanism of substitution of each coarse particle with the same volume filled by the fine phase determined the predominance of the fine earth pores. When the mechanisms of filling (open areas between the coarse particles are filled by finer particles) or of shrinkage prevailed, there were two distinct types of pores in the mixtures: fine earth pores and coarse lacunar pores. These latter pores correspond to the vacant volume that was left when the volume of the soil phase (with its solid particles and their own packing pores) and the volume of solid glass particles were subtracted from the total volume.

Soil micromorphological studies have quantified the pore structure and distribution of rock fragments (Koppi and McBratney, 1991) and of limestone fragments (Khormali et al., 2006), but they didn't analyzed quantitatively the soil pores formation induced by the presence and distribution of the rock fragments.

The purpose of our work was to investigate the effect of the interaction between different sizes and concentrations of rock fragments and soils with different shrinkage-swelling dynamics and plasticity on the mechanisms of soil structure formation.

For this purpose an experimental test in pots was performed by adding rock fragments of different sizes and shapes and in different concentrations in five soils different in shrinkage-swelling dynamics and plasticity. After several wetting-drying cycles was quantified, by means of soil two-dimensional image analysis, the effect of rock fragments on pore size distribution and surface cracking of the soils tested.

4.2 Materials and methods

4.2.1 Soils selection

From a set of 14 soils from different Italian locations were selected four soils characterized by different shrinkage-swelling characteristics and different plasticity. Cylindrical specimens were prepared for each of 14 soils and were subjected to one wetting and drying (W/D) cycle to identify those with greater or smaller swelling-shrinkage capacity. After the W/D cycle the reduction of the diameter of cylindrical specimens was measured. Soil plasticity was also measured on thoroughly puddled samples of each soil at a water content where maximum plasticity is expressed, according to the field method described in the Soil survey manual (Soil Survey Division Staff, 1993).

The values obtained from measurements of the reduction of diameter of cylindrical samples at the end of one W/D cycle were used to obtain a relative index of shrinkage normalizing these values respect to the highest value, which corresponded to the soil with highest shrinkage dynamics. Thus was obtained a relative index of shrinkage where the value 1 corresponds to the soil with higher shrinkage dynamics. The values obtained from thickness measurements of puddled samples prepared for test of plasticity have been normalized respect to the lowest value, which was that of the soil with greater plasticity. The inverse of these normalized values was calculated in order to obtain a relative index of plasticity where the value 1 corresponds to the soil with greatest plasticity.

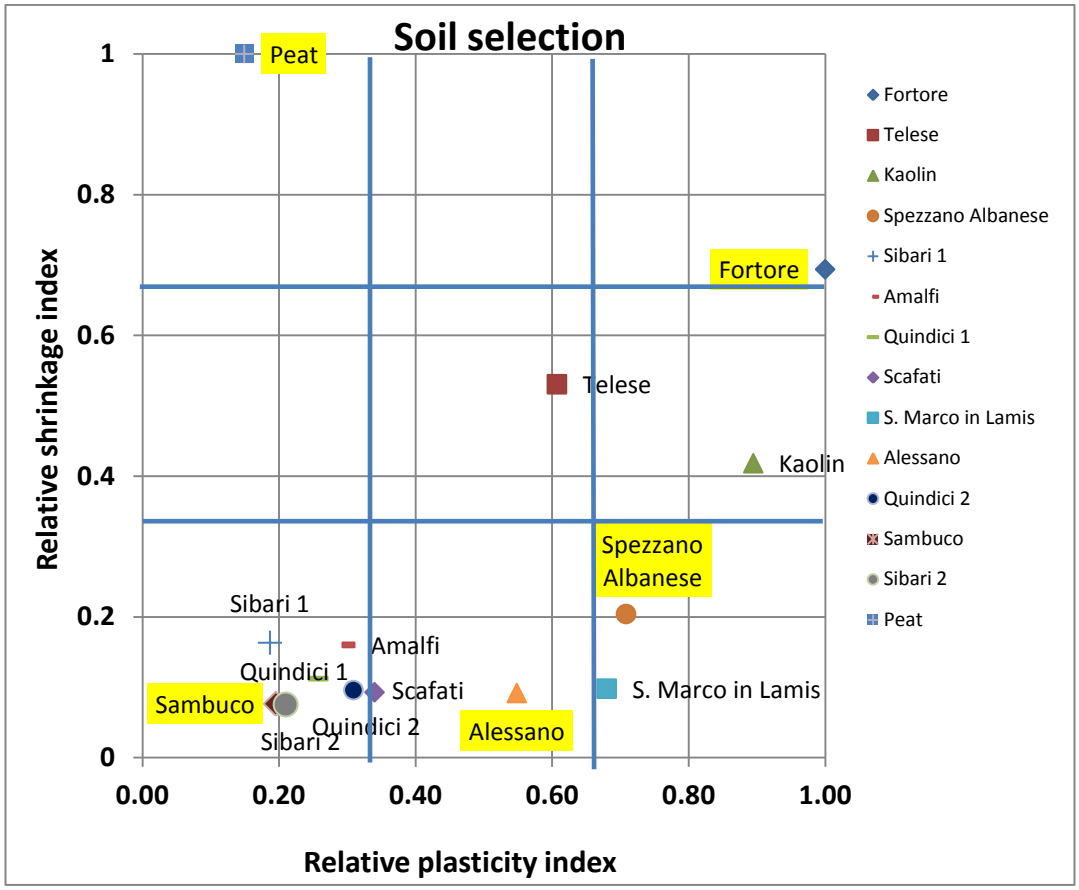

Figure 1. Scheme of relative shrinkage and plasticity properties of the 14 soils tested.

Then the following 4 soils were identified as those with the most extreme properties of shrinkage-swelling characteristics and of plasticity:

- A Vertisol sampled in San Bartolomeo in Galdo (Benevento, South Italy, 41°27'3.00"N, 15°1'51.00"E) characterized by high shrinkage-swelling capacity and high plasticity.
- An Andosol sampled in Sambuco (Salerno, South Italy, 40°40'22.00"N, 14°37'4.00"E), characterized by low shrinkage-swelling capacity and low plasticity.
- An Entisol sampled in Spezzano Albanese (Cosenza, South Italy, 39°43'40.80"N, 16°20'7.20"E), characterized by low shrinkage-swelling capacity and high plasticity.
- A peat purchased as professional substrate from a company that supplies agricultural products (Floragard).

- In addition to these 4 soils we tested the effect of the presence of stones even on a terra rossa that is typically characterized by a compact structure and problems of asphyxia. The terra rossa was sampled in Alessano (Lecce, South Italy, 39°52'48.06"N, 18°21'18.60"E).

Prior to the experiment, all five soil were dried at 40 °C for 72 hours and sieved to 2 mm. Substrates were analyzed for grain size distribution (GSD) by sieving a humid sample, for the fractions between 0.2 and 2 mm, and by sedimentation (pipette method) (Day, 1965), using Stockes law, for <0.2 mm fractions.

Soil chemical analyses were completed by following standard methods. Soil pH was determined potentiometrically with a pHmeter (10pH/ISE, Beckman) in soil: water suspensions (ratio of 1:2.5) and in soil solution NaF (ratio 1:50). (Peech, 1965). Organic carbon content was determined with the Walkley and Black (1934) method, by means of organic matter oxidation with potassium bichromate, in the presence of sulfuric acid. Electrical conductivity was measured in soil:water suspensions (ratio of 1:5) using a conductivity meter (microCM 2201,CRISON) (Rhoades, 1996). Total carbonates were determined using a Dietrich-Fruehling calcimeter (Loeppert and Suarez, 1996).

4.2.2 Experimental desing

For the experiment irregular basaltic rock fragments of three increasing sizes were added to each soil at two different concentrations, according to the experimental design shown in Table 1.

Soil	**Rock fragment**									**Glass beads**
	2-4mm		**4-8mm**					**12-16mm**		
Vertisol	10%	25%		10%		25%		10%	25%	10%
Andosol	10%	25%		10%		25%		10%	25%	10%
Peat	10%	25%		10%		25%		10%	25%	10%
Entisol	10%	25%	5%	10%	15%	25%	35%	10%	25%	10%
Terra rossa			5%	10%	15%	25%	35%			10%

Table 1. Experimental design with the used concentrations expressed in volumetric percentage.

Because the terra rossa and Entisol are characterized in nature by a compact structure, for these two soils was tested the effect of 5 increasing concentration of rock fragment of 4-8mm size. Glass beads with a diameter of 6 mm were also added to each soil at a concentration of 10% in volume, in order to compare their effect with that of the 4-8mm rock fragments. The samples were prepared by mixing the wet soil with a given concentration of stones or glass beads and filling two pots (replicates) of 15 cm in diameter. The skeleton and glass beads were added and mixed to wet soil to aid the distribution in the entire sample. Two control pots for each soil without rock fragment were also prepared.

In order to induce soil structure development the samples were put in a tank and subjected to nine wetting/drying (W/D) cycles, consisting of a wetting phase of 24 hours at 25 °C and drying phase of 32 °C for 6 days. In order to avoid possible soil structure artefacts induced by drop impact or runoff, wetting (with deionized water) was performed via capillary action from the bottom of the container.

4.2.3 Two-dimensional image analysis

Before impregnation the samples were further dried for another 10 days. A mixture of acetone and polyester resin (Crystic 17449, Scott-Bader Ltd.) was added with fluorescent dye (Uvitex OB, Ciba Ltd.), having a spectral emission in the blue band under UV illumination (365 nm). The samples were saturated with that mixture under a moderate vacuum. This procedure yielded a low viscosity mixture for optimal resin penetration into the pore networks (Fitzpatrick, 1993). After resin polymerization, the soil blocks were cut into regular parallelepipeds. Digital images (20 μm pixel resolution) of the four vertical sections (3 x 5 cm) were acquired under UV illumination. A Nikon D200 camera was used, controlled by a PC using Nikon Capture 4.1 software. To merge the variability of the two replicates, four images of each sample were placed side by side to obtain a single large 2D image (36 x 5 cm) consisting of all twelve vertical sections of the treatment (Fig. 1). Images were pre-processed and segmented using a technique of supervised "thresholding" using Corel Photo-Paint X3, in order to obtain binary images where the two separate solid and pore phases are in black and white, respectively.

Image analysis was performed using Solicon - PC Version 1.0 software (Cattle *et al.*, 2000) to determine total porosity. Pore size distribution was determined by image analysis using Micromorph 1.4 (TRANSVALOR 2000), through the application of the "opening" algorithm (Horgan, 1998; Serra, 1982), which classifies the pore phase according to the spacing from the walls.

At the end of the last cycle and before impregnation digital images (47 μm pixel resolution) of the samples surfaces were acquired, in order to analyse the network of cracks developed on their surfaces. A Nikon D200 camera was used, controlled by a PC using Nikon Capture 4.1 software. The digital images were segmented using a technique of supervised "thresholding" using Corel Photo-Paint X3, in order to obtain binary images.

The analysis of the network of cracks was performed measuring the cracking density and the mean width of the cracks. The cracking density was determined obtaining the skeleton of the cracks network (Soille, 2004) (see fig.2) and measuring the ratio between the number of pixels of the skeleton and the number of pixels of the total image.

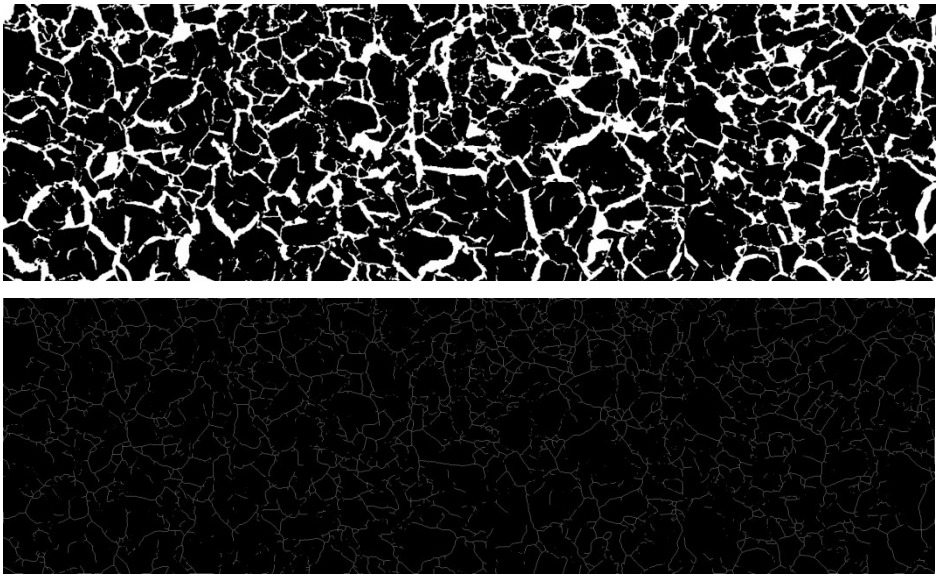

Figure 2. Binary image and skeleton of network obtained.

4.3 Results

The main properties of the five soils used in the experimental test are given in Table 2.

Table 2. Properties of the soil used in the experiment.

	GSD[a]							
Soils	Sand (%)	Silt (%)	Clay (%)	pH (NaF)	pH (H_2O)	EC[b] ($\mu S\ cm^{-1}$)	OM (%)	$CaCO_3$ (%)
Vertisol	48.5	30.7	20.8		7.9	200	2.6	0.5
Entisol	24.2	46.0	29.9		6.6	3790	1.36	11.5
Terra Rossa	29.2	26.3	44.5		7.1	1174	1.31	25.7
Andosol	9.3	29.7	60.9	10.4	6.4	264	9.77	absent
Peat					5.2	841		absent

[a] Grain size distribution obtained by sieve method.
[b]electrical conductivity.
[c]organic matter.

In this paragraph will be discussed the main results of two-dimensional image analysis performed on images of vertical sections of samples of Vertisol and Entisol soils, characterized respectively by high and low shrinkage dynamics, treated with increasing concentrations of rock fragment of 4-8mm size. For each measurement perfomed on the two replicates of each treatment mean values were calculated and were reported in the following graphs.

4.3.1 Comparison between Vertisol and Entisol

In figures 3 and 4 are shown images representing the different soil pore system organizations obtained in Vertisol and Entisol controls and samples treated with increasing concentrations of rock fragments of 4-8mm size.

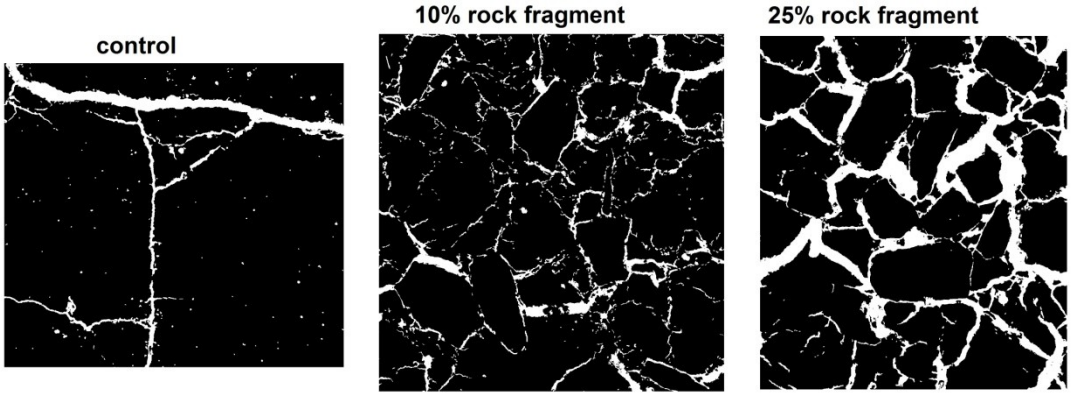

Figure 3. Binary images of vertical section of Vertisol samples (solid phase in black and pore phase in white).

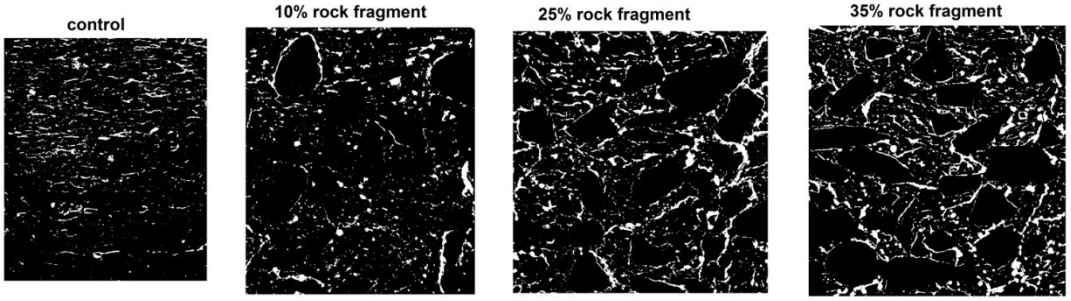

Figure 4. Binary images of vertical section of Entisol samples (solid phase in black and pore phase in white).

The graph reported in fig.5 show that after 9 W/D cycles total porosity of Vertisol control was higher (7.3%) than total porosity of Entisol control (4%). This difference between controls of two soils can also be observed in the comparison between their pore size distributions shown in figures 8 and 9. The PoSD of Entisol control is characterized by pore classes no larger than 400μm, while Vertisol control have a pore size distribution characterized by pore classes up to 1600μm.

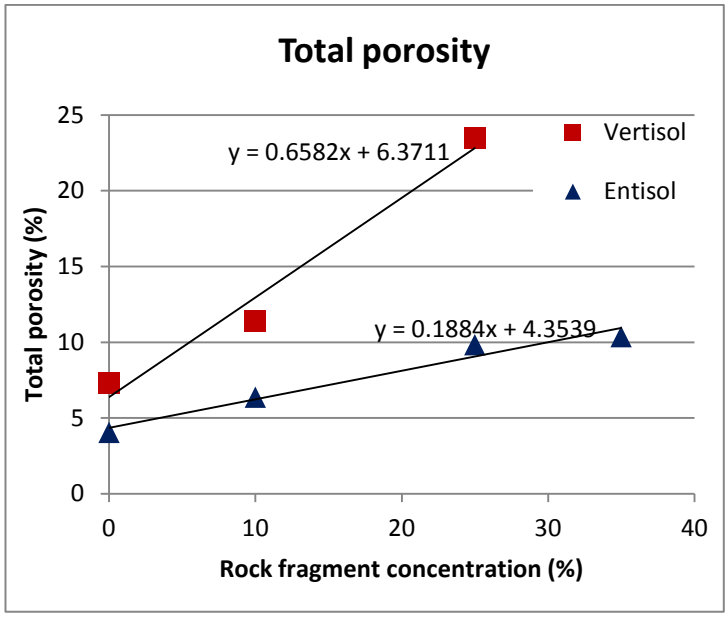

Figure 5. Comparison of total porosity trends versus rock fragments concentration between Vertisol and Entisol samples.

It was observed that the addition of rock fragments induced an increase in total porosity after 9 W/D cycles in both soils, but the magnitude of this increase was different in the two soils. As you can see from the slope of trend lines of the two soils, Vertisol showed a higher reactivity to the addition of rock fragments, with a greater enhance in porosity with increasing concentrations of added rock fragments.

In fact, total porosity of the samples treated with 10% rock fragment by volume increased from 7.3% (control) to 11.4% in Vertisol and from 4% (control) to 6.4% in Entisol. And after the addition of 25% rock fragments by volume, there was a further increase of total porosity in Vertisol (23.4%) and in Entisol (9.8%). With the addition of 35% rock fragments by volume total porosity increased to 10.4% in Entisol samples.

From the graph in fig.6 it is also possible to observe an increase of mean width of pores, albeit with some fluctuations, with increase of concentration of added rock fragments in both soils. As observed for total porosity, even for the mean widht of pores the slope of the trend lines was higher for Vertisol samples than for Entisol samples. In particular, after the addition of 10% stones the mean width of pores was lower (405μm) than the control (447 μm) in Vertisol samples and after the addition of 25% rock fragments increased to 739 μm. In all Entisol samples treated with

increasing concentration of rock fragments the mean width of pores was greater than the control, with the highest value (535 μm) obtained after the addition of 10% rock fragments.

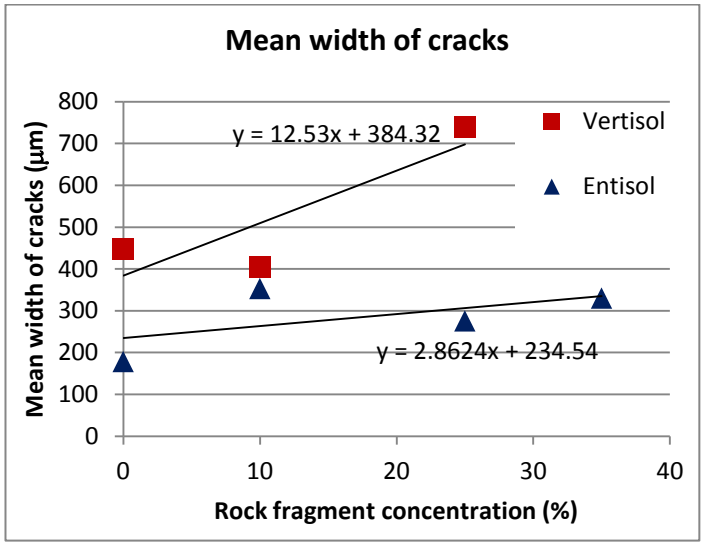

Figure 6. Comparison of mean width of cracks trends versus rock fragments concentration between Vertisol and Entisol samples.

The results obtained from the measurement of cracking density carried out by measuring the total length of the skeleton of the network of pores in relation to the surface of the image are reported in fig.7. Despite some fluctuations, cracking density improved with increasing concentrations of rock fragments in both soils. From the slope of the trend lines obtained for the two soils can be observed that, although very similar values were obtained for the control, this increase was greater in Vertisol samples.

At the same concentration of rock fragments, in fact, the value of cracking density was greater in Vertisol than in Entisol samples. Furthermore, with increasing concentrations in Vertisol samples the value of density of cracks always increased with increasing concentration from 0.65% of control to 0.95% with 10% rock fragment and to 1.9% with 25% rock fragments. In Entisol samples instead with 10% rock fragments value of density of cracks was lower (0.59%) than the control (0.69%), and this value increased compared to control after the addition of both 25% and 35% rock fragments. Even if the value of density of cracks of samples treated

with 35% rock fragments was lower (1.06%) than the value obtained with 25% rock fragments (0.95%).

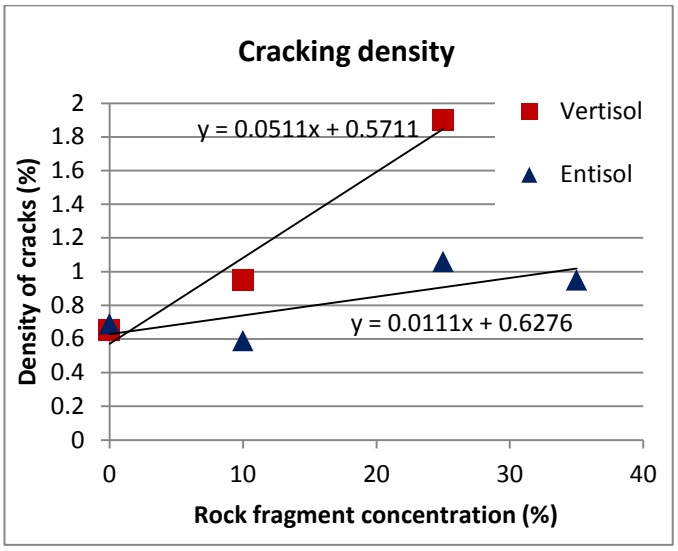

Figure 7. Comparison of cracking density trends versus rock fragments concentration between Vertisol and Entisol samples.

Regarding the effect of the addition of rock fragments on the pore size distribution from the graph in fig. 8 can be observed that in Entisol samples the frequency of pore size classes larger than 120 μm increased gradually, compared with control, with increasing concentrations of rock fragments added. The treatment with 10% rock fragments induced a reduction of pore size classes smaller than 120 μm and an increase of all pore size classes larger than 120μm. Following the addition of 25% rock fragments was observed an increase in the frequency of all pores size classes larger than 80 μm and with the addition of 35% rock fragment, there was an increase of all pore size classes larger than 120μm.

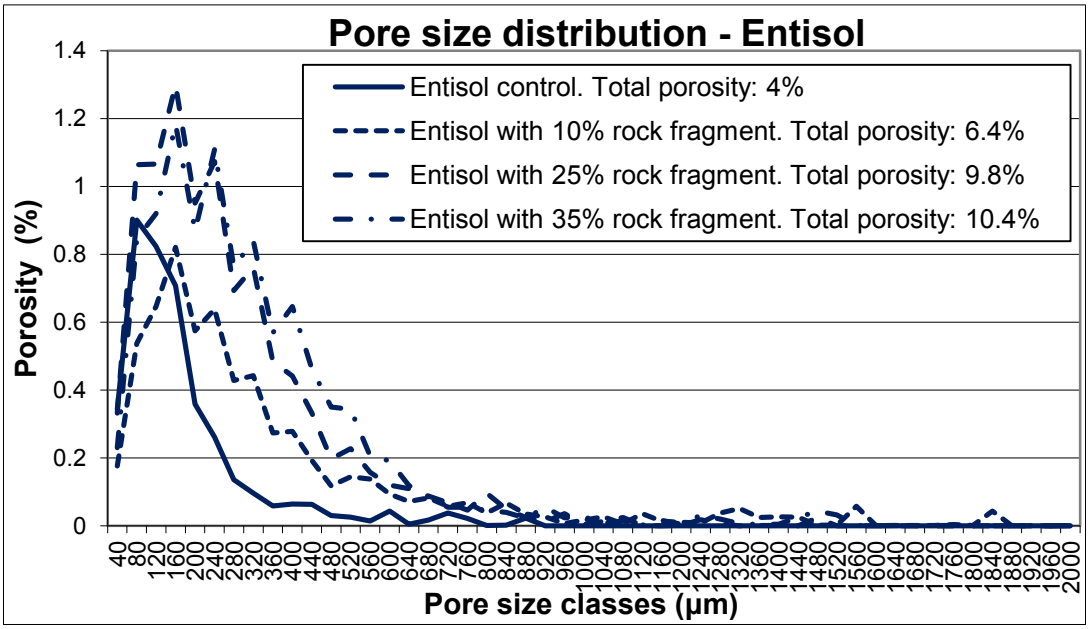

Figure 8. Pore size distribution of Entisol samples.

From the graph in fig.9 it can be noted that both concentrations of rock fragments added to Vertisol samples induced an increase in all pore size classes respect to the control. In particular, while with 10% rock fragment there was a greater increase compared to the control of pore size classes smaller than 160µm, with 25% rock fragment the greatest increase in frequency regarded pore size classes larger than 200µm.

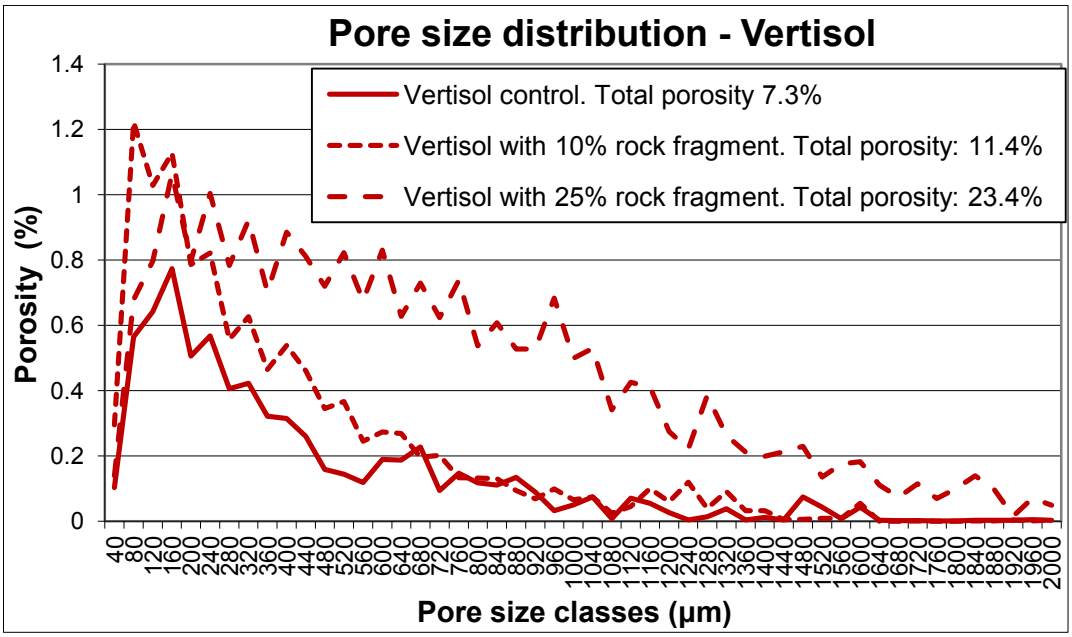

Figure 9. Pore size distribution of Vertisol samples.

4.3.2 Comparison between surface and vertical section of Vertisol samples

After the experimental test with 9 W/D cycles on the surface of all Vertisol samples was observed the formation of a network of surface cracks. Then was carried out an analysis of this network of cracks in order to compare the results related to the surface with those related to the vertical sections of the samples. From the measurement of cracking density (fig.10) was noted both on surface and in section an increase of cracking process with the increase of rock fragments concentrations.

From the values of slope of the trend lines it was possible to note that the magnitude of this increase is the same both in surface and in vertical section, even if the values of the density of cracks were found, with the same rock fragments concentration, higher in vertical section than in surface. In the controls density of cracks resulted 0.65% in the vertical section and 0.36% in depth. Following the addition of 10% rock fragment was observed an increase to 0.95% in vertical section and to 0.8% in surface, and with the addition of 25% rock fragments the density of cracks increased further to 1.9% in the vertical section and 1.63% at the surface.

From the graph of the trend of mean width of pores with the variation of rock fragments concentration (fig.10) it was observed on the surface a reduction of mean width of pores with increasing rock fragments concentrations. In fact, the mean width of cracks decreased from 1514μm (control) to 1096μm after the addition of 10% rock fragments and to 594μm with 25% rock fragments.

In vertical section instead with increasing concentration of rock fragments, there was a positive trend of the mean width of cracks, although with some fluctuations. The mean width of cracks reduced from 447μm (control) to 405μm with 10% rock fragments, and subsequently increased to 739μm with 25% rock fragments.

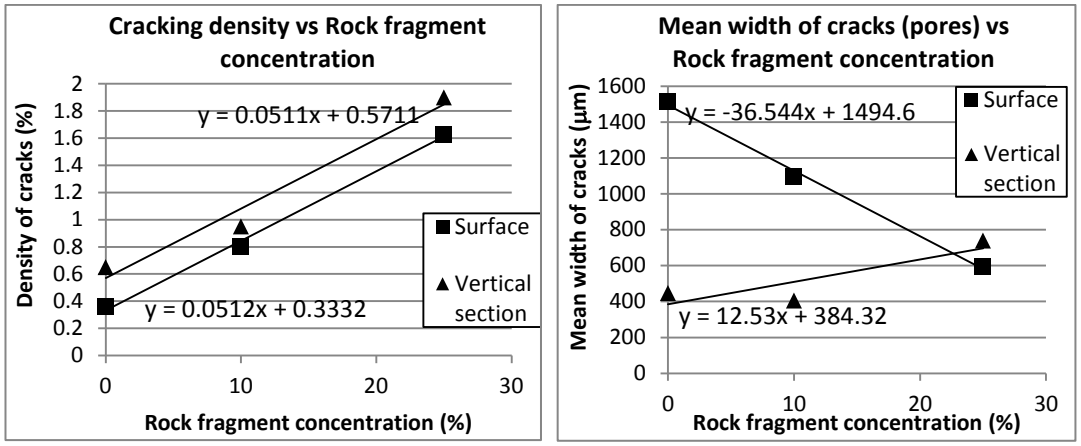

Figure 10. Comparison of cracking density and mean width of cracks trends versus rock fragments concentration between surface and vertical section of Vertisol samples.

4.3.3 Effect of rock fragment on surface cracking in Vertisol samples

After the acquisition of the images of the surface of Vertisol samples, the analysis of the network of surface cracks was performed measuring cracking density and mean width of the cracks.

The figure 11 shows the effect of different sizes of rock fragments on the surface cracking density of Vertisol samples. It can be observed, for all rock fragments sizes, an increase of surface cracking density with increasing rock fragments concentrations. And from the slope of the trend lines can be observed that this positive trend is more evident with smaller rock fragments size. In fact, with the same concentration of rock fragments added the cracking density resulted greater for the smaller rock fragments size. In particular with 2-4mm rock fragments the cracking density increased from 0.36% of the control to 1.35% in samples treated with 10% rock fragments and to 2.34% in samples treated with 25% rock fragments. With 4-8mm rock fragments the density of cracks increased from 0.36% (control) to 0.8% after the addition of 10% rock fragments and further increased to 1.63% with 25% rock fragments. And with 12-16mm rock fragments surface cracking density increased from 0.36% (control) to 0.48% with 10% rock fragments and to 0.79% with 25% rock fragments.

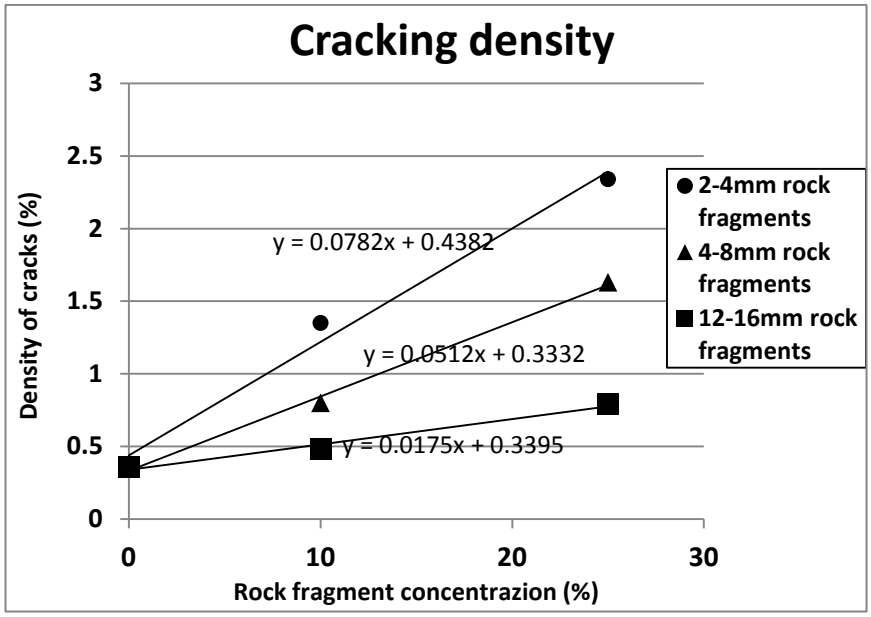

Figure 11. Comparison of cracking density trends versus rock fragments concentration between Vertisol samples treated with different sizes of rock fragments.

The fig.12 shows the effect of different sizes of rock fragments on the mean width of surface cracks of Vertisol samples. With increasing concentrations of 2-4mm rock fragments mean width of surface cracks decreased. In fact, the mean width of cracks reduced from 1514µm (control) to 470µm for samples treated with 10% rock fragments. The further increase of concentration of rock fragments (25%) resulted in further reduction of the mean width of cracks to 369µm, a value, however, close to that obtained with 10% rock fragment.

After the addition of rock fragments of 4-8mm size (see fig.11) was observed, with increasing concentrations of rock fragments, negative trend of mean width of cracks. In particular, the mean width of cracks reduced from 1514µm (control) to 1096µm with 10% rock fragments and to 594µm with 25% rock fragments.

Unlike that observed with rock fragments of smaller size, for the treatment with rock fragments of 12-16mm size has been observed a positive trend of mean width of cracks with increasing concentrations of rock fragments. Mean width of cracks increased from 1514µm (control) to 1939µm after treatment with 10% rock fragments and to 2328µm with 25% rock fragments.

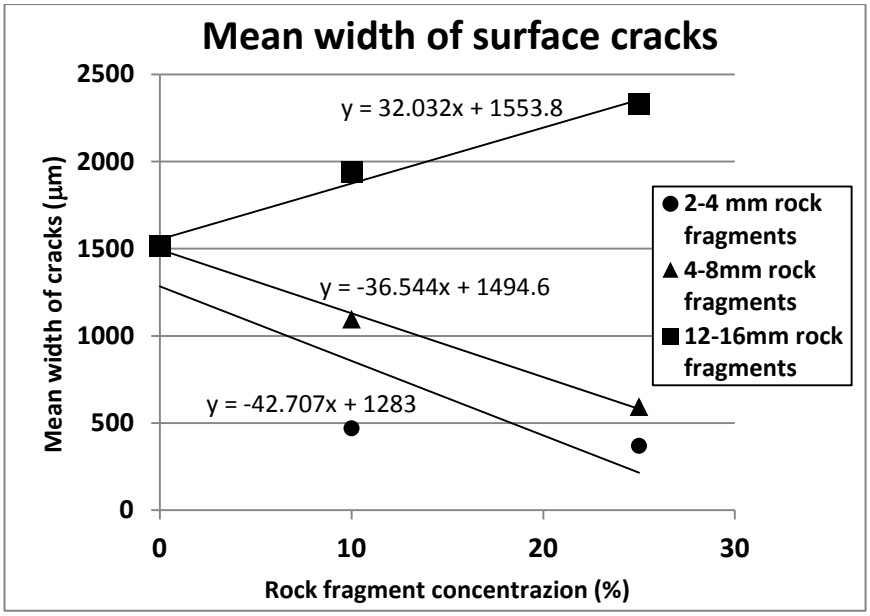

Figure 12. Comparison of mean width of surface cracks trends versus rock fragments concentration between Vertisol samples treated with different sizes of rock fragments.

In order to make an assessment of the effect of the shape of skeleton on soil pore development have been compared the results obtained for Vertisol samples treated with 10% by volume of rock fragments of 4-8 mm size and with 10% grass beads of comparable size (6mm). From the figure 13 it was observed that in both cases the cracking density increased compared to control (0.36%), but this increase was greater with the addition of 10% rock fragments (0.80%) than with 10% glass beads (0.70%). The reduction in mean width of cracks was similar following the addition of glass beads and rock fragments. In fact, the mean width of cracks decreased from 1514µm (control) to 1114µm with 10% glass beads and 1096µm with 10% rock fragments.

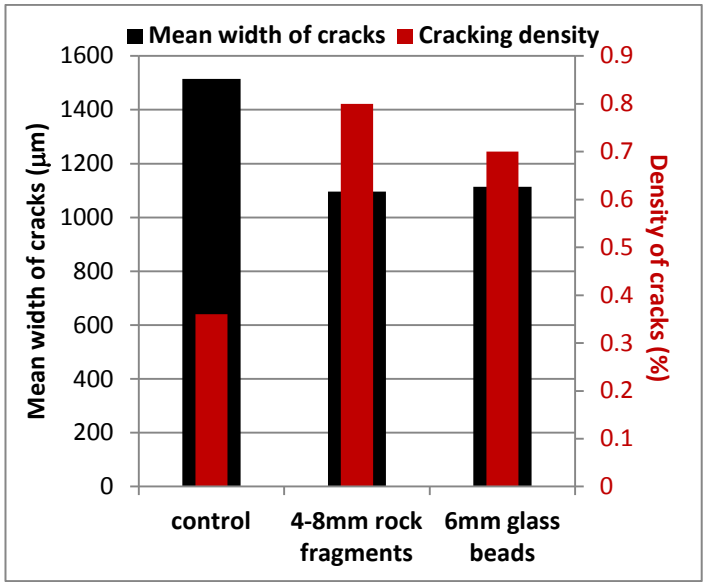

Figure 13. Comparison of cracking density and mean width of surface cracks variations between Vertisol samples treated with 10% rock fragments (4-8mm size) and 10% glass beads (6mm size).

4.4 Discussion

In this work it was possible to observe the different process of soil pore development in Vertisol and in Entisol soils, characterized by different shrinkage dynamics, after the addition of increasing concentrations of rock fragments and after 9 W/D cycles. Their different swelling-shrinkage dynamics during W/D cycles determined their different self structuring capacity and may explain the observed differences in total porosity and mean width of cracks between the controls for the two soils (fig. 4 and 5) .

Although similar values of cracking density were obtained for the controls for the two soils (fig. 6), actually from the figures 2 and 3 and from the PoSDs reported in figures 7 and 8 can be observed that soil pore system organization resulted very different for the two soils. In fact control of Entisol showed after 9 W/D cycles the formation of a soil pore system characterized by many sub-horizontal pores smaller than 160µm, while the control of Vertisol was characterized by a more complex soil structure with larger pores.

Different shrinkage-swelling dynamics of this two soils has also led to the different responses in terms of soil pore formation following the addition of increasing concentrations of rock fragments.

It was observed that the addition of rock fragments and the 9 W/D cycles induced a mechanism of pore development in both soils, but the magnitude of this development was different in the two soils.

The Vertisol, characterized by higher shrinkage-swelling dynamics resulted more reactive to the addition of rock fragment, both in terms of total porosity, mean width of pores, cracking density and pore size distribution. In fact, the values of slope of the trend lines obtained from these different measurements resulted larger than the values obtained for Entisol.

Total porosity of Vertisol samples in fact increased with increasing concentrations of rock fragments added. Pore development was determined by increased cracking density with increasing concentration of rock fragments. And this increase of porosity mainly involved small pores after the addition of 10% rock fragments, as has been possible to observe from the values of mean width of pores and from PoSD (fig.5 and 7). While with the addition of 25% rock fragments pore development regarded mainly large pores.

It was also observed that even in a soil characterized by poor self structuring properties, as the Entisol used in our experimental test, the addition of rock fragments induced a positive effect on pores development and thus on the formation of soil structure. In fact, in this soil, although to a lesser extent than the Vertisol, with increasing concentration of rock fragments was observed an increase in porosity.

In Entisol samples, even if there was a positive trend of the cracking process with increasing concentration, actually with the addition of 10% rock fragments was observed a reduction in cracking density. This reduction was probably due to an effect of substitution with rock fragments of sub horizontal microporosity present in the control. This phenomenon of reduction of porosity regarded pores lesser than 120μm, producing a consequent increase in mean width of pores compared to the control. The mean value of the width of pores was also greater than those observed in samples treated with higher concentrations of rock fragments, because in these samples prevailed the process of induction of new pores even in smaller pore size range.

With the addition of 25% and 35% rock fragments, was observed an increase in both the frequency of all pores size classes and in the mean width of pores. It was noted however, that respect to the concentration of 25% the cracking density did not increased further, but is slightly decreased, after the addition of 35% rock fragments, probably because the concentration of 35% rock fragments cannot induce a further development of cracks in the soil matrix, but began to prevail a substitution effect of pores with the solid phase of rock fragments.

The comparison between the network of cracks produced on the surface and in vertical section with to the addition of rock fragments in Vertisol samples showed in both cases the same positive trend of cracking density with increasing concentrations of rock fragments (fig. 9). Then rock fragments increased the cracking process of Vertisol not only in the internal structure of the soil but also on its surface. Although the trend is the same, however, have been recorded values of density of cracks highest in vertical section than in surface, and this result showed that the cracking process in Vertisol samples is more evident inside than on the soil surface.
It has been noted however that with increasing concentrations of rock fragments the mean width of pores decreased on the soil surface and instead increased in vertical section. Thus the increase of cracking density with increasing concentrations of rock fragments on the surface corresponded to an increase of small cracks, while in depth generally corresponded to an increase of larger cracks. The oscillation of this trend in the vertical section at the concentration of 10% of rock fragments can be explained, as mentioned above, by the largest increase of small pores.

Regarding the analysis of the network of cracks developed on the surface of Vertisol samples in figures 10 and 11 are reported two summary graphs that allow us to make some general remarks on the effect of size and concentration of rock fragments on the surface cracking density and on the mean width of surface cracks. The histogram in fig. 10 show that cracking density increased with increasing concentrations of rock fragments, and this increase became progressively smaller with increasing size of rock fragments. In fact, the density of cracks with the same concentration of rock fragments decreased with increasing rock fragment size.

With regard to the mean width of surface cracks in fig. 11 is shown that the mean width of cracks decreased with increasing concentrations of rock fragments of 2-4mm and 4-8mm sizes, increased with increasing concentrations of rock fragments of 12-16 mm size. With the same concentration of rock fragments the mean width of cracks increased with the size of rock fragments added.

So it can be stated that with the reduction of the size of rock fragments in the Vertisol it was observed the formation of a more complex network of surface cracks with a mean width of cracks gradually smaller.

4.5 Conclusion

In this work was evaluated the effect of increasing concentrations of rock fragments with different size in the formation of the pore system of soils characterized by different shrinkage-swelling dynamics.

The results obtained showed that the presence of the skeleton in two soils (a Vertisol and an Entisol) characterized by high and less shrinkage dynamics induced an increase of the soil pore development.

It was observed that the magnitude of this increase was dependent on the shrinkage and swelling dynamics of the two soils, resulting greater in the Vertisol characterized by higher shrinkage-swelling dynamics.

Actually also in the Entisol, characterized by poor self structuring properties, the addition of rock fragments induced a positive effect on the pores development and thus on the formation of soil structure.

The analysis of the network of cracks formed on the surface of Vertisol samples showed a clear influence of both concentration and size of rock fragments on the cracking process.

The results of the soil pore image analysis obtained in this work have shown that in order to make a comparison of the effect of rock fragments on the soil structure formation of two different soils is not sufficient to evaluate only the values of total porosity, but also measurements such as cracking density and mean width of pores, in addition to pore size distribution, can give an important contribution to the

quantitative understanding of the mechanisms of structure formation induced by stones in the soil.

5. Soil fauna activity and soil structure: characterization by micromorphological image analysis

5.1 Introduction

The soil biological communities are characterized by higher diversity, by several orders of magnitude, compared to aboveground biomass(Heywood, 1995). Soil fauna and plant roots play an important role in the formation and stabilization of soil structure.

In organic horizons, soil fauna exert a profound influence on the soil structure. Their excrement (faecal pellets) constitute most of the microaggregates in organic horizons (Babel, 1975; Ponge, 1991; Barois et al., 1998; Phillips and Fitzpatrick, 1999). Faecal materials can accumulate to such an extent that they dominate the horizons.

Also known as ‘‘ecosystem engineers’’ (Jones et al., 1994), earthworms produce structural features at three different scales of soil porosity. Much work deals with the characterization of burrow networks created by earthworm species (Capowiez et al., 1998; Jégou et al., 1999). In relation to macropore space (>1 mm), burrow networks act as preferential flow paths (Bouché and Al-Addan, 1997). At a smaller scale, earthworms may change the pore space between mineral and organic particles, i.e. the microporosity, and the stability of soil structure (Blanchart et al., 1993; Chauvel et al., 1999). In cultivated soil at low level of earthworm densities, the enchytraeids can play an important role in creating a stable soil structure and porosity (Topoliantz et al., 2000).

Micromorphological techniques provide an excellent tool to understand the role of soil fauna and their impact on an array of soil properties since evidence of animal activities such as burrowing and deposition of excrement (faecal pellets) can be identified and quantified (Kooistra et al., 2010). Fauna-induced features are found in all types of soils and can be so abundant that they determine the nature and intensity of active physical and chemical processes.

For many years, soil organisms, particularly in organic horizons, have been studied micromorphologically. For example Bal (1970) investigated the extent to which soil fauna influenced the development of humus profiles under two contrasting tree types.

Righi et al. (1982) stated that soil fauna influence the structure of the spodic horizon. In 1991 Kooistra illustrated the specific micromorphological techniques used to study interactions between soil structure and soil biota. Dawod and FitzPatrick (1993) studied the effects of enchytraeid populations on the structure of some Scottish soils. These previous works performed qualitative interpretations of the faunal influence on the soil structure (VanderBygaart et al., 2000). A movement toward a quantitative estimate in two dimension of the influence of earthworm activity on soil structural attributes of shape and size was performed by VanderBygaart et al. (2000) that proposed a method for estimating earthworm-influenced soil structure using techniques in morphometric image analysis of soil micromorphology. They compiled a learning set of mammillated vughs, the pores most likely developed by the burrowing of earthworms.

Davidson et al. (2002, 2006) presented results of a project designed to investigate the interactions between the activity of fauna and soil structure based on the investigation of excremental pedofeatures by means micromorphological and image analysis. In this project they used a protocol for image analysis (Bruenau et al, 2004) developed to segment void space and excremental features. The method consisted in to separate areas dominated by small features (dominantly enchytraeid excrement) from those dominated by large features. Moreover they measure only two types of pores: large voids (>1000μm^2) and small voids (50-500μm^2).

The aim of this preliminary work was to use a micromorphological image analysis approach in order to discriminate and to quantify the effect of different biological features on soil structure formation. In particular, to provide an additional contribution to the results of previous works that used micromorphological image analysis, we used an image analysis approach based on mathematical morphology that allowed to quantify the contribution of different biological activities on size distribution of both pore and solid phase.

5.2 Material and method

Using a large collection of soil thin sections from organic horizons of different soils, microsites with specific features of biological activities were detected. The approach used to characterize biological pedofeatures is based on the work of Babel (1975), Bullock et al. (1985) and Fitzpatrick (1993).

The images of the areas of thin sections where the biological features have been identified were acquired under transmitted light (TL) and circular polarized light (CPL) with a resolution of 7µm.

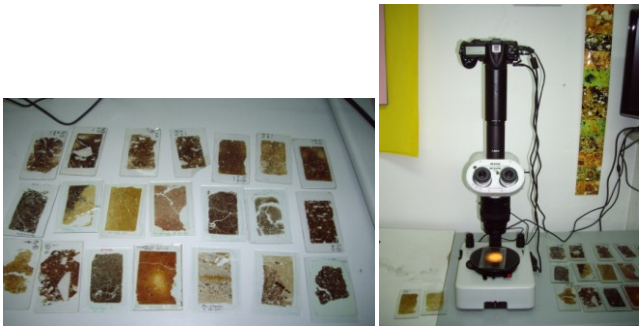

Figure 1. Soil thin sections analysed and optical microscopy with digital camera for the acquisition of digital images.

The difference between the two images acquired under two different lights was obtained in order to discriminate between pores and mineral grains that appeared as pores in transmitted light.

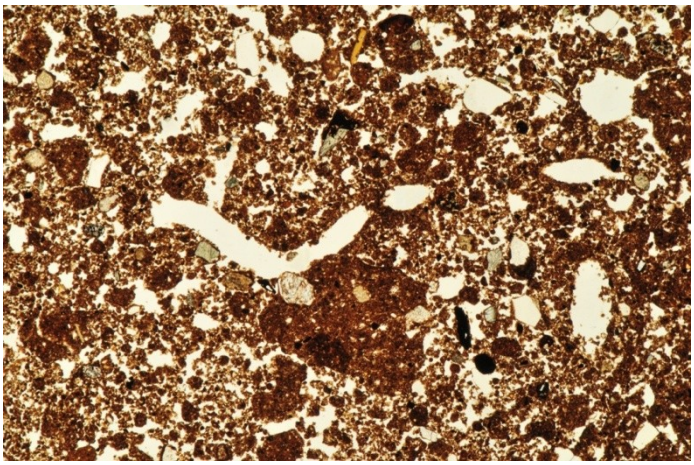

Figure 2. Digital image acquired under transmitted light.

Figure 3. Digital image acquired under circular polarized light.

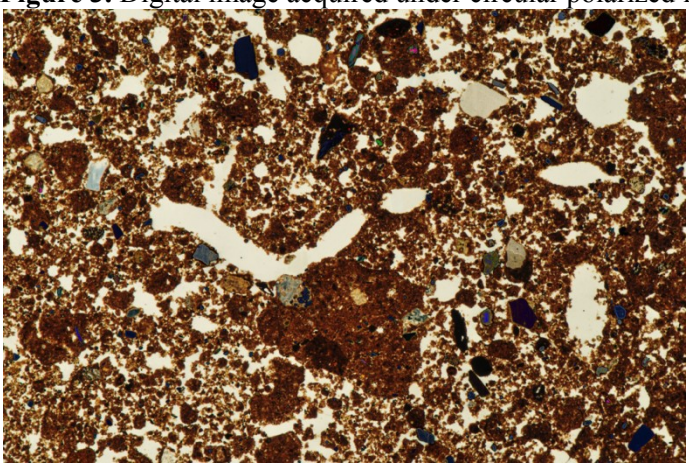

Figure 4. The image obtained from the difference between the two images acquired under two different lights.

Each biological feature was characterized by morphometric object analysis using Image-Pro Plus 6.0, in order to calculate its morphometric parameters.

The following morphometric parameters were measured:

- Aspect: ratio between major axis and minor axis of ellipse equivalent to object.
- Area/Box: ratio between area of object and area of its bounding box.
- Radius ratio: ratio between maximum radius and minimum radius.
- Roundness: (perimeter^2)/(4*π*area).

The difference images were segmented using a technique of supervised "thresholding" using Corel Photo-Paint X3, in order to obtain binary images where the two separate solid and pore phases are in black and white, respectively. Successively they were analysed. Pore size distribution was determined by image

analysis using Micromorph 1.4, through the application of the "successive opening" algorithm (Horgan, 1998), which classifies the pore phase according to the spacing from the walls. Using the inverted images in which solid and pore phases are in white and black respectively, aggregate size distribution was determined with the same procedure used for the porous phase.

Pore size distribution and aggregate size distribution were determined for the total image and for each specific biological feature identified.

5.3 Results and discussion

5.3.1 Identification and characterization of biological features

From the observation of thin sections were identified and analyzed five common biological features: excrements of earthworm and enchytraeids, faecal pellets characterized by excrements of beetle larvae and enchytraeids, soil fauna burrows and fragments of plant roots.

Below are reported the images obtained from the difference between the two digital images acquired from the thin sections under TL and CPL lights. And in the following tables are reported the mean values of morphometric parameters obtained by means object analysis of each biological feature.

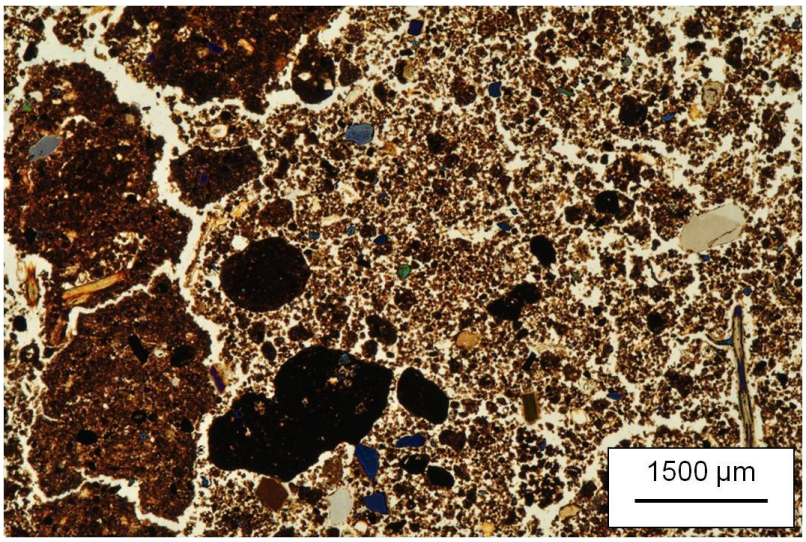

Figure 5. Difference image of soil thin section with excrement of earthworm and enchytraeids.

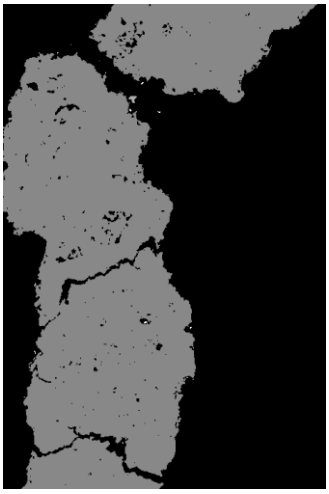

Morphometric parameter	Mean value
Area (μm^2)	2857220
Aspect	1.39
Area/Box	0.61
Mean Diameter (μm)	1573
Holes	23.50
Radius Ratio	2.14
Roundness	4.94

Figure 6 Results of the object analysis performed on the excrements of earthworm.

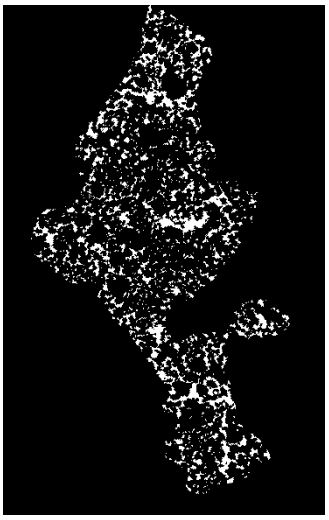

Morphometric parameter	Mean value
Area (μm^2)	4226
Aspect	1.65
Area/Box	0.67
Mean Diameter (μm)	71
Holes	0
Radius Ratio	2.35
Roundness	1.16

Figure 7. Results of the object analysis performed on the excrements of enchytraeids.

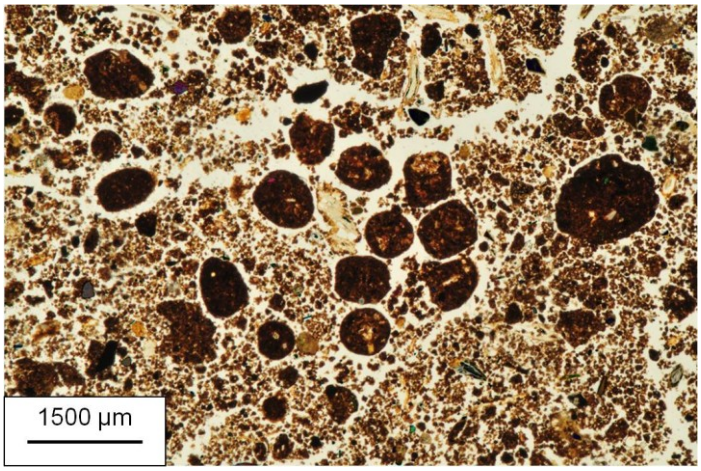

Figure 8 Difference image of soil thin section with excrement of beetle larvae and enchytraeids.

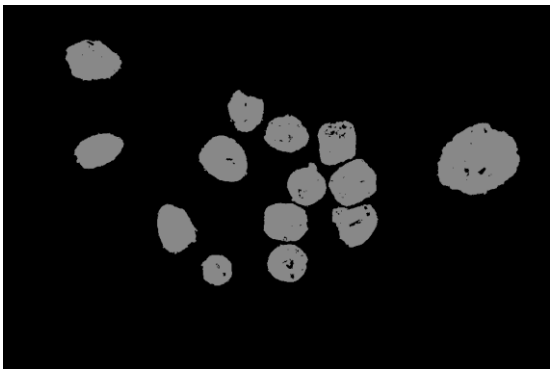

Morphometric parameter	Mean value
Area (µm^2)	287869
Aspect	1.20
Area/Box	0.72
Mean Diameter (µm)	586
Holes	7.71
Radius Ratio	1.44
Roundness	2.56

Figure 9 Results of the object analysis performed on the beetle larvae excrements.

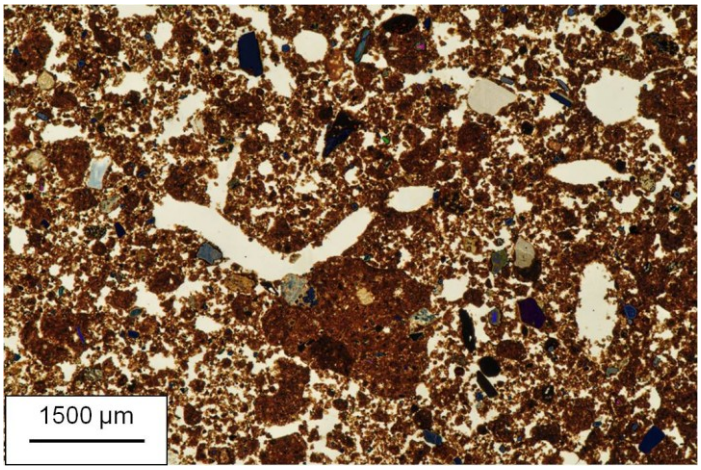

Figure 10. Difference image of soil thin section with soil fauna burrows.

Morphometric parameter	Mean value
Area (μm^2)	711040
Aspect	3.33
Area/Box	0.31
Mean Diameter (μm)	1220
Holes	4
Radius Ratio	7.50
Roundness	9.24

Figure 11. Results of the object analysis performed on the soil fauna burrow.

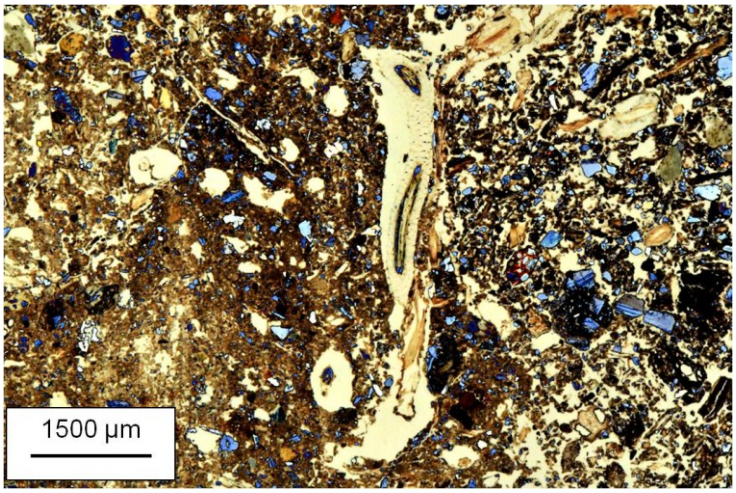

Figure 12. Difference image of soil thin section with fragments of plant roots.

Morphometric parameter	Mean value
Area (μm^2)	1464809
Aspect	6.90
Area/Box	0.28
Mean Diameter (μm)	1087
Holes	114
Radius Ratio	17.29
Roundness	82.66

Figure 13 Results of the object analysis performed on the longitudinal section of plant roots.

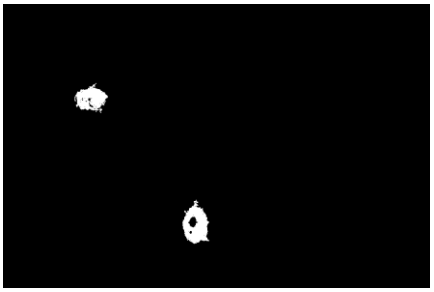

Morphometric parameter	Mean value
Area (μm^2)	168683
Aspect	1.42
Area/box	0.54
Mean Diameter (μm)	477
Holes	5.50
Radius Ratio	1.99
Roundness	6.45

Figure 14 Results of the object analysis performed on the transversal section of plant roots.

The morphometric parameters determined by the object analysis that better describe specific morphological characteristics of different biological features and that allow to discriminate among different biological features are resulted "aspect" for the longitudinal section of plant roots fragments, "radius ratio" for the soil fauna burrow and "roundness" for excrements of beetle larvae and of enchytraeids. These parameters can be used to discriminate among different biological activities in the soil thin section and can be usefully chosen as filter to try procedures of automatic segmentation.

5.3.2 Contribution of biological features to soil structure

Image analysis performed on the whole soil thin section containing biological features and on the specific areas characterized only by the presence of biological features have allowed to obtain pore size distribution and aggregate size distribution related to both the total section and to the biological features specifically.

The results have allowed to determine the contributions of different biological features to pore size distribution and aggregate size distribution of the total area of thin section analyzed.

In Fig. 15 is shown the pore size distribution of the area of soil thin section containing earthworm and enchytraeids excrements. It can be seen that packing pores within cast deposits of enchytraeids contribute to the porous phase characterized by pore sizes between 14μm and 84μm, and especially pores of 14-42μm size. The pores around excrements of earthworms contribute to the pore size classes in the 14-210μm range. In particular, the presence of earthworms excrements produces pores larger than 168μm.

Therefore the production of casts by enchytraeids contributes mainly to the presence of micropores in the size range 14-42µm, still present in the soil analyzed. As you can see from the second mode of the pore size distribution in fig.15, pore size classes larger than 168µm are characterized only by pores produced by earthworms. Therefore the presence of earthworms casts results in the formation of pores that otherwise would not be present in the soil matrix analyzed and contributes to the multimodality of the PoSD.

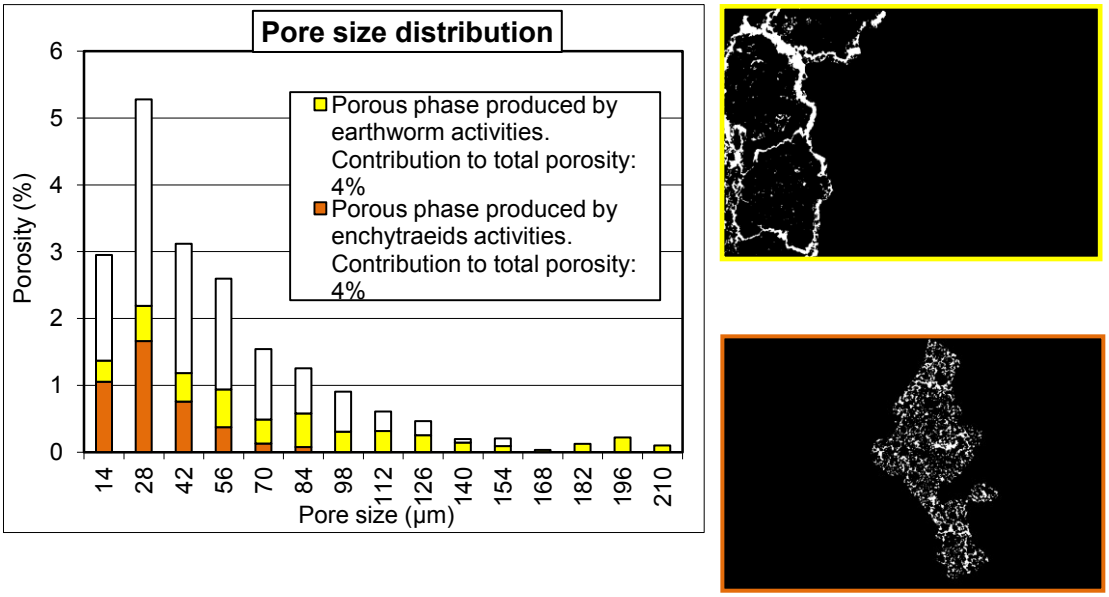

Figure 15. Contribution to pore size distribution of earthworm and enchytraeids activity. In white is reported the remaining porosity that cannot be attributed to the presence of biological features identified. Total porosity of the total image: 20%.

In Fig. 16 is reported the aggregate size distribution obtained from the image analysis of the area of soil thin section containing earthworms and enchytraeids excrements. Can be observed that the solid phase of 1232-1428µm size range is characterized exclusively by earthworms casts. Then they determine the formation of aggregates larger than 1232µm that would lack in the absence of earthworms in this soil.

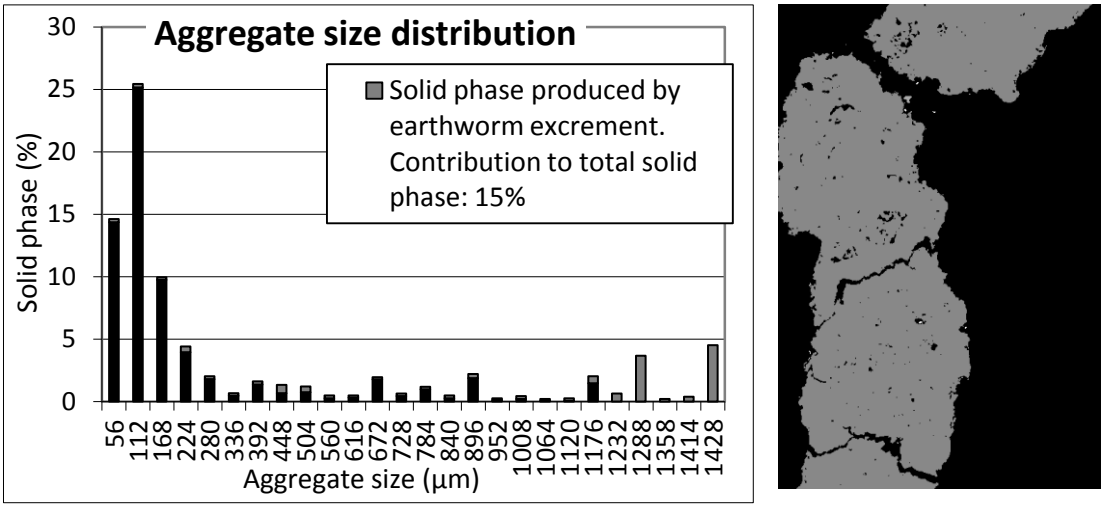

Figure 16. Contribution to aggregate size distribution of earthworm excrements. In black is reported the remaining solid phase that cannot be attributed to the presence of biological features identified. Total solid phase of the total image: 80%.

In Fig. 17 is shown the pore size distribution of the area of soil thin section containing beetle larvae and enchytraeids excrements. Is possible to observe that packing pores within enchytraeids casts contribute to the porous phase in the 14-98µm pore size range. And pores among excrements of beetle larvae contribute to pore sizes classes between 14 and 210µm. In particular they contribute to the pores of 112-154µm size.

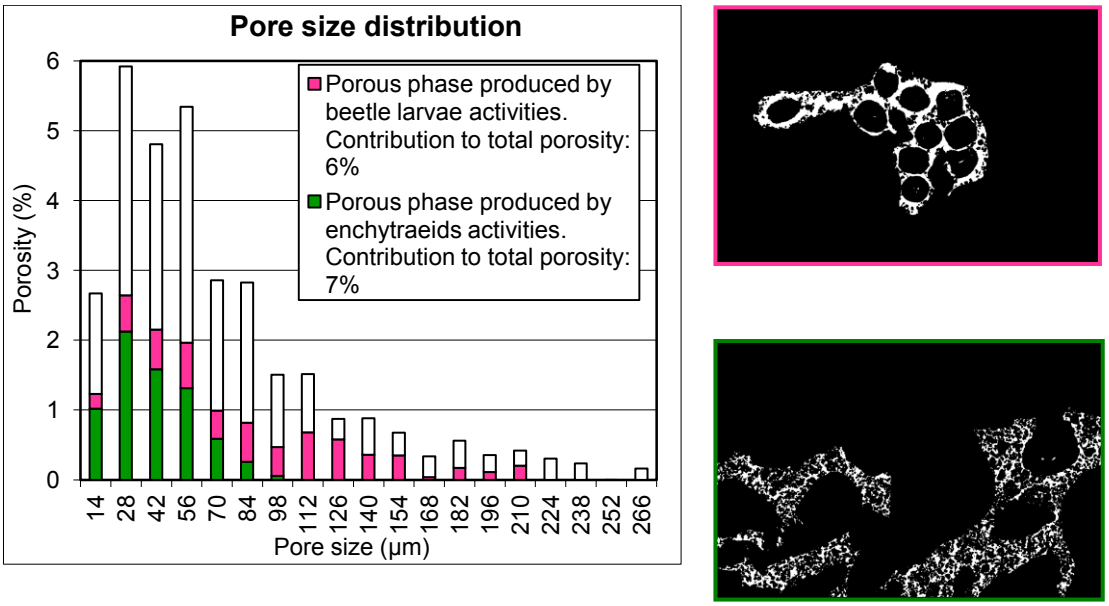

Figure 17 Contribution to pore size distribution of beetle larvae and enchytraeids activity. In white is reported the remaining porosity that cannot be attributed to the presence of biological features identified. Total porosity of the total image: 32%.

It was then observed that the presence of excrements of different soil organisms contributes to the formation of pores in different size ranges. Consequently, as can be seen from figures 15 and 17 the presence of different organisms in the same soil, such as earthworms and enchytraeids or beetle larvae and enchytraeids, may contribute to the multimodality of the pore size distribution.

In fig.18 is reported the aggregate size distribution of the area of soil thin section containing beetle larvae and enchytraeids excrements. It is possible to observe that the beetle larvae excrements represent the majority of aggregates of sizes between 392 and 560µm in the analyzed area of thin section. They determine the presence of the second mode visible in the aggregate size distribution (fig. 18) of the area of thin section analyzed. Thus they contribute to the multimodality of the aggregate size distribution.

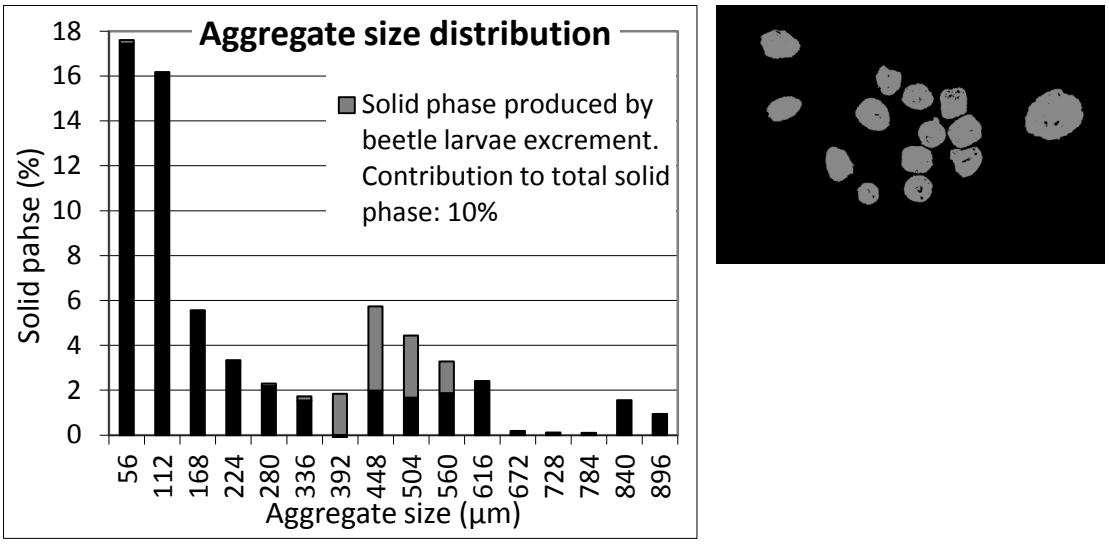

Figure 18 Contribution to aggregate size distribution of beetle larvae excrements. In black is reported the remaining solid phase that cannot be attributed to the presence of biological features identified. Total solid phase of the total image: 68%.

In fig.19 is shown the pore size distribution of the area of soil thin section characterized by the presence of soil fauna burrowing activity. It is possible to observe that the burrowing activity of organisms in the soil has resulted in the formation of pores with size between 14 and 490µm. In particular pore size classes larger than 238µm are characterized almost exclusively by faunal burrows. The burrowing activities of organisms leads to the formation of pores having width of

238-294µm and 406µm and 490µm that otherwise would not be present in the soil matrix analyzed. Therefore soil fauna burrows increase the multimodality of PoSD.

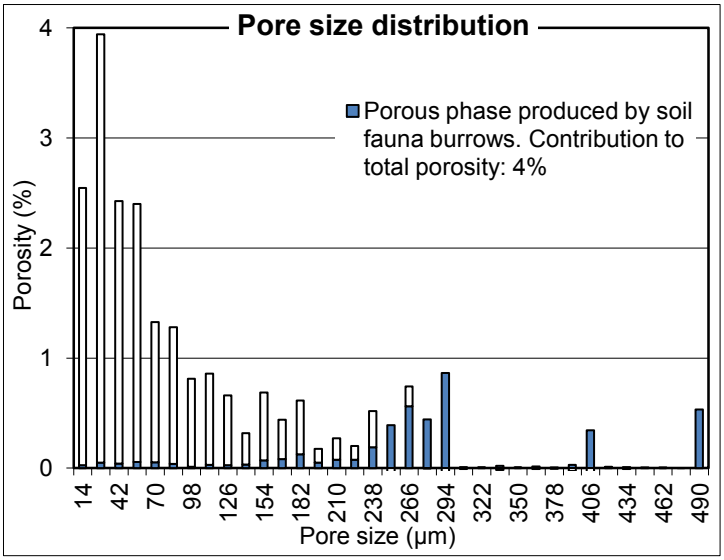

Figure 19 Contribution to pore size distribution of soil fauna burrowing activity. In white is reported the remaining porosity that cannot be attributed to the presence of biological features identified. Total porosity of the total image: 22%.

In Fig. 20 is reported the pore size distribution of the area of soil thin section characterized by the presence plant roots fragments. Is possible to assess the contribution of the transversal and longitudinal sections PoSD of plant roots fragments. Longitudinal section of plant roots fragments produce pores in the range 14-392µm, and in particular the pores larger than 210µm are produced only by plant root fragments. Transversal section of plant roots fragments produce pores of 238µm.

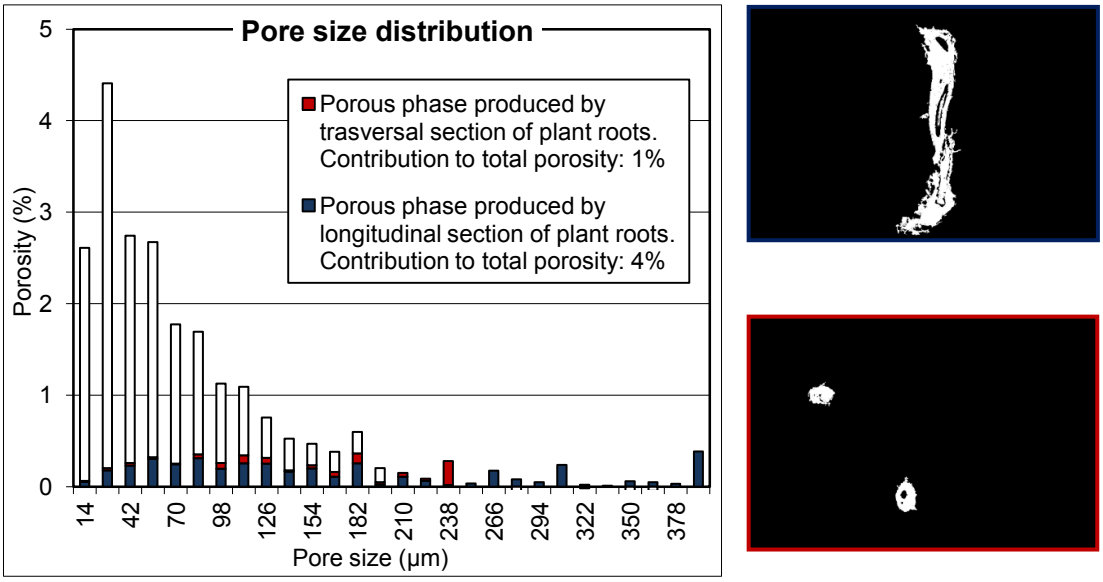

Figure 20. Contribution to pore size distribution of plant roots fragments. In white is reported the remaining porosity that cannot be attributed to the presence of biological features identified. Total porosity of the total image: 22%.

The soil structure is more complex and therefore consists of different habitats with increasing number of different pores size classes. Consequently, the quantification of the contribution of different organisms to the formation of pores and aggregates of different sizes allows a better understanding of their role in the development of soil structure.

For example, results reported above have shown that the presence of excrements of different soil organisms contributes to the formation of pores in different size ranges. As you can see from figures 15 and 17, the presence of different organisms in the same soil, such as earthworms and enchytraeids or beetle larvae and enchytraeids, may contribute to the multimodality of the pore size distribution, and thus to the heterogeneity of the soil pore system.

Also the burrowing activity of soil fauna in the soil thin section analysed contribute to the heterogeneity of the soil pore system increasing the multimodality of the pore size distribution (fig.19).

Earthworm excrements contribute to increasing the multimodality, and thus the complexity, not only of the pore size distribution but also of the aggregate size

distribution of the soil analyzed. And also casts of beetle larvae produce a mode in the aggregate size distribution of the soil matrix analyzed.

In soil thin section analyzed the presence of excrements of earthworm and beetle larvae induce pores development in the same size range, but they produce more specific signals in the aggregate size distribution, therefore in some cases morphometry of solid phase is more useful to discriminate the contribution of different organisms to soil structure.

Moreover, results showed, overall, that the contribution to the porosity due to biological activity can be easier detected when it produces large pores, but specific contribution in pore size distribution are also present in the micropore range, as in the case of enchytraeids activity.

5.4 Conclusion

The micromorphological image analysis approach used in this work allowed to discriminate the contribution of different biological activities to the soil structure. First of all these different biological features have been identified: excrements of earthworms and enchytraeids, faecal pellets characterized by excrements of beetle larvae and enchytraeids, soil fauna burrows and fragments of plant roots.

Successively have been quantified specific contributions to pore size distribution attributable to the presence of fragment of plant roots, soil fauna burrows and faecal pellets of enchytraeids, earthworm and beetle larvae.

It is important to emphasize that the results showed that the combination of different biological activities in the same soil produce a pronounced multimodal pore size distribution; this finding is much important for the fertility of soils.

It was observed that the image analysis of solid phase also can be used to discriminate the effects of different biological activities on soil structure. In fact for example excrements of beetle larvae and of earthworms produce more specific signals in aggregate size distribution, than in pore size distribution.

6. Conclusions

The importance of soil structure for terrestrial ecosystems is well known. A large bulk of scientific literature addresses factors influencing soil structure and soil pore development, but little is still known concerning the underlying physical mechanisms of their action. In this work, whose chapters are organized as collection of papers, we attempted to investigate physical mechanisms of soil pore development by means an experimental approach using soil 2D image analysis and standard soil micromorphology.

After the first introductory chapter, the second one investigates some problems related to the acquisition stage of image analysis in order to provide a contribution to the standardization of this procedure. The results obtained, although still far from providing a standardized procedure may be used as guidelines or recommendations that should be followed during the digital acquisition of image analysis.

The experimental work reported in the third chapter was performed by means of the addition of calcium carbonate ($CaCO_3$) and iron (Fe) oxides on three simplified soil-like systems in which soil structure formation was induced by several wetting and drying cycles. The obtained results showed changes in the pore size distribution, in some cases very large, and allowed the identification of specific mechanisms of pore modification induced by Fe and micrite pedofeatures produced by the mobilization in suspension of Fe oxides and $CaCO_3$. Our results, even if obtained on simplified substrates, give a contribution in the understanding of the physical role of $CaCO_3$ and Fe oxides pedofeatures in pore formation in real soils.

The second experimental work, reported in the fourth chapter was performed in order to investigate the effect of the interaction between different sizes and concentrations of rock fragments and soils with different shrinkage-swelling dynamics on the mechanisms of soil structure formation.

The results obtained showed that the presence of the gravel material in two soils (a Vertisol and an Entisol) characterized by high and less shrinkage dynamics induced an increase of the soil pore development. It was observed that the magnitude of this increase was dependent on the shrinkage and swelling dynamics of the two soils,

resulting greater in the Vertisol characterized by higher shrinkage-swelling dynamics. Actually also in the Entisol, characterized by poor self structuring properties, the addition of rock fragments induced a positive effect on the pores development and thus on the formation of soil structure. These results highlighted the contribution of rock fragments in soil pore development.

It was observed that the micromorphological image analysis approach proposed in the technical note reported in the fifth chapter allowed to discriminate the contribution of different biological activities to pore size distribution and aggregate size distribution. Although this approach can be further ameliorated it is important to emphasize that the results demonstrate the possibility to quantify the combined contribution of different biological activities to the formation of a pronounced multimodal pore size distribution; which is an indicator of high physical quality important for the fertility of soils.

Overall the results of the thesis highlighted the enormous potential of the experimental tests in pots combined with soil micromorphology and image analysis techniques for understanding the mechanisms of development of soil structure and showed the need to reassess physical simulation tests in order to quantitatively investigate combined effects of factors influencing soil structure formation.

Bibliography

Abrahams, A.D. & Parsons, A.J. 1991. Relation between infiltration and stone cover on a semiarid hillslope, southern Arizona. Journal of Hydrology, 122, 49–59.

Agassi, M. & Levy, G.J. 1991. Stone-cover and rain intensity: effects on infiltration, erosion and water splash. Australian Journal of Soil Research, 29, 565–575.

Ajmone Marsan, F., Pagliai, M., Pini, R. 1994. Identification and properties of fragipan soils in the Piemonte Region (Italy). Soil Sci. Soc. Am. J. 58, 891-900.

Angers, D.A., Caron, J., 1998. Plant-induced changes in soil structure. Applied Soil Ecology 10, 11-19.

Arduino, E., Barberis, E., Boero, V., 1989. Iron oxides and particle aggregation in B horizons of some Italian soils. Geoderma 45, 319–329.

Babel, U., 1975. Micromorphology of soil organic matter. In: Gieseking, J.E. (Ed.), Soil Components, Vol. 1. Organic Components. Springler, Berlin, pp. 369–473 (Chapter 4).

Baghernejad, M., Dalrymple JB., 1993. Colloidal suspensions of calcium-carbonate in soils and their likely significance in the formation of calcic horizons. Geoderma. 58, 17-41.

Bal, L., 1970. Morphological investigation in two moder-humus profiles and the role of the soil fauna in their genesis. Geoderma 4, 5–36.

Barois, I., Dubroeucq, D., Rojas, P., Lavelle, P., 1998. Andosolforming process linked with soil fauna under the perennial grass Mulhembergia mascroura. Geoderma 86, 241–260.

Barral, M.T., Arias M., Guerif J. 1998. Effects of iron and organic matter on the porosity and structural stability of soil aggregates. Soil Till. Res. 46, 261-272.

Bartoli, F., Genevois-Gomendy, V., Royer, J.J., Niquet, S., Vivier, H. & Grayson, R. 2005. A multiscale study of silty soil structure. European Journal of Soil Science, 56, 207–224.

Baveye, P., Rogasik, H., Wendroth, O., Onasch, I., Crawford, J.W., 2002. Effect of sampling volume on the measurement of soil physical properties: simulation with X-ray tomography data. Measurement Science & Technology 13, 775–784.

Bear, J., 1972. Dynamics of Fluids in Porous Media. Elsevier, New York, NY, USA, 764 pp.

Bear, J., Bachmat, Y., 1984. Transport phenomena in porous media—basic equations. In: Bear, J., Corapeioglu, M.Y. Eds.., Fundamentals of Transport Phenomena in Porous Media. NATO ASI Series, M. Nijhoff, Dordrecht.

Bignell, D.E., Holt, J.A., 2002. Termites. In: Lal, R. (Ed.), Encyclopedia of Soil Science. Marcel Dekker, New York, NY, pp. 1305–1307.

Blanchart, E., Bruand, A., Lavelle, P., 1993. The physical structure of casts of Millosonia anomala (Oligochaeta: Megascolecidae) in shrub savanna soils (Coˆte d'Ivoire). Geoderma 56, 119– 132.

Bockheim, J.G. Gennadiyev, A.N., 2009. The value of controlled experiments in studying soil-forming processes: A review. Geoderma, 152: 208–217

Boix-Fayos, C., Calvo-Cases, A., Imeson, A.C., Soriano-Soto, M.D. 2001. Influence of soil properties on the aggregation of some Mediterranean soils and the use of aggregate size and stability as land degradation indicators. Catena. 44, 47-67.

Bouché, M.B., Al-Addan, F., 1997. Earthworms, water infiltration and soil stability: some new assessments. Soil Biology & Biochemistry 29, 441– 452.

Bouma, J. 1990. Using morphometric expressions for macropores to improve soil physical analyses of field soils. Geoderma. 46, 3-11.

Brakensiek, D.L. & Rawls, W.J. 1994. Soil containing rock fragments: effects on infiltration. Catena, 23, 99–110.

Bresson, L.M., Moran, C.J., 2003. Role of compaction versus aggregate disruption on slumping and shrinking of repacked hardsetting seedbeds. Soil Science 168, 585–594.

Bronick, C.J. and Lal, R. 2005. Soil structure and management: a review. Geoderma. 124, 3 –22.

Brown, G.G., Barois, I., Lavelle, P., 2000. Regulation of soil organic matter dynamics and microbial activity in the drilosphere and the role of interactions with other edaphic functional domains. Eur. J. Soil Biol. 36, 177–198.

Bruneau P. M.C., Davidson D. A., Grieve, I. C., 2004. An evaluation of image analysis for measuring changes in void space and excremental features on soil thin sections in an upland grassland soil. Geoderma 120:165–175.

Bullock, M.S., Kemper, W.D., Nelson, S.D., 1988. Soil cohesion as affected by freezing water content, time and tillage. Soil Sci. Soc. Am. J. 52, 770–776.

Bullock, P. and Thomasson, A.J., 1979. Rothamsted studies of soil structure, II. Measurement and characterization of macroporosity by image analysis and comparison with data from water retention measurements. J. Soil Sci., 30:391-413.

Bullock, P., Fedoroff, N., Jongerius, A., Stoops, G., Tursma, T., Babel, U., 1985. Handbook for Soil Thin Section Description. Waine Research Publications, Wolverhampton.

Capowiez, Y., Pierret, A., Daniel, O., Monestiez, P., Kretzschmar, A., 1998. 3D skeleton reconstructions of natural earthworm burrow systems using CAT scan images of soil cores. Biology and Fertility of Soils 27, 51– 59.

Carof, M.S. de Tourdonnet, Y. Coquet, V. Hallaire & J. Roger-Estrade, 2007. Hydraulic conductivity and porosity under conventional and no-tillage and the effect of three species of cover crop in northern France. Soil Use and Management, 23: 230–237.

Cattle, S.R., Farrell, R.A., McBratney, A.B., Moran, C.J., Roesner, E.A., Koppi, A.J., 2000. Solicon – PC Version 1.0. The University of Sidney and Cotton Research and Development Corporation.

Cerda`, A. 2001. Effects of rock fragment cover on soil infiltration, interrill runoff and erosion. European Journal of Soil Science, 52, 59–68.

Chantigny M.H., Angers D.A., Prévost D., Vèzina L-P e Chalifour F-P.,1997. Soil aggregation and fungal and bacterial biomass under annual and perennial cropping systems. Soil Sci. Soc. Am. J., 61: 262-267.

Chauvel, A., Grimaldi, M., Barros, E., Blanchart, E., Desjardins, T., Sarrazin, M., Lavelle, P., 1999. An Amazonian earthworm compacts more than a bulldozer. Nature 398, 32– 33.

Chenu, C., Le Bissonnais, Y., Arrouays, D., 2000. Organic matter influence on clay wettability and soil aggregate stability. Soil Sci. Soc. Am. J. 64, 1479–1486.

Colombo, C. and Torrent, J. 1991. Relationships between aggregation and iron oxides in Terra Rossa soils from southern Italy. Catena. 18, 51-59.

Czarnes S., Hallett P.D.,Bengough A.G. & Young I.M., 2000. Root- and microbial-derived mucilages affect soil structure and water transport. European Journal of Soil Science 51: 435-443.

Dagesse D., 2011.Effect of freeze-drying on soil aggregate stability. Soil Science Society of America Journal, 75: 2111-2121.

Dathe, A., Baveye, P., 2003. Dependence of the surface fractal dimension of soil pores on image resolution and magnification. European Journal of Soil Science 54, 453–466.

Davidson, D.A., Bruneau, P.M.C., Grieve, I.C., Young, I.M., 2002. Impacts of fauna on an upland grassland soil as determined by micromorphological analysis. Appl. Soil Ecol. 20, 133–143.

Davidson, D.A., Grieve, I.C., 2006. Relationships between biodiversity and soil structure and function: Evidence from laboratory and field experiments. Applied Soil Ecology 33: 176–185.

Dawod, V., FitzPatrick, E.A., 1993. Some population sizes and effects of the Enchytraeidae (Oligochaeta) on soil structure in a selection of Scottish soils. Geoderma 56, 173–178.

Day, P.R. 1965. Particle fractionation and particle-size analysis. In: Black, C.A. (ed.), Methods of Soil Analysis, Part 1: American Society of Agronomy. Soil Science Society of America, Inc. Madison, Wisconsin, pp. 545-567.

Dexter, A.R., 1988. Advances in characterization of soil structure. Soil Tillage Res., 11: 199-238.

Dexter, A.R., Richard, G. 2009. The saturated hydraulic conductivity of soils with n-modal pore size distributions. Geoderma. 154, 76–85.

Díaz-Zorita, M., Perfect, E., Grove, J. H. 2002. Disruptive methods for assessing soil structure. Soil Till. Res. 64, 3-22.

Dunkerley, D.L. 1995. Surface stone cover on desert hillslopes: parameterizing characteristics relevant to infiltration and surface runoff. Earth Surface Processes & Landforms, 20, 207–218.

Duwig, C., Delmas, P., Muller, K., Prado, B., Morin, H., Ren, K., 2008. Quantifying fluorescent tracer distribution in allophanic soils to image solute transport. European Journal of Soil Science 59, 94–102.

Edwards, A.P., Bremner, J.M.,1967. Microaggregates in soils. J. Soil Sci., 18:64–73.

Edwards, C.A., Bohlen, P.J., 1996. Biology and Ecology of Earthworms. Chapman & Hall, London, 426 pp.

Elliot, T.R., Heck, R.J., 2007. A comparison of optical and X-ray CT technique for void analysis in soil thin section. Geoderma 141, 60–70.

El-Swaify S. A., Emerson, W. W. 1975. Changes in the Physical Properties of Soil Clays Due to Precipitated Aluminum and Iron Hydroxides: I. Swelling and Aggregate Stability After Drying. Soil Science Society of America Journal, 39: 1056-1063.

Falsone, G., Catoni, M., Bonifacio, E. 2010. Effects of calcite on the soil porous structure: natural and experimental conditions. Agrochimica. 54, 1 -12.

Fies J.C.; De Louvigny N.; Chanzy A. 2002. The role of stones in soil water retention. European Journal of Soil Science, 53: 95-104.

Fisher, C., 1971. The new quantimet 720. The Microscope 19, 1–20.

Fitzpatrick, E.A. 1993. Soil Microscopy and Micromorphology. Wiley, Chichester.

FitzPatrick, E.A., 1984. Micromorphology of Soils. Chapman and Hall, London, 433 pp.

Francis, G.S., Fraser, P.M., 1998. The effects of three earthworm species on soil macroporosity and hydraulic conductivity Applied Soil Ecology 10, 11-19

Gale, W.J., Cambardella, C.A., Bailey, T.B., 2000. Root-derived carbon and the formation and stabilization of aggregates. Soil Sc. Soc. Am. J. 64, 201-207.

Gargiulo, L. 2008. Indagini innovative sulla strutturazione del suolo. Graduation thesis in Applied Pedology, University Federico II of Naples.

Gile, L.H., Peterson, F.F., Grossman, R.B. 1966. Morphological and genetic sequences of carbonate accumulation in desert soils. Soil Sci. 101, 347-360.

Głab, T., Kulig, B., 2008. Effect of mulch and tillage system on soil porosity under wheat (Triticum aestivum). Soil & Tillage Research 99, 169–178.

Gleton, W.G.and Dani, O. 2002. Particle-Size Analysis. In: Dane, J.H., Topp G.C. (Eds.), Methods of Soil Analysis. Part 4 Physical Methods SSSA Book Ser. 5. Soil Science Society of America. Inc. Madison, WI, pp. 255-288.

Groenevelt, P.H. and Grant, C.D. 2004. Analysis of soil shrinkage data. Soil Till. Res. 79, 71-77.

Gulser, C., 2006. Effect of forage cropping treatments on soil structure and relationship with fractal dimensions. Geoderma 131, 33-44.

Heywood V.H., 1995. Global Biodiversity Assessment. Cambridge University Press, Cambridge.

Hillel, D. 1980. Fundamentals of soil physics. Academic Press, New York.

Holt, J.A., Lepage, M., 2000. Termites and soil properties. In: Abe, T., Bignell, D.E., Higashi, M. (Eds.), Termites: Evolution, Sociality, Symbioses, Ecology. Kluwer Academic Publishers, Dordrecht, pp. 389–407.

Horgan, G.W. 1998. Mathematical morphology for analyzing soil structure from images. Eur. J. Soil Sci. 49, 161-173.

Horn, R., Taubner, H., Wuttke, M., Baumgartl, T. 1994. Soil physical properties related to soil structure. Soil Till. Res. 30, 187-216.

Hubert, F., Hallaire, V., Sardini, P., Caner, L., Heddadj, D., 2007. Pore morphology changes under tillage and no-tillage practices. Geoderma 142, 226–236.

Hussein, J., Adey, M.A., 1998. Changes in microstructure, voids and b-fabric of surface samples of a Vertisol caused by wet/dry cycles. Geoderma 85, 63–82.

Igwe, C.A., Akamigbo, F.O.R, Mbagwu J.S.C. 1999. Chemical and mineralogical properties of soils in southeastern Nigeria in relation to aggregate stability. Geoderma, **92,** 111–123.

Imhoff, S., da Silva, A.P., Dexter, A. 2002. Factors contributing to the tensile strength and friability of Oxisols. Soil Sci. Soc. Am. J. 66, 1656–1661.

Jacks, G.V., 1963. The biological nature of soil productivity. Soils & Fert. 26: 147–150.

Jégou, D., Hallaire, V., Cluzeau, D., Tre´hen, P., 1999. Characterisation of the burrow system of the earthworms using X-ray computed tomography and image analysis. Biology and Fertility of Soils 29, 314– 318.

Jones, C.G., Lawton J.H., Shachak M., 1994. Organisms as ecosystem engineers. Oikos 69, 373-386.

Jongerius A., Schoonderbeek D., Jager, A., Kowalinski T., 1972. Electro-optical soil porosity investigation by means of Quantimet-B equipment. Geoderma, 7, 177-198.

Jongerius, A., Schoonderbeek, D., Jager, A., Kowalinski, S., 1972. Electro-optical soil porosity investigation by means of Quantimet-B equipment. Geoderma 7 (3–4), 177–198.

Jungerius, P.D., van den Ancker, J.A.M., Mucher, H.J., 1999. The contribution of termites to the microgranular structure of soils on the Uasin Gishu Plateau, Kenya. Catena 34, 349-363.

Kay, B.D., 1998. Soil structure and organic carbon: a review. In: Lal, R., Kimble, J.M., Follett, R.F., Stewart, B.A. (Eds.), Soil Processes and the Carbon Cycle. CRC Press, Boca Raton, FL, pp. 169– 197.

Kemper, D.W. and Rosenau, R.C. 1986. Aggregate stability and aggregate size distribution. In: Methods of Soil Analysis, Part 1. ASA-SSSA (ed. A. Klute). Soil Science Society of America, Inc. Madison, WI , pp. 425-442.

Khormali F; Abtahi A; Stoops G, 2006. Micromorphology of calcitic features in highly calcareous soils of Fars Province, Southern Iran. Geoderma, 132: 31-46.

Kooistra, M.J., 1991. A micromorphological approach to the interactions between soil structure and soil biota. Agric. Ecosyst. Environ. 34, 315–328.

Koppi, A. J. and McBratney, A. B., 1991. A basis for soil mesomorphological analysis. Journal of Soil Science, 42: 139–146.

Kuka, K., Franko, U., Rühlmann, J. 2007. Modelling the impact of pore space distribution on carbon turnover. Ecol. Model. 208, 295–306.

Lal, R. 2006. Encyclopedia of Soil Science. Second Edition, Vol I, Vol II. Taylor and Francis, Boca Raton, FL.

Lal, R., Shukla, M.K., 2004. Principles of soil physics. Marcel Dekker, Inc.

Lehrsch, G.A., 1998. Freeze–thaw cycles increase near-surface aggregate stability. Soil Sci. 163, 63–70.

Li, D.C., Velde, B., Zhang, T.L., 2004. Observations of pores and aggregates during aggregation in some clay-rich agricultural soils as seen in 2D image analysis. Geoderma, 118: 191-207.

Li, J.H., Zhang, L.M., 2010. Geometric parameters and REV of a crack network in soil. Computers and Geotechnics, 37: 466–475.

Loeppert, R.H., Suarez, D.L. 1996. Carbonate and gypsum. In: Sparks, D.L. (ed.),Methods of Soil Analysis, Part 3, Chemical Methods SSSA Book Ser. 5. American Society of Agronomy and Soil Science Society of America, Madison, Wisconsin, USA.

Marcelino, V., Cnudde, V., Vansteelandt, S., Caro, F., 2007. An evaluation of 2D-image analysis techniques for measuring soil microporosity. European Journal of Soil Science 58, 133–140.

Martens, D.A., 2000. Plant residue biochemistry regulates soil carbon cycling and carbon sequestration. Soil Biol. Biochem. 32, 361– 369.

McBratney, A.B. and Moran, C.J., 1990. A rapid analysis method for soil macropore structure, II. Stereological model, statistical analysis, and interpretation. Soil Sci. Soc. Am. J., 54: 509- 515.

McKeague, J.A., Guertin, R.K., Valentine, K.W.G., Belisle, J., Bourbeau, G.A., Howell, A., Michalyna, W., Hopkins, L., Page, F.. Bresson, L.M. 1980. Estimating illuvial clay in soils by micromorphology. Soil Sci. 129, 386-388.

Meadows, A., Meadows, P. S., Wood, D. M. & Murray, J. M. H., 1994. Microbiological effects on slope stability – an experimental analysis. Sedimentology 41: 423-435.

Mele G., Basile A., Leone A.P., Moreau E., Terribile F., Velde B., 1999. The study of soil structure by coupling serial sections and 3D image analysis, Modelling of transport processes in soils. Int. Workshop of EurAgEng's Field of interest on Soil and Water. Edited by Feyen & K.Wiyo. Leuven, 103-117.

Miralles-Mellado I., Canton Y., Sole-Benet A., 2011. Two-Dimensional Porosity of Crusted Silty Soils: Indicators of Soil Quality in Semiarid Rangelands? Soil Science Society of America Journal, 75: 1330-1342.

Mooney, S.J., Tams, A.R. , Berry, P.M., 2006. A reliable method for preserving soil structure in the field for subsequent morphological examinations. Geoderma 133: 338– 344.

Moreau, E., 1997. Etude de la morphologie et de la topologie 2D et 3D d'un sol argileux par analyse d'images. Ph.D. Thesis. Université de Poitiers, France.

Moreau, E., Velde, B., Terrible, F., 1999. Comparison of 2D and 3D images of fractures in a Vertisol. Geoderma 92, 55– 72.

Muggler, C.C., van Griethuysen, C., Buurman, P., Pape, T., 1999. Aggregation, organic matter, and iron oxide morphology in Oxisols from Minas Gerais, Brazil. Soil Sci. 164, 759–770.

Muneer, M. and Oades, J.M. 1989. The role of ca-organic interactions in soil aggregate stability .1. Laboratory studies with glucose-C-14, $CaCO_3$ and $CaSO_4.2H_2O$. Aust. J. Soil Res. 27, 389-399.

Murphy, C.P. 1983. Point counting pores and illuvial clay in thin section. Geoderma. 31, 133-150.

Murphy, C.P., Bullock, P., Biswell, K.J., 1977b. Measurement and characterization of voids in soil thin-sections by image analysis .2. Applications. Journal of Soil Science 28, 509–518.

Murphy, C.P., Bullock, P., Turner, R.H., 1977a. Measurement and characterization of voids in soil thin-sections by image analysis .1. Principles and techniques. Journal of Soil Science 28, 498–508.

Nawrath, R., Serra, J., 1979a. Quantitative image analysis — applications using sequential transformations. Microscopica Acta 82, 113–128.

Newman, A.C.D., Thomasson, A.J., 1979. Rothamsted studies of soil structure: III. Pore size distributions and shrinkage processes. Journal of Soil Science 30, 415–439.

Oades, J.M., 1984. Soil organic matter and structural stability: mechanisms and implications for management. Plant Soil, 76: 319–337.

Oades, J.M., Gillman, G.P., Uehara, G., 1989. Interactions of soil organic matter and variable-charge clays. In: Coleman, D.C., Oades, J.M., Uehara, G. (Eds.), Dynamics of Soil Organic Matter in Tropical Ecosystems. Hawaii Press, Honolulu, pp. 69–95.

Oades, J.M., Waters, A.G., 1991. Aggregate hierarchy in soils. Aust. J. Soil Res. 29, 815–828.

Ohrstrom, P., Hamed, Y., Persson, M., Berndtsson, R., 2004. Characterizing unsaturated solute transport by simultaneous use of dye and bromide. Journal of Hydrology 289, 23–35.

Padmanabhan, E. and Mermut, A.R. 1996.Submicroscopic structure of Fe-coatings on quartz grains in tropical environments. Clays Clay Miner. 44, 801- 810.

Pagliai M., La Marca G., Lucamente G., Genovese L., 1984. Effects of zero and conventional tillage on the length and irregularity of elongated pores in a clay loam soil under viticulture, Soil Tillage Res., 4: 433-444.

Pagliai, M. Vignozzi, N. 2002. Image analysis and microscopic techniques to characterize soil pore system, in: Blahovec, J., Kutílek, M (Eds.), Physical methods in agriculture: approach to precision and quality. Kluwer Academic Plenum Publishers, New York, pp. 13-38.

Pagliai, M., La Marca, M., Lucamante, G., 1987. Changes in soil porosity in remolded soils treated with poultry manure. Soil Science 144, 128–140.

Pagliai, M., Vignozzi N. and Pellegrini S. 2004. Soil Structure and the Effect of Management Practices. Soil & Tillage Research 79:131-143.

Pawluk, S. and Dumanski, J. 1973. Ferruginous concretions in a poorly drained soil of Alberta. Proc. Soil Sci. Soc. Am. 37, 124-127.

Peech, M. 1965. Hydrogen-ion activity. In: Black, C.A. (Ed.), Methods of Soil Analysis, Part 2. American Society of Agronomy and Soil Science Society of America, Inc. Madison, Wisconsin, USA.

Pendleton, D.E., Dathe, A., Baveye, P., 2005. Influence of image resolution and evaluation algorithm on estimates of the lacunarity of porous media. Physical Review E 72 (4) Art. No. 0413062005.

Phillips, D.H., Fitzpatrick, E.A., 1999. Biological influences on the morphology and micromorphology of selected Podzols (Spodosols) and Cambisols (Inceptisols) from the eastern United States and north-east Scotland. Geoderma 90, 327–364.

Piccolo, A., Pietramellara, G., Mbagwu, J.S.C., 1997. Use of humic substances as soil conditioners to increase aggregate stability. Geoderma 91, 311–326.

Pires L. F. Bacchi, O. S.; Reichardt, K., 2007. Assessment of soil structure repair due to wetting and drying cycles through 2D tomographic image analysis. Soil and Tillage Research, 92: 537-545.

Pires, L.F., Cooper, M., Cássaro, F.A.M., Reichardt, K. Bacchi, O.O.S., Dias, N.M.P. 2008. Micromorphological analysis to characterize structure modifications of soil samples submitted to wetting and drying cycles. Catena. 72, 297-304.

Poesen J., Lavee, H. 1994. Rock fragment in top soils: significance and processes. Catena 23: 1-28

Ponge, J.F., 1991. Food resources and diets of soil animals in a small area of Scots pine litter. Geoderma 49, 33–62.

Protz, R., Shipitalo, M.J., Mermut, A.R. and Fox, C.A., 1987. Image analysis of soils – present and future. Geoderma, 40: 115-125.

Puget, P., Drinkwater, L.E., 2001. Short-term dynamics of root- and Shoot-derived carbon from a leguminous green manure. Soil Sci. Soc. Am. J 65, 771-779.

Rhoades, J.D. 1996. Salinity: Electrical conductivity and Total Dissolved Solids. In: Sparks D.L. (Ed.), Methods of Soil Analysis, Part 3, Chemical Methods SSSA Book Ser. 5. American Society of Agronomy and Soil Science Society of America, Madison, Wisconsin, USA.

Rhoton, F. E., Römkens, M.J.M., Bigham, J.M., Zobeck, T.M., Upchurch, D.R. 2003. Ferrihydrite influence on infiltration, runoff, and soil loss. Soil Sci. Soc. Am. J. 67, 1220–1226.

Righi, D., Van Ranst, E., De Coninck, F., Guillet, B., 1982. Microprobe study of a Placohumod in the Antwerp Campaine Belgium.. Pedologie 32, 117–134.

Ringrose-Voase, A. J. 1990, One-dimensional image analysis of soil structure. I. Principles. Journal of Soil Science, 41: 499–512.

Ringrose-Voase, A., 1987. A scheme for the quantitative description of soil macrostructure by image analysis. Journal of Soil Science, 38: 343–356.

Ringrose-Voase, A.J. 1991. Micromorphology of Soil Structure: Description, Quantification, Application. Australian Journal of Soil Research 29:777-813.

Ringrose-Voase, A.J. 1996. Measurement of soil macropore geometry by image analysis of sections through impregnated soil. Plant and Soil, 183, 27–47.

Ringrose-Voase, A.J., Bullock, P., 1984. The automatic recognition and measurement of soil pore types by image analysis and computer programs. Journal of Soil Science 35, 673–684.

Sauer, T.J. & Logsdon, S.D. 2002. Hydraulic and physical properties of stony soils in a small watershed. Soil Science Society of America Journal, 66, 1947–1956.

Schutter, M.E., Dick, R.P., 2002. Microbial community profiles and activities among aggregates of winter fallow and cover-cropped soil. Soil Sci. Soc. Am. J. 66, 142– 153.

Schwertmann, U., Fanning, D.S. 1976. Iron-manganese concretions in hydrosequences of soils in loess in Bavaria. Soil Sci. Soc. Am. J. 40, 731-738.

Schwertmann, U., Taylor, R.M. 1989. Iron oxides. In: Dixon, J.B., Weed, S.B. (Eds.), Minerals in the Soil Environment, pp. 379–437. Soil Science Society of America, Madison, WI.

Scott, H.D. 2000. Soil physics: agricultural and environmental applications. Iowa State University Press, Iowa.

Serra, J. 1982. Image Analysis and Mathematical Morphology. Academic Press, London.

Six, J., Bossuyt, H., Degryze, S., Denef, K. 2004. A history of research on the link between (micro)aggregates, soil biota, and soil organic matter dynamics. Soil Till. Res. 79, 7-31.

Six, J., Elliott, E.T., Paustian, K., 2000. Soil structure and soil organic matter. II. A normalized stability index and the effect of mineralogy. Soil Sci. Soc. Am. J. 64, 1042–1049.

Six, J., Feller, C., Denef, K., Ogle, S.M., Sa, d.M.J.C., 2002. Soil organic matter, biota and aggregation in temperate and tropical soils—effects of no-tillage. Agronomie 22, 755–775.

Sleutel, S., Cnudde, V., Masschaele, B., Vlassenbroek, J., Dierick, M., Van Hoorebeke, L., Jacobs, P., De Neve, S., 2008. Comparison of different nano- and micro-focus X-ray computed tomography set-ups for the visualization of the soil microstructure and soil organic matter. Computers & Geosciences 34, 931–938.

Soil Survey Division Staff. 1993. Soil survey manual. Soil Conservation Service Handbook 18, chapter 3. U.S. Department of Agriculture.

Soille, 2004. Morphological image analysis: principles and applications. Springer.

Spomer, L.A. 1980.Pediction and control of porosity and water retention in sand-soil mixtures for drained turf sites, Agronomy Journal, 72: 361-362.

Stewart, V.I., Adams, W.A. and Abdulla, H.H., 1970. Quantitative pedological studies on soils derived from silurian mudstones: II the relationship between stone content and the apparent density of the fine earth. J. Soil Sci., 21: 248-255.

Sugden, A., Stone, R., Ash, C. 2004. Ecology in the Underworld. Science. 304, 1613.

Summer, M.E. and Miller, W.P. 1996. Cation exchange capacity and exchange coefficients. In: Sparks, D.L. (Ed.), Methods of Soil Analysis, Part 3, Chemical Methods SSSA Book Ser. 5. American Society of Agronomy and Soil Science Society of America, Madison, Wisconsin, USA.

Sweeney, S.J., 1994. Macropore characterization and water movement in a fractured glacial till unit of southern Alberta, Canada. Unpublished PhD Dissertation 1330 pp.

Taina, I. A.; Heck, R. J.; Elliot, T. R., Scaiff, N., 2010. Micromorphological and X-ray μCT study of Orthic Humic Gleysols under different management conditions. Geoderma. 158, 110-119.

Tariq, A.U.R., Durnford, D.S. 1993. Soil volumetric shrinkage measurements: a simple method. Soil Sci. 155, 325–330.

Telfair, D., Gardner, M.R., Miars, D., 1957. The restoration of a structurally degenerated soil. Soil Science Society of America Journal Proceedings 21, 131–134.

Terribile, F. and FitzPatrick, E.A., 1992. The application of multilayer digital image processing techniques to the description of soil thin sections. Geoderma, 55: 159-174.

Thompson, M.L., Singh, P., Corak, S. and Straszheim, W.E., 1992. Cautionary notes for the automated analysis of soil pore-space images. In: A.R. Mermut and L.D. Norton (Editors), Digitization, Processing and Quantitative Interpretation of Image Analysis in Soil Science and Related Areas. Geoderma, 53:399-415.

Tisdall, J.M. and J.M. Oades. 1982. Organic matter and water-stable aggregates in soil. J. Soil Sci. 33:141–163.

Topoliantz, S., Ponge, J.F., Viaux, P., 2000. Earthworm and enchytraeid activity under different arable farming systems, as exemplified by biogenic structures. Plant and Soil 225, 39– 51.

Torri, D. Poesen, Monaci, J.F. Busoni, E., 1994. Rock fragment content and fine soil bulk density. Catena, 23: 65-71

Towner, G.D. 1988. The influence of sand- and silt-size particles on the cracking during drying of small clay-dominated aggregates. Journal of Soil Science, 39: 347-356.

TRANSVALOR 2000. Micromorph Version 1.4 CMM. Ecole des Mines, Armines.

Urbanek E., Shakesby R. A., 2009. Impact of stone content on water movement in water-repellent sand. European Journal of Soil Science, 60, 412–419.

Van Wesemael, B., Poesen, J. De Figueiredo, T., 1995. Effects of rock fragments on physical degradation of cultivated soils by rainfall. Soil & Tillage Research, 33: 229-250.

VandenBygaart, A. J., Fox, C. A., Fallow, D. J., Protz R., 2000. Estimating Earthworm-Influenced Soil Structure by Morphometric Image Analysis. Soil Sci. Soc. Am. J. 64:982–988.

VandenBygaart, A.J., Protz, R., 1999. The representative elementary area (REA) in studies of quantitative soil micromorphology. Geoderma 89, 333–346.

Velde, B. 1999. Structure of surface cracks in soil and muds. Geoderma. 93, 101-124.

Vogel, H. J. 2000. A numerical experiment on pore size, pore connectivity, water retention, permeability, and solute transport using network models. Eur. J. Soil Sci., 51: 99-105.

Vogel, H.J., 1997. Morphological determination of pore connectivity as a function of pore size using serial sections. European Journal of Soil Science, 48: 365-377.

Walkley, A. and Black, I.A. 1934. An examination of the Degtjareff method for determining organic carbon in soils: Effect of variations in digestion conditions and of inorganic soil constituents. Soil Sci. 63, 251-263.

Wallwork, J. A., 1975. The Distribution and Diversity of Soil Fauna. Hollett & Son.

Wilson, M.J. 1987. A Handbook of Determinative Methods in Clay Mineralogy. Chapman and Hall, New York.

Wuddivira, M. N. and Camps-Roach, G. 2007. Effects of organic matter and calcium on soil structural stability. Eur. J. Soil Sci. 58, 722–727.

Yerima, P.K. and Van Ranst, B. E. 2005. Introduction to Soil Science: Soils of the Tropics. Trafford Publishing, Victoria, BC.

Young M., Crawford, J. W. 2004. Interactions and Self-Organization in the Soil-Microbe Complex. Science, 304: 1634.

Young, I. M., Ritz, K. 2000. Tillage, habitat space and function of soil microbes. Soil Tillage Res., 53: 201-213.

Young, I.M., Crawford, J.W., Rappoldt, C. 2001. New methods and models for characterizing structural heterogeneity of soil. Soil Till. Res. 61, 33-45.

Zhang, X., Bengough, A. G., Crawford, J. W.,. Young, I. M, 2002. A lattice BGK model for advection and anisotropic dispersion equation. Advances in Water Res., 25: 1-8.

Zhou Z.C., Shangguan Z.P., 2007. The effects of ryegrass roots and shoots on loess erosion under simulated rainfall. CATENA, 70, 350-355.

Zhou, B.B., Shao, M.A., Shao, H.B., 2009. Effects of rock fragments on water movement and solute transport in a Loess Plateau soil. Surface geosciences (Hydrology – Hydrogeology). C. R. Geoscience 341: 462–472.